Sterile Neutrino Oscillation Sensitivity Simulation in SBN

Costas Andreopoulos, Dominic Barker, Chris Backhouse, Steve Dennis, Guanqun Ge, Daniele Gibin, Thomas Ham, Rhiannon Jones, Georgia Karagiorgi, Tereza Kroupova, Jacob Larkin, Andy Mastbaum, Ornella Palamara, Gray Putnam, Marco Roda, Mark Ross-Lonergan, Glória de Sá Pereira, Elizabeth Worcester, Bruno Zamorano, Joseph Zennamo

Institutes

Abstract

Keywords:

Contents

1. Introduction

Following the observation of neutrino oscillations and the confirmation that neutrinos are massive particles, many experiments have taken advantage of the numerous sources of neutrinos to learn more about their behaviour, particularly in the context of flavour oscillations. Conflicting results have since emerged between existing oscillation data and the three flavour neutrino framework in short-baseline experiments, and are consequently under investigation. The anomalies hint towards the existence of an additional mass eigenstate at around $\Delta m^2 = 1$ eV^2 such that the oscillations of active neutrinos to this new state are fast, and consequently undetectable by long-baseline experiments.

If there does exist a fourth type of neutrino, it must be 'sterile', such that it is unable to interact via the weak force. This requirement is necessary to maintain consistency with the three-flavour active neutrino picture defined by LEP [1] [2]. Given that they do not couple to the weak bosons, sterile neutrinos are unobservable both directly and indirectly in current neutrino oscillation experiments and their existence can only be determined through inconsistencies with the active-only neutrino oscillation picture.

In most short baseline neutrino experiments, a sterile neutrino oscillation measurement is made via one of the three channels,

- $\nu_\mu \to \nu_\mu$ (ν_μ disappearance)
- $\nu_\mu \to \nu_e$ (ν_e appearance)
- $\nu_e \to \nu_e$ (ν_e disappearance)

where the sensitivity of the measurement is dependent on the energy, baseline and neutrino source of the experiment. Measurements may also be made through the analogous channels with anti-neutrinos. In each disappearance case, a deficit in the observed event rate relative to predictions given by the three-flavour neutrino model could indicate that the active neutrino flavour eigenstate oscillated to a sterile flavour eigenstate. Similarly, in the electron neutrino appearance case, an excess of observed electron neutrinos could be due to the oscillation of a sterile flavour eigenstate into the active flavour state.

Following the determination of an excess or deficit in the expected rate of three-flavour neutrino oscillations and the subsequent postulation of an additional neutrino flavour eigenstate,

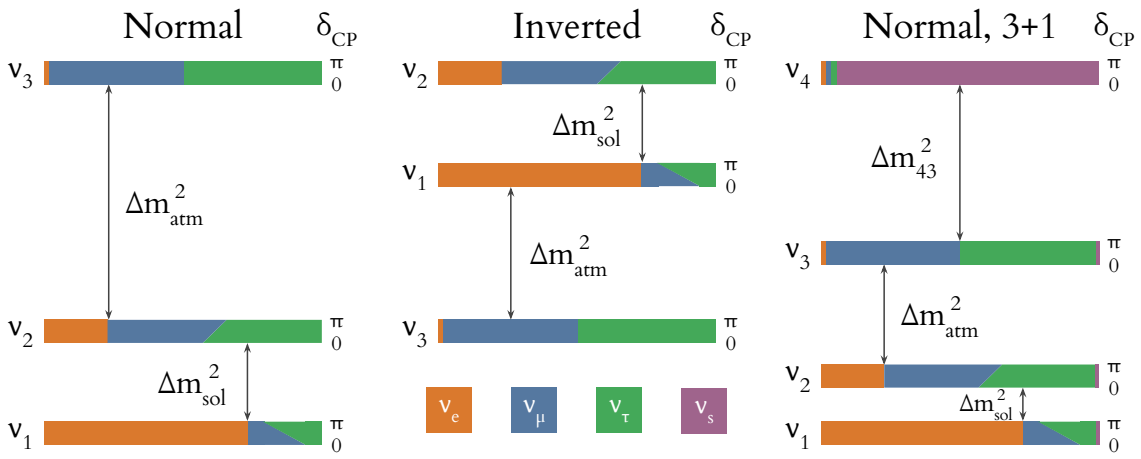

Figure 1: A demonstration of how the neutrino flavour eigenstates contribute to the neutrino mass hierarchy in each of the normal, inverted and (3+1) sterile cases. The sterile neutrino mass splitting, Δm^2_{43} is included in the normal-ordering scheme to demonstrate the (3+1) model amendment to the active neutrino picture. The sterile splitting is likely to be more than 10 times larger than the active splittings [3].

it is necessary to update the parameterisation of neutrino oscillations to incorporate this additional member of the neutrino family.

The simplest extension to the active neutrino picture which has been proposed to explain these short baseline anomalies is the 3+1 (active+sterile) hypothesis. The sterile component of each active neutrino must be small enough to minimise conflict with the LEP three-flavour constraint, but still allow for oscillations to occur between active and sterile flavour eigenstates. Adding in a single sterile neutrino to the mass hierarchy is shown for normal-ordering in Figure 1.

The constraints set by existing anomalous neutrino oscillation data suggest that the third mass splitting is at least 10 times larger than the active mass splittings. The approximation $\Delta m^2_{41} = \Delta m^2_{21,sol} + \Delta m^2_{32,atm} + \Delta m^2_{43}$ is therefore assumed to be true and allows for the assumption that, $\Delta m^2_{sol} \approx \Delta m^2_{atm} \approx 0$ [3], reducing the parametrisation of a sterile neutrino oscillation measurement in the (3+1) framework to only include the single mass splitting, Δm^2_{41}.

Incorporating the (3+1) sterile neutrino model into the mixing matrix in order to determine the probability of oscillations between the active and sterile flavours involves the addition of a single row and column to the PMNS matrix [3],

$$U_{\alpha k} = \begin{pmatrix} U_{e1} & U_{e2} & U_{e3} & U_{e4} \\ U_{\mu 1} & U_{\mu 2} & U_{\mu 3} & U_{\mu 4} \\ U_{\tau 1} & U_{\tau 2} & U_{\tau 3} & U_{\tau 4} \\ U_{s1} & U_{s2} & U_{s3} & U_{s4} \end{pmatrix}. \quad (1)$$

Parameterised by the sterile mixing angles and mass splitting, the probability of each of the short baseline ν_μ and ν_e appearance and disappearance oscillations occurring in the (3+1) picture is as follows [**?**],

$$P_{\mu\to\mu} = \sin^2(2\theta_{\mu\mu}) \sin^2\left(1.27\frac{\Delta m^2 L}{E}\right) \quad (2)$$

$$P_{e\to e} = \sin^2(2\theta_{ee}) \sin^2\left(1.27\frac{\Delta m^2 L}{E}\right) \quad (3)$$

$$P_{\mu\to e} = \sin^2(2\theta_{\mu e}) \sin^2\left(1.27\frac{\Delta m^2 L}{E}\right), \quad (4)$$

where the effective sterile mixing angles are defined as [3],

$$\sin^2(2\theta_{\mu\mu}) = 4(1 - |U_{\mu 4}|^2)|U_{\mu 4}|^2 \quad (5)$$

$$\sin^2(2\theta_{ee}) = 4(1 - |U_{e4}|^2)|U_{e4}|^2 \quad (6)$$

$$\sin^2(2\theta_{\mu e}) = 4|U_{e4}|^2|U_{\mu 4}|^2. \quad (7)$$

2. Oscillation Analysis Paradigm

The SBN oscillation analysis procedure involves a simultaneous fit of systematic and oscillation parameters to kinematic distributions of topological event samples from all SBN detectors, providing an indirect extrapolation from the near to the far detectors. The method is summarised graphically in Figure 2.

Event rate predictions are constructed in each sample, beam and detector defined in the analysis. A physics hypothesis may then be combined with any prior systematic uncertainties and both are applied to the event rate predictions. These predictions and the

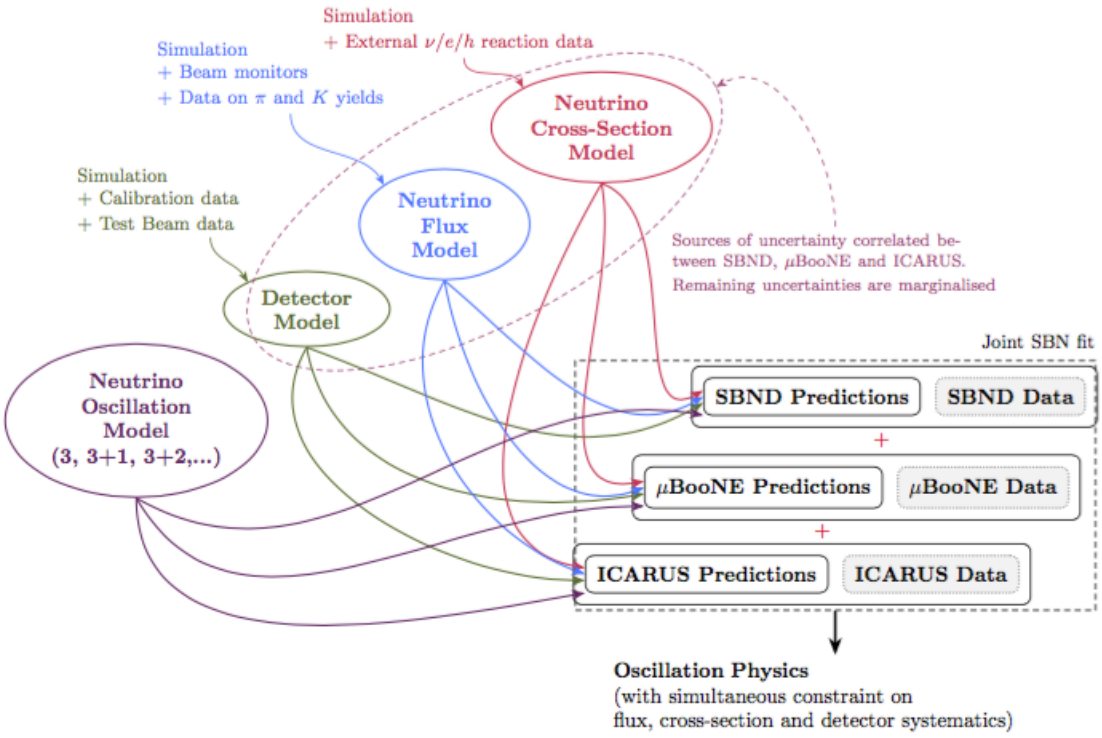

Figure 2: SBN oscillation analysis strategy

corresponding observations from any number of detectors and samples can then be combined in a fitting procedure, from which the sensitivity to the physics hypothesis can be determined at a given confidence level.

Section 8 will present analyses of the SBN sensitivity to the (3+1) sterile oscillation model through the observation of ν_μ disappearance, ν_e-appearance and ν_e-disappearance in SBN. The physics hypothesis used in the construction of the MC predictions for this analysis will be discussed here.

Given that existing results suggest $\Delta m^2_{41} \gg \Delta m^2_{sol,atm}$ in the (3+1) sterile neutrino hypothesis, the effective two-flavour oscillation probability can be employed. This probability is parameterised by Δm^2_{41} and $\sin^2 2\theta_{\mu\mu}$ for ν_μ disappearance searches, as per equation 26. SBN will be sensitive to the same region of parameter space previously explored by other experiments, where $10^{-2} < \Delta m^2_{41}$ eV^2, $10^{-3} < \sin^2 2\theta_{\mu\mu} < 1$, $10^{-4} < \sin^2 2\theta_{\mu e} < 1$, $10^{-2} < \sin^2 2\theta_{ee} < 1$. SBN will aim to push below the existing $\sin^2 2\theta$ limits.

Due to the short baseline of the SBN experiment, along with the validity of the approximation that $\Delta m^2_{41} \gg \Delta m^2_{sol,atm}$, $\Delta m^2_{sol} = \Delta m^2_{atm} = 0$, SBN is completely insensitive to active neutrino oscillations. The active neutrino oscillation hypothesis is therefore not applied alongside the sterile hypothesis in the SBN (3+1) sensitivity analyses and $\sin^2 2\theta_{\mu\mu}$ is the relevant mixing parameter in the two-flavour approximation.

3. Monte Carlo Event Simulation

3.1. ν_μ Production

Presently, the reconstruction in both SBND and ICARUS is under active development, such that a completely validated production is not yet available in either detector. The primary samples used in this analysis are therefore truth-based, with simple modifications applied to emulate shape and rate differences which might be expected in fully-reconstructed events in each of the three detectors. The samples of neutrino scattering events used in the main analyses in this note are constructed in the following way,

1. Generate $\mathcal{O}(10^6)$ ν_μ GENIE neutrino scattering events in the active volume of each detector
2. Propagate the final state particles through GEANT4 in each detector

3. Apply a combination of threshold cuts and smearing to the propagated particles, to emulate a 'reconstructed' sample

4. Select only the charged-current neutrino interaction events from the 'reconstructed' sample

5. Define the 'reconstructed' neutrino energy in each selected event.

Steps 1 and 2 will be discussed in the following subsections 3.3 and 3.4. Steps 3-through-5 will be discussed in section 4.1.

3.2. SBN geometries

The SBN volume definitions are given in Table 1, and refer to the active and fiducial volumes of each detector. An active volume is a geometry definition which contains all the liquid argon, and extends to the outer walls of each detector. The fiducial volumes are smaller geometries, entirely contained within one of the active volumes in a detector. A fiducial volume is used to minimise the number of tracks and showers which leave the active volume following a neutrino interaction, such that the number of particles it is possible to reconstruct is maximised in the event. A fiducial volume also provides shielding from external activity in the detector volume.

SBND has a single active volume with two fiducial volumes separated by the CPA. MicroBooNE has a single active volume with a single fiducial volume contained within it. In the case of ICARUS, there are two separate cryostats, each with two TPC's, therefore the ICARUS detector comprises 2 active and 4 fiducial volumes.

3.3. Muon neutrino interaction generation with GENIE

The GENIE interaction generator determines which of the neutrinos present in the flux and entering a given detector's geometry interact, and how that interaction is characterised. GENIE is a multi-purpose tool, primarily built for the Monte Carlo (MC) generation of neutrino interactions with varying nuclear structures spanning energies from 1 MeV to 1 PeV. Within GENIE, neutrino interactions are simulated using a combination of nuclear physics, cross-section, hadronization and hadron transport models according to how theoretical models define the available phase space. One GENIE tool allows for the combination of different versions of each of these models, to form unique configurations in a given simulation.

Volume	X [cm]		Y [cm]		Z [cm]	
	Active	Fiducial	Active	Fiducial	Active	Fiducial
SBND TPC1	-199.15, 199.15	-190.0, 5.6	-200.0, 200.0	-185.0, 185.0	0.0, 500.0	15.0, 415.0
SBND TPC2		10.9, 190.9		-185.0, 185.0		15.0, 415.0
MicroBooNE	-1.6, 254.8	13.5, 239.8	-115.5, 117.5	-100.5, 102.5	0.1, 1036.9	15.1, 956.9
ICARUS TPC1	-364.5, -67.9	-356.2, -224.5	-177.4, 143.4	-158.4, 128.4	-910.0, 880.0	-895.0, 800.0
ICARUS TPC2		-207.9, -76.2		-158.4, 128.4		-895.0, 800.0
ICARUS TPC3	67.94, 364.5	76.2, 207.9	-177.4, 143.4	-158.4, 128.4	-910.0, 880.0	-895.0, 800.0
ICARUS TPC4		224.5, 356.2		-158.4, 128.4		-895.0, 800.0

Table 1: The active and fiducial volume definitions used throughout the analyses for SBND, MicroBooNE and ICARUS.

Neutrino interactions generated using multiple GENIE model configurations contributed to the analyses presented in this note. Included are the historical GENIE v2 'Default+MEC'[1] model and from version 3 the configuration which fit best to MicroBooNE neutrino scattering data [4] defined according to the GENIE naming convention, G18_10a_02_11a [5]. Finally, variations of the CC QE+2p2h model components are substituted into the configuration from GENIE v3, including,

[1]Note that MEC and 2p2h may be used interchangeably throughout this explanation, this is simply to reference names as they are/were defined in each situation. However 2p2h is the more-correct definition of the scattering mode itself.

- **Llewellyn Smith + Empirical 2p2h, LS-E**: Default CC QE+2p2h model from GENIE v2 [6].
- **Nieves**: Also known as the 'Valencia' model. The CC QE+2p2h model used in the G18_10a_02_11a configuration [7]
- **SuSAv2**: 'Super-Scaling Approach version 2' [8]
- **Smith-Moniz**: QE(Running M_A), no CC 2p2h [9].

A summary of the contents of these model configurations are shown in Table 2. Bold elements of the table highlight components of the configuration which have been switched out from the previous model (when reading from left to right). A comparison of the GENIE v2 Default+MEC and GENIE v3 G18_10a_02_11a model configurations is shown with the MicroBooNE ν_μ CC Inclusive cross-section measurement in Figure 3 [4].

3.4. Muon neutrino interaction propagation with GEANT4

Having simulated the neutrino interaction and determined the particles leaving the nucleus along with their kinematics, the next step is to model their transport through the argon itself using a GEANT4-based simulation in LArSoft [20] [21].

First, the particles which successfully left the nucleus following an interaction are propagated through the detector geometry until they either leave it, or they range-out. As they traverse the liquid argon, the drift of the ionisation electrons is simulated and propagated onto the wire planes of the detector. Upon reaching the wire planes, the charge and timing information for every electron is recorded and the true energy of each deposition on each wire is calculated.

The charge, energy and timing information from every electron is combined for each simulated particle as a whole. If the total energy for a single particle is high enough for its type to be visible in the detector, and the particle remained entirely within the detector volume, then the truth-level information about the particle is stored. These truth-level particles are also tagged to be either a `Track` or an electromagnetic `Shower`. Particle hierarchies can then be constructed from each of the simulated particles in order to describe the relationship between all the final state particles produced in the neutrino interaction.

	GENIE Model Configuration				
Configuration component	'Default+MEC' v02.12.10	LS-E v03.00.06	G18_10a_02_11a v03.00.06	SuSAv2 v03.02.00	Smith-Moniz v03.02.00
Nuclear	RFG, Bodek-Ritchie [10]	**LFG** [11]	LFG	LFG	LFG
CC QE	Llewellyn Smith [6]	Llewellyn Smith	**Nieves** [7]	**SuSAv2** [8]	**Smith-Moniz** [9]
NC El	Ahrens [12]	Ahrens	Ahrens	Ahrens	Ahrens
CC 2p2h	Empirical [13]	Empirical	**Nieves**	**SuSAv2**	**N/A**
NC 2p2h	Empirical	Empirical	Empirical	Empirical	Empirical
Resonant, π, γ	Rein-Sehgal [14]	**Berger-Sehgal** [15]	Berger-Sehgal	Berger-Sehgal	Berger-Sehgal
Coherent, π	Rein-Sehgal [16]	**Berger-Sehgal** [17]	Berger-Sehgal	Berger-Sehgal	Berger-Sehgal
DIS	Bodek-Yang [18]	Bodek-Yang	Bodek-Yang	Bodek-Yang	Bodek-Yang
Hadronization	AGKY [5]	AGKY	AGKY	AGKY	AGKY
FSI	*hA* [5]	***hA*, 2018**	*hA*, 2018	*hA*, 2018	*hA* 2018

Table 2: A summary of the model configuration components used in the analyses presented in this note. The left-most column breaks down the model which may be 'plugged in' to construct the configuration. Included (from left-to-right) are the historical GENIE v2 Default configuration with an empirical form of the 2p2h interaction, the model configuration which best-describes MicroBooNE neutrino scattering data, G18_10a_02_11a [5] [19], with the historical CC QE+2p2h model plugged in, and three variants of this configuration, each substituted with different CC QE+2p2h models. Note that the Smith-Moniz configuration employs the 'Running-M_A' CC QE model and consequently doesn't include a CC 2p2h component. The elements in **bold** indicate models which have been replaced with respect to the configuration to its left.

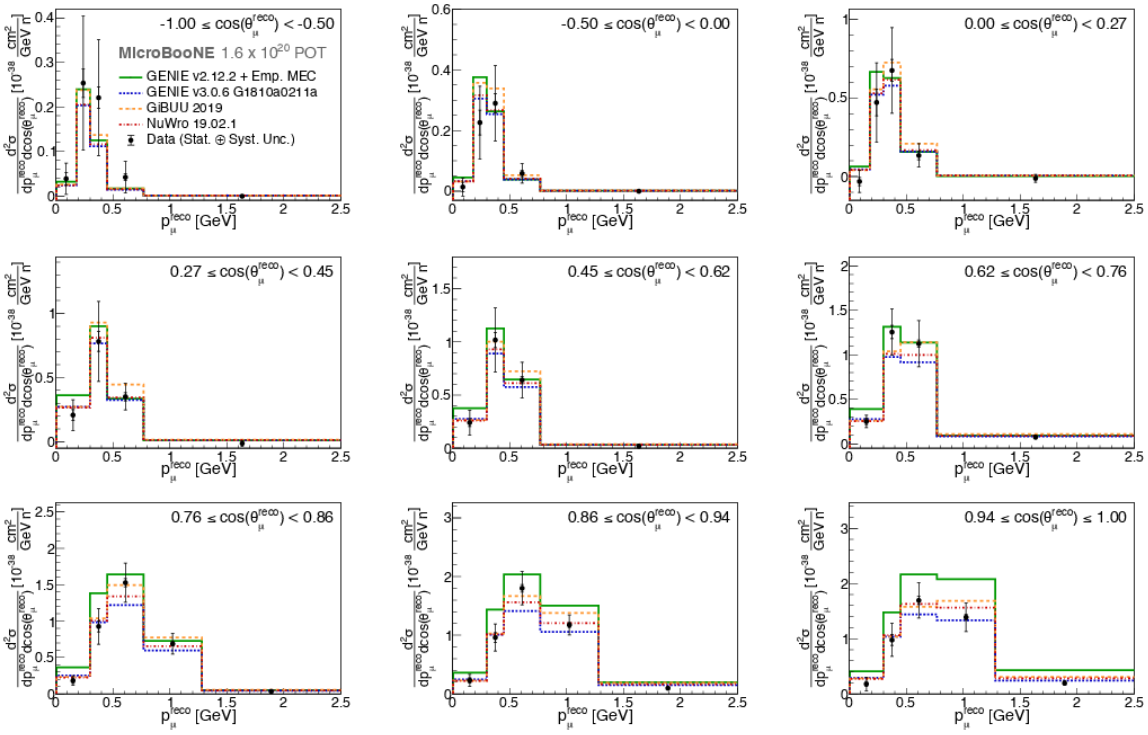

Figure 3: ν_μ CC Inclusive double-differential cross-section MicroBooNE data and multiple model configurations. The data (black dots and error bars) is presented as a function of reconstructed muon momentum in discrete muon scattering angle bins with both statistical and systematic uncertainties. The blue line shows the MicroBooNE-selected new GENIE model whilst the green line shows the historical default+MEC GENIE model [4].

3.5. ν_e Production

The ν_e production followed the same steps described in section 3.1, however, in addition to generating an intrinsic ν_e sample, an oscillated $\nu_\mu \rightarrow \nu_e$ sample, a dirt sample and a cosmic sample were also produced. The oscillated sample is used to mimic the ν_e appearance signal whereas the dirt and cosmic samples are backgrounds. The other major background associated with a ν_e analysis involves ν_μ. A dedicated sample was not produced to emulate this, but instead the events from the ν_μ production were also ran through the ν_e selection as mentioned in section 4.3. Table 3.5 outlines the number of events produced for each sample for each detector. The dirt events were produced with an additional filter at the generation stage which discarded any events where a shower above 10 MeV in the active volume was not present. This filter was used in order to remove any delta rays. Only about 1% of dirt events would pass this filter so the number of dirt events used in the ν_e selection was ∼100,000.

Sample	Events Produced
Intrinsic ν_e	∼1,000,000
Oscillated ν	∼1,000,000
ν_μ	See ν_μ sample
Dirt	∼10,000,000
Cosmic_Dirt	∼100,000

Table 3: The number of events initially produced for each sample in each of the three SBN detectors as part of the ν_e analysis.

4. Event Selections and Assumed Performance

4.1. Selection of Muon-Neutrino Charged-Current Events

The pseudo-reconstruction method employed in this analysis is based on the studies performed at time of the SBN proposal [22] in which fake reconstruction and a ν_μ CC event selection are applied simultaneously. The main reason for utilising this approach is that when the new SBN fitting frameworks were developing their analysis procedures, the SBN proposal served as a reference for validation. Having now completed this analysis validation, some features of the proposal-era method have been necessarily updated to account for fundamental modifications to the SBN program.

Given that this entire procedure is a placeholder for when fully-reconstructed samples become available, additional development of the finer details, such as the magnitude of the kinematic thresholds, has not been conducted since the SBN proposal was written. The combined pseudo-reconstruction and selection is described below, followed by a summary of the quantitative, detector-specific definitions.

The first step is to reconstruct and identify muon-neutrino-like interactions from the sample, which involves finding the primary track in every event as follows,

1. Generate events as per steps 1 & 2 above
2. Remove any events whose true interaction vertex is not located in the fiducial volume
3. Remove any events which do not produce a muon or a charged pion track. Events in which muons are produced are the CC signal events, whilst events with no muon but instead have a leading pion are candidate NC background events

4. Remove events in which the primary track,
   (a) Has a true kinetic energy, $E_k < 21$ MeV
   (b) Is entirely contained in the detector but their full trajectory length, $L_c < 50$ cm. This removes any NC backgrounds which aren't likely to be mis-identified in data from the sample
   (c) Exits the detector but their full trajectory length, $L_e < 100$ cm. This accounts for the ability to reconstruct escaping tracks
5. Assume an 80% reconstruction efficiency by removing 20% of all true signal events. This accounts for the estimated rate of neutrino interaction contamination in the external background removal, along with all other unaccounted-for losses.

Having selected the event, more pseudo-reconstruction can be performed on the remaining tracks in the sample for the purpose of calculating the 'reconstructed' neutrino energy and defining the 'reconstructed' content of the events for exclusive sample definitions. The resulting neutrino-induced sample contamination of the pseudo-selected ν_μ CC Inclusive event rate is 2%.

4.2. Reconstructed sample and energy definitions

First, any tracks with true $E_k < 21$ MeV are removed from the event. The true kinetic energy of any remaining tracks are then smeared by selecting a value from a Gaussian with $\mu = E_{k,true}$ and $\sigma = \alpha E_{k,true}$, where,

$$\alpha = \begin{cases} 0.05 & \text{Non-primary tracks} \\ 0.02 & \text{Contained, primary track,} \end{cases} \tag{8}$$

where 'primary' tracks refer to the leading lepton (in this case the muon) and 'non-primary' tracks refer to everything else in the final state.

In the case of escaping primary tracks, the amount by which to smear the kinetic energy is defined as a function of track length to emulate Multiple Coulomb Scattering (MCS),

$$\alpha = -A \ln(BL), \tag{9}$$

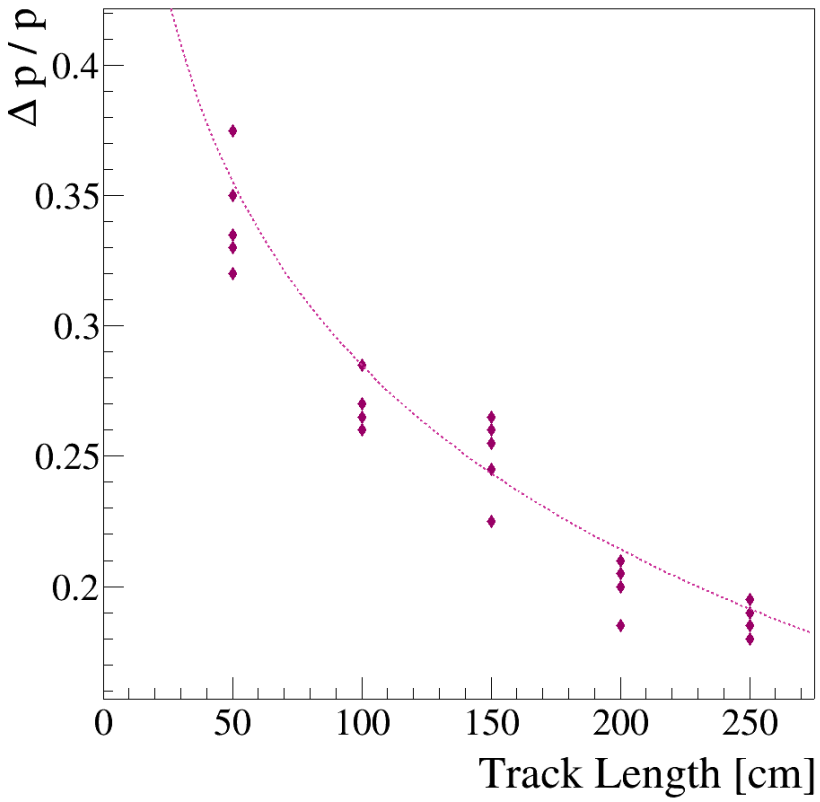

Figure 4: The momentum resolution of reconstructed muons as a function of track length, plotted from data in [23]. The functional form of the line-of-best-fit follows equation 9 with $A = 0.102$ and $B = 0.0006121$ cm^{-1}.

where $A = 0.102$ and $B = 0.0006121$ cm^{-1}. The functional form of equation 9 and values of A and B are shown in Figure 4 and were defined following a study conducted by the ICARUS experiment [23].

No smearing of shower-like particles is performed in the construction of the charged-current inclusive sample. The 'reconstructed' neutrino energy is then simply calculated by,

$$E_\nu = \sum_{n=0}^{N_t} E^n_{smeared}, \tag{10}$$

where N_t is the number of tracks above the true kinetic energy threshold and $E^n_{smeared}$ is the smeared total energy of each track.

4.3. Selection of Electron-Neutrino Charged-Current Events

The ν_e selection follows a similar basis to the ν_μ selection described in section 4.1. Different criteria for the selection were applied to beam induced TPC events, dirt events and cosmic events each of which are outlined below.

4.3.1. Beam induced active volume events

1. Remove any events whose true interaction vertex is not located in the fiducial volume.
2. Showers arising from the vertex are identified and the reconstructed energy is found from smearing the ionisation deposition. If more than one shower with energy above 100 MeV exists, the event is removed. This removes neutral pion events where the pion decays into two photon showers.
3. If there is only one photon candidate in the event, a conversion gap cut is applied. If the vertex is deemed visible, due to the presence of at least 50 MeV of hadronic kinetic energy, and the photon starts to shower further than 3 cm from the vertex the event is removed.
4. Remaining photons undergo a dE/dx cut resulting in a 94% background rejection.
5. If a misidentified photon originates from a resonant ν_μ CC interaction, the muon lepton is identified. Events where a muon travels greater than 1 m are assumed to be from ν_μ CC interactions and the event is removed.
6. Events where the shower has an energy less than 200 MeV are removed
7. A weight of 0.8 is applied to all selected events to account for an assumed 80% reconstruction efficiency.

4.3.2. Dirt Events

The selection procedure for dirt events is similar to that of events occurring in the TPC outlined above. However, since the vertex for dirt events occurs outside the detector volume, the conversion gap and muon track length cuts are not undertaken.

4.3.3. Cosmic Events

A largely separate analysis is applied for cosmic events which is as follows:

1. If a cosmic photon initially interacts outside the fiducial volume the event is removed.
2. Cosmic events which occur outside the beam spill time window are removed if there is no other activity in the TPC during the beam spill time.
3. 95% of cosmic events occurring within the beam spill window are removed by use of the PDS and CRT systems and taking advantage of the bucket structure of the beam.
4. Same dE/dx cut as described above.
5. Events below a reconstructed energy of 200 MeV are removed.
6. A topological cosmic cylinder cut is applied to cosmic photons which originate from cosmic muons that pass through the TPC. These can be removed by a fiducial volume cut corresponding to a cylinder of radius 15 cm around the cosmic muon.

5. Systematic Error Assignments

All systematic parameters used in the SBN oscillation analyses are defined through the construction of 'universes', in which one or more systematic parameters are varied within their prior uncertainty, at known n-σ intervals, to produce an alternative sample of MC events. Many such universes can be constructed to characterise the variations of a given parameter/set. If the variations are well-approximated by a Gaussian distribution, a covariance matrix can be constructed in a chosen kinematic parameter space to represent that parameter. The standard deviation of the Gaussian distribution corresponds to a 1-σ variation. If the parameter is not normally distributed, cubic splines can instead be constructed in true-reco kinematic parameter space to directly represent the behaviour of the n-σ parameter/set variations. An example application of these representations of the SBN flux and interaction systematic parameters will be discussed further with respect to the VALOR fitting framework implementation in section vii.

5.1. Flux systematic parameters

The flux systematic parameter set is separated into three categories, the hadronic cross-section parameters, the optical flux parameters and the hadronic neutrino production parameters. This section will define the main contributions to each set and is mostly informed by this paper [24], where much more detail can be found.

i. Hadronic cross-section and optical parameters.

The flux parameters involving the interaction cross-section of hadrons in the Beryllium target and Aluminium horn are categorised based on three broad interaction types. The distinction is made between those affecting the total cross-section, σ_{TOT}, the inelastic cross-section, σ_{INEL}, and the quasi-elastic cross-section, σ_{QE}, which is a subset of the inelastic interactions concerning elastic-like collisions similar to those between hadrons and free nucleons.

The split largely stems from the availability of σ_{TOT} and inelastic data sets, along with the omission of a distinct σ_{EL} parameter due to the lack of data in the relevant kinematic

region for interactions within the BNB. The elastic cross-section can instead be inferred from σ_{TOT} and σ_{INEL} by the relation $\sigma_{TOT} = \sigma_{INEL} + \sigma_{EL}$.

The σ_{TOT} cross-section is modelled and compared to n-Be interaction data at similar energies to the BNB. The agreement is sufficient to extend the use of the model to p-Be and $\pi^{\pm}$-Be interactions. The variation between model and data gives the prior systematic uncertainty on the total cross-section.

The global inelastic cross-section data set is much more abundant at the BNB energies, therefore σ_{INEL} for nucleons and pion interactions on both Beryllium and Aluminium can be inferred directly from data, without any need for a comparison with theory. In contrast, the subset of quasi-elastic data is sparse, therefore theoretical models are once again employed to help parametrise the cross-section between nucleons, pions and the target materials.

Variations performed to simulate these parameters take into consideration their relations in the following way:

- While σ_{TOT} is varied, σ_{INEL} is held constant to allow only σ_{EL} to change
- While σ_{INEL} is varied, σ_{EL} is allowed to float within a fixed σ_{TOT}
- The total σ_{INEL} also remains unchanged whilst σ_{QE} is varied, such that only other inelastic processes are allowed to float.

ii. Optical flux parameters.

The horn current and skin effect quantify the strength of the magnetic field in the horn and the magnitude of the field's permeation into the surrounding conducting cylinder respectively. Varying the horn current impacts the focussing properties of the horn and therefore the shape of the neutrino flux. The skin effect can induce a variation in the magnitude of the magnetic field following the permeation of the current into the material surrounding the horn.

iii. Hadronic neutrino production flux parameters.

Neutrinos observed in the SBN experiments are primarily produced through the decay of hadronic particles exiting the Beryllium target of the BNB. The differential cross-section of each of these particles are parametrised separately through fits to experimental p-Be cross-section data.

This section will serve as a brief summary of the extremely detailed explanation given in [24] and will primarily focus on charged pions since π^+ decay is by far the dominant neutrino production mechanism in the BNB.

1. $\pi^{\pm}$: The Sanford and Wang (SW) parametrisation of the differential cross-section as a function of meson kinematics, p, θ, and incident proton momentum, p_B, is used to describe charged pion production using equation 11,

$$\frac{d^2\sigma}{dpd\theta} = c_1 p^{c_2} \left(1 - \frac{p}{p_B - c_9}\right) \exp\left(-c_3 \frac{p^{c_4}}{p_B^{c_5}} - c_6\theta(p - p_B c_7 cos^{c_8}\theta)\right), \tag{11}$$

   where $c_{\{1..9\}}$ are determined through fits to the HARP p-Be data at 8.89 GeV/c. It is these 9 correlated parameters which are varied within their uncertainty in the simulation of the charged pion systematic parameters

2. K^+: There is insufficient data for K^+ production following proton-Beryllium interactions at 8.89 GeV/c to apply the SW differential cross-section parametrisation. Instead, Feynman scaling is utilised to translate measurements made at different proton energies to those relevant for SBN

3. K^0_L: The long lifetime and the fact that neutral kaons cannot be focused contribute to the reduced rate of neutrino production from their decay. Forward going data ($< 5°$) from a number of experiments is therefore used in fits to constrain the SW parametrisation

4. K^-: Contrary to the methods of parametrising the other hadronic production mechanisms, a Monte Carlo simulation of p-Be interactions is produced using GEANT4 to determine the K^- differential cross-section. This is once again a method of combating the scarcity of available K^- production data from p-Be interactions at energies relevant to SBN.

The complete list of flux systematic parameters along with the prior 1σ uncertainties are

given in Tables 4, 5 and 6. These are associated with the optical parameters, hadronic parameters and parameters respectively.

Parameter	Description	Uncertainty	
		Be	Al
$f_{\sigma^N_{INEL}}$	Secondary nucleon interactions in the target (Be) and horn (Al), inelastic cross-section	±5%	±10%
$f_{\sigma^N_{QE}}$	Secondary nucleon interactions in the target (Be) and horn (Al), quasi-elastic cross-section	±20%	±45%
$f_{\sigma^N_{TOT}}$	Secondary nucleon interactions in the target (Be) and horn (Al), total cross-section	±15%	±25%
$f_{\sigma^\pi_{INEL}}$	Secondary pion interactions in the target (Be) and horn (Al), inelastic cross-section	±10%	±20%
$f_{\sigma^\pi_{QE}}$	Secondary pion interactions in the target (Be) and horn (Al), quasi-elastic cross-section	±11.2%	±25.9%
$f_{\sigma^\pi_{TOT}}$	Secondary pion interactions in the target (Be) and horn (Al), total cross-section	±11.9%	±28.7%

Table 4: Hadronic secondary interaction flux unisim systematic uncertainties, the cross-sections are treated separately for Aluminium and Beryllium [22].

Parameter	Description	Uncertainty
$f_{SkinEffect}$	Depth that the current penetrates the horn conductor	$< 18\%$
$f_{HornCurrent}$	Current running in the horn conductor	±0.6%

Table 5: Optical, beam focusing flux unisim systematic uncertainties [24].

5.2. Neutrino-Nucleus Interactions

The method for simulating the neutrino interaction systematic parameters involves varying each parameter within their prior uncertainty using the GENIE ReWeight functionality, which will be briefly summarised in the following section. A complete description of GENIE ReWeight can be found here [26].

Parameter	Description	Uncertainty			
		ν_μ	$\bar{\nu}_\mu$	ν_e	$\bar{\nu}_e$
f_{π^+}	ν production mechanism: π^+	$\pm$11.7%	$\pm$1.0%	$\pm$10.7%	$\pm$0.03%
f_{π^-}	ν production mechanism: π^-	$\pm$0.0%	$\pm$11.6%	$\pm$0.0%	$\pm$3.0%
f_{K^+}	ν production mechanism: K^+	$\pm$0.2%	$\pm$0.1%	$\pm$2.0%	$\pm$0.1%
f_{K^-}	ν production mechanism: K^-	$\pm$0.0%	$\pm$0.4%	$\pm$0.0%	$\pm$3.0%
f_{K^0}	ν production mechanism: K^0	$\pm$0.0%	$\pm$0.3%	$\pm$2.3%	$\pm$21.4%

Table 6: Hadron production flux multisim systematic uncertainties [25].

ν_μ		$\bar{\nu}_\mu$	ν_e	$\bar{\nu}_e$
Range [GeV]	Width [GeV]	Bin edges [GeV]		
0.3-0.6	0.1	0.0	0.0	0.0
0.6-1.2	0.05	0.7	0.5	2.5
1.2-1.5	0.3	1.0	0.7	10.0
1.5-3.0	0.5	1.5	0.8	-
3.0-10.0	7.0	2.5	1.5	-
	-	10.0	2.5	-
	-	-	10.0	-

Table 7: The binning definitions in each neutrino flavour which are used in the construction of the flux multisim covariance matrix.

5.3. GENIE ReWeight

The GENIE ReWeight method begins by assigning a corresponding systematic parameter, x_P, to each physics parameter, P, with standard deviation, $\approx \delta P$. The relation between the tweaked physics parameter, P' and the nominal value with respect to this systematic parameter is given in equation 12,

$$P' = P\left(1 + x_P \cdot \frac{\delta P}{P}\right), \tag{12}$$

such that if $x_P = \pm 1$, $P' = P \pm \delta P$ and if $x_P = 0$, $P' = P$, i.e. the nominal value. The systematic parameter x_P can be associated to many different forms of physics parameters, from single variables to a complex system such as an entire MC prediction.

Interaction parameters propagated from GENIE

In the case of cross-section modelling uncertainties, the event weight, w_σ^{evt}, associated to a particular variation of a systematic parameter is calculated directly from the resulting neutrino interaction probability variation and is defined as per equation 13,

$$w_\sigma^{evt}(x_P) = \left(\frac{d^n\sigma'_\nu}{dK^n}\right) \Big/ \left(\frac{d^n\sigma_\nu}{dK^n}\right), \tag{13}$$

where $\frac{d^n\sigma'_\nu}{dK^n}$ and $\frac{d^n\sigma_\nu}{dK^n}$ are the varied and nominal n-dimensional differential cross-sections for the interaction in the n-dimensional kinematic space, K^n , respectively. The event weight, w_σ^{evt} is therefore a function of the systematic parameter, x_P.

For further details on how the event weight functionality is implemented for hadron transport parameters and other direct examples of its application, see [26].

MEC uncertainty

The MEC, or 2p-2h, interaction mode was only added as a permanent component of neutrino event generation in the last decade or so. In addition to the relative novelty of the model, the physics system it encapsulates is incredibly complex. Consequently, the corresponding systematic uncertainty associated to it is less understood than that of the other processes making up the total neutrino interaction cross-section.

Consequently, a well-validated systematic parameter has not yet been propagated from the GENIE event generator for use in the SBN oscillation analysis. Instead, an arbitrary 100% normalisation uncertainty is applied across all energies to account for the missing parameter. The uncertainty is defined to be maximal to encompass the complexity of the 2p-2h process.

Intranuclear hadron transport parameters

Intranuclear re-interactions occur frequently and cause the composition and kinematics of the observed final state to differ from the initial neutrino interaction. They are therefore a major source of systematic uncertainty in any neutrino-nuclear interaction measurement. This section will provide a high level summary of the intranuclear hadron transport model and reweighting scheme, a much more thorough explanation can be found here [26].

The events simulated in the SBN oscillation analysis utilise the internal GENIE INTRANUKE/hA model to propagate neutrino interaction products through the nucleus. This serves as an alternative to a full cascade model, which are much more complex and subsequently don't lend themselves to a reweighting scheme. The GENIE INTRANUKE/hA model instead utilises the total cross-section of each nuclear process for pions and nucleons as a function of energy and is data-driven. The model takes into consideration the fact that hadrons produced in the neutrino interaction will not re-interact with their full cross-section, which is determined from the mean free path, and allows for pion (not nucleon) absorption and production.

The intranuclear systematic uncertainties fall into two categories:

- Uncertainties associated with the total rescattering probability of hadrons produced in the neutrino interaction
- Uncertainties associated with the relative probability of each rescattering mechanism, once the hadron has been determined to reinteract

which are further separated for nucleons and pions.

Variations due to the rescattering probability depend on the mean free path, λ^h, of the hadron, h, and this parameter is modified in the reweighting scheme according to equation 14,

$$\lambda^h \rightarrow \lambda^{h'} = \lambda^h \left(1 + x^h_{mfp} \cdot \frac{\delta\lambda^h}{\lambda^h}\right), \tag{14}$$

where $\lambda^{h'}$ is the modified mean free path, $\delta\lambda^h$ is it's corresponding uncertainty and x^h_{mfp} is the systematic parameter associated to it.

The weight associated to variations of the re-scattering probability, w^h_{mfp}, depends on the nominal and tweaked survival probabilities of each hadron, P^h_{surv} & $P^{h'}_{surv}$,

$$P^{h^{(\prime)}}_{surv} = \int \exp\left(\frac{-r}{\lambda^{h^{(\prime)}}}\right) dr, \tag{15}$$

each of which is a function of the corresponding mean free path, $\lambda^{h^{(\prime)}}$, along the hadron's trajectory, r,

$$w^h_{mfp} = \begin{cases} \dfrac{1 - P^{h'}_{surv}}{1 - P^h_{surv}}, & h \text{ re-interacts} \\ \\ \dfrac{P^{h'}_{surv}}{P^h_{surv}}, & h \text{ escapes.} \end{cases} \tag{16}$$

Having determined that a hadron will re-interact, the mode by which this occurs must be defined, m. The mode corresponds to one of the following eventualities,

- Elastic scatter
- Inelastic scatter
- Charge exchange
- Absorption[2]
- Pion production

and the probability of each mode occurring, P_m^h, is calculated using hadron-nucleus cross-section data,

$$P_m^h = \frac{\sigma_m^{hA}}{\sigma_{total}^{hA}}, \tag{17}$$

where σ_m^{hA} is the hadron-nucleon (hA) cross-section for the re-scattering mode, m, and σ_{total}^{hA} is the total hadron-nucleon cross-section. The distribution of such probabilities for re-scattered pions, π, and nucleons, N, is shown as a function of the kinetic energy in Figure 5.

The determination of the weight associated with the re-scattering mode of the hadron follows the same re-weighting procedure as in the cross-section and mean-free-path cases. First, the cross-section associated to each re-scattering mode is tweaked,

$$\sigma_m^{hA} \rightarrow \sigma_m^{hA\prime} = \sigma_m^{hA} \left(1 + x_m^h \cdot \frac{\delta\sigma_m^{hA}}{\sigma_m^{hA}}, \right) \tag{18}$$

where once again, $\sigma_m^{hA\prime}$ is the tweaked cross-section, $\delta\sigma_m^{hA}$ is the associated uncertainty and x_m^h is the systematic parameter used to represent the tweak. Finally, the weight is defined,

$$w_m^h = \sum_m \delta_{m;m'} \cdot x_m^h \cdot \frac{\delta\sigma_m^{hA}}{\sigma_m^{hA}}, \tag{19}$$

[2]Refers to the emission of 2 or more nucleons with no pions in the final state. This can refer to either the absorption of a pion or, if no pion was ever produced, simply multi-nucleon knockout.

where m corresponds to the list of possible re-scattering modes and m' is the actual mode by which the hadron scattered.

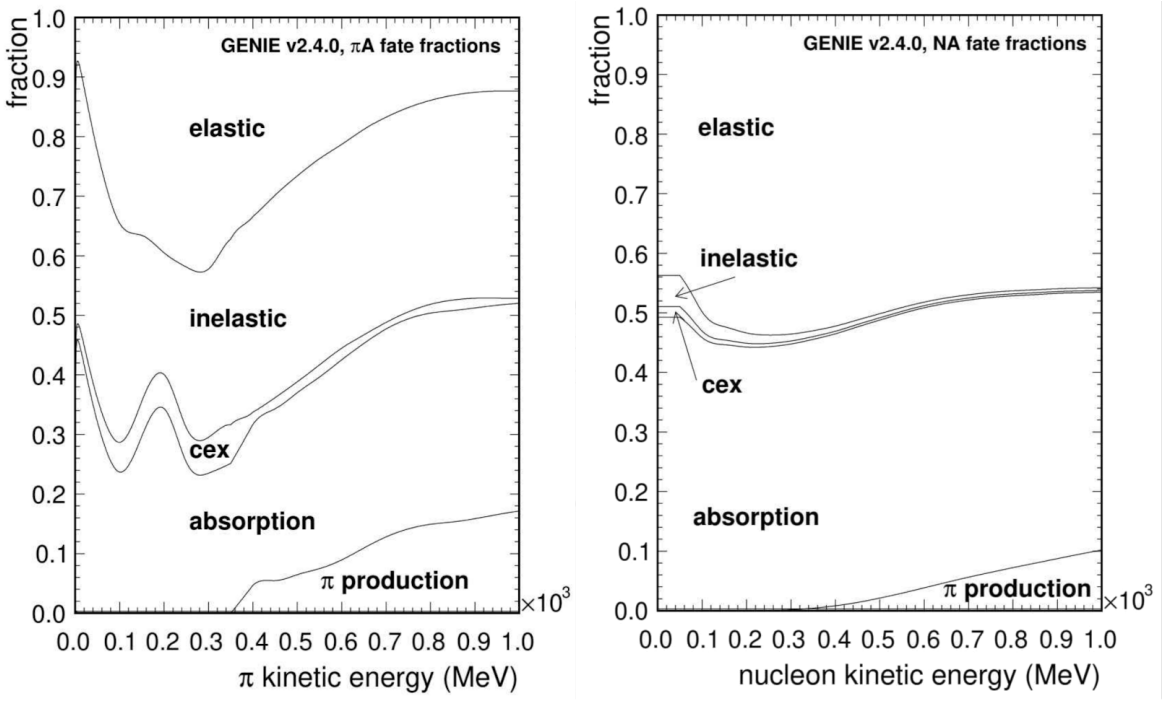

Figure 5: Relative intranuclear re-scattering rates defined in GENIE. On the left is the pion case and on the right is the nucleon case. The sum of all integrated modes for each case should always be 1 [26].

Finally, the total weight applied to a single hadron based on it's probability of interacting combined with, if relevant, the mode by which it is determined to interact is simply,

$$w^h = w^h_{mfp} \cdot w^h_m, \tag{20}$$

and this is propagated to the event-level from the single-particle level in the following product,

$$w^{evt}_{HT} = \prod_j w^h_j, \tag{21}$$

where j corresponds to all primary hadrons in the event. As is this case for the entire interaction systematic section, more information can be found here [26].

All interaction systematic uncertainties considered in the SBN oscillation analyses concern the GENIE stage of the simulation. There are currently no uncertainties implemented for the subsequent interactions of final state particles as they are propagated by GEANT4 through the liquid argon, following their emission from the argon nucleus. A complete list of the interaction parameters considered in the SBN oscillation analyses along with the prior uncertainties used in the construction of the universe variations are given in Tables 8, 9 and 10.

Parameter	Description	$\delta P/P$
$f_{M_A^{CCQE}}$	Axial mass for CC quasi-elastic	-15% +25%
$f_{M_A^{CCRes}}$	Axial mass for CC resonance neutrino production	±20%
$f_{M_A^{NCRes}}$	Axial mass for NC resonance neutrino production	±20%
f_{NC}	Additional error on NC/CC ratio	±25%
$f_{nR_{\nu n}^{CC1\pi}}$	Non-resonance bkg normalisation in νn CC1π reactions	±50%
$f_{nR_{\nu p}^{CC1\pi}}$	Non-resonance bkg normalisation in νp CC1π reactions	±50%
$f_{nR_{\nu n}^{CC2\pi}}$	Non-resonance bkg normalisation in νn CC2π reactions	±50%
$f_{nR_{\nu p}^{CC2\pi}}$	Non-resonance bkg normalisation in νp CC2π reactions	±50%
$f_{nR_{\bar{\nu} n}^{CC1\pi}}$	Non-resonance bkg normalisation in $\bar{\nu} n$ CC1π reactions	±50%
$f_{nR_{\bar{\nu} p}^{CC1\pi}}$	Non-resonance bkg normalisation in $\bar{\nu} p$ CC1π reactions	±50%
$f_{nR_{\bar{\nu} n}^{CC2\pi}}$	Non-resonance bkg normalisation in $\bar{\nu} n$ CC2π reactions	±50%
$f_{nR_{\bar{\nu} p}^{CC2\pi}}$	Non-resonance bkg normalisation in $\bar{\nu} p$ CC2π reactions	±50%
$f_{nR_{\nu n}^{NC1\pi}}$	Non-resonance bkg normalisation in νn NC1π reactions	±50%
$f_{nR_{\nu p}^{NC1\pi}}$	Non-resonance bkg normalisation in νp NC1π reactions	±50%
$f_{nR_{\nu n}^{NC2\pi}}$	Non-resonance bkg normalisation in νn NC2π reactions	±50%
$f_{nR_{\nu p}^{NC2\pi}}$	Non-resonance bkg normalisation in νp NC2π reactions	±50%
$f_{nR_{\bar{\nu} n}^{NC1\pi}}$	Non-resonance bkg normalisation in $\bar{\nu} n$ NC1π reactions	±50%
$f_{nR_{\bar{\nu} p}^{NC1\pi}}$	Non-resonance bkg normalisation in $\bar{\nu} p$ NC1π reactions	±50%
$f_{nR_{\bar{\nu} n}^{NC2\pi}}$	Non-resonance bkg normalisation in $\bar{\nu} n$ NC2π reactions	±50%
$f_{nR_{\bar{\nu} p}^{NC2\pi}}$	Non-resonance bkg normalisation in $\bar{\nu} p$ NC2π reactions	±50%

Table 8: SBN proposal-era neutrino interaction cross-section systematic parameters considered in GENIE [26].

Parameter	Description	$\delta P/P$
$f_{M_A^{NCEl}}$	Axial mass for NC elastic	±25%
$f_{\eta^{NCEl}}$	Strange axial form factor for NC elastic	±30%
f_{2p2h}	Normalisation uncertainty for 2p2h interactions	±100%
$f_{M_V^{CCRes}}$	Vector mass for CC resonance neutrino production	±10%
$f_{M_V^{NCRes}}$	Vector mass for NC resonance neutrino production	±10%
$f_{A_{HT}}$	Higher-twist parameter A for NC and CC DIS events	±25%
$f_{B_{HT}}$	Higher-twist parameter B for NC and CC DIS events	±25%
$f_{C_{v1u}}$	Valence p.d.f. correction factor C_{v1u} for DIS events	±30%
$f_{C_{v2u}}$	Valence p.d.f. correction factor C_{v2u} for DIS events	±40%
$f_{M_A^{Coh}}$	Axial mass for NC and CC coherent pion production	±50%
$f_{R_0^{Coh}}$	Nuclear size parameter controlling π absorption	±20%
$f_{\Delta\to N\gamma}$	Branching ratio for Δ radiative decay	±50%

Table 9: The additional neutrino interaction cross-section systematic parameters considered in GENIE [26] with respect to those available in the SBN proposal analysis. Note the 2p2h parameter is not propagated from the event generator.

Parameter	Description	$\delta P/P$
f_{λ_π}	Intranuclear mean free path for pions	±20%
$f_{R_\pi^{CEx}}$	Intranuclear charge exchange rescattering fraction for pions	±50%
$f_{R_\pi^{Inel}}$	Intranuclear inelastic rescattering fraction for pions	±40%
$f_{R_\pi^{\pi}}$	Intranuclear pion-production rescattering fraction for pions	±20%
$f_{R_\pi^{Abs}}$	Intranuclear absorption fraction for pions	±20%
f_{λ_N}	Intranuclear mean free path for nucleons	±20%
$f_{R_N^{CEx}}$	Intranuclear charge exchange rescattering fraction for nucleons	±50%
$f_{R_N^{Inel}}$	Intranuclear inelastic rescattering fraction for nucleons	±40%
$f_{R_N^{\pi}}$	Intranuclear pion-production rescattering fraction for nucleons	±20%
$f_{R_N^{Abs}}$	Intranuclear absorption fraction for nucleons	±20%

Table 10: Intranuclear hadron transport (FSI) systematic parameters [26].

6. Oscillation Fitting Frameworks

The SBN oscillation analysis paradigm outlined in Sec. 2 was implemented in three independent fitting frameworks: CAFAna (Sec. 6.2), SBNFit (Sec. 6.3) and VALOR (Sec. 6.4). The same MC generated event samples, event selections and systematic error inputs were used in all fitting frameworks. However, the three different frameworks treat systematic inputs slightly differently, and make use of different approximations, as described in the following subsections. As such they provide interesting insights on the impact of these approximations and systematics treatment on the SBN oscillation sensitivity.

6.1. Common analysis choices

In addition to the input central values being identical, the following fitting choices are common to all three fitting frameworks.

The ν_μ binning (edge-to-edge) has 19 bins in reconstructed neutrino energy, defined as xxxx, which are bounded as follows:

- 2 0.1-GeV bins from 0.2-0.4 GeV,
- 12 0.05-GeV bins from 0.4-1.0 GeV,
- 2 0.25-GeV bins from 1.0-1.5 GeV and
- 3 0.5-GeV bins from 1.5-3 GeV.

The ν_e binning (edge-to-edge) has 11 bins in reconstructed neutrino energy, defined as xxxx, which are bounded as follows:

- 6 0.15-GeV bins from 0.2-1.1 GeV,
- 2 0.2-GeV bins from 1.1-1.5 GeV,
- 2 0.25-GeV bins from 1.5-2.0 GeV and
- 1 bin from 2.0-3.0 GeV.

The input spectra are provided in Fig. 16 for the ν_μ analyses.

6.2. CAFAna

in progress, adapting text from DUNE CDR

The CAFAna framework was developed for the NOvA experiment and has been used for ν_μ-disappearance, ν_e-appearance, and joint fits, plus sterile neutrino searches and cross-section analyses. CAFAna has now been adapted for use in the DUNE and SBN sensitivity analyses and upcoming NOvA/T2K joint fit.

In the sensitivity studies, the compatibility of a particular oscillation hypothesis with the data is evaluated using the likelihood appropriate for Poisson-distributed data [27]:

$$\chi^2 = -2\log\mathcal{L} = 2\sum_{i}^{N_{\text{bins}}}\left[M_i - D_i + D_i\ln\left(\frac{D_i}{M_i}\right)\right] \tag{22}$$

where M_i is the Monte Carlo expectation in bin i and D_i is the observed count. For these studies the bins here represent reconstructed neutrino energy, but other observables, such as reconstructed kinematic variables or event classification likelihoods may also be used. Multiple samples with different selections can be fit simultaneously, as can multi-dimensional distributions of reconstructed variables.

Event records representing the reconstructed properties of neutrino interactions and, in the case of Monte Carlo, the true neutrino properties are processed to fill the required histograms. Oscillated predictions are created by populating 2D histograms, with the second axis being the true distance travelled divided by neutrino energy, for each oscillation channel ($\nu_\alpha \to \nu_\beta$). These are then reweighted as a function of the true energy axis according to an exact calculation of the oscillation weight at the bin center and summed to yield the total oscillated prediction:

$$M_i = \sum_{\alpha}^{e,\mu}\sum_{\beta}^{e,\mu,\tau}\sum_{j} P_{\alpha\beta}(E_j)M_{ij}^{\alpha\beta} \tag{23}$$

where $P_{\alpha\beta}(E)$ is the probability for a neutrino created in flavor state α to be found in flavor state β at the desired baseline. $M_{ij}^{\alpha\beta}$ represents the number of selected events in bin i of the reconstructed variable with true L_j/E_j, taken from a simulation where neutrinos of flavor α from the beam have been replaced by equivalent neutrinos in flavor β. Various oscillation calculations are available, *e.g.* three-flavor oscillations with matter effects or full four-flavor

sterile oscillations. For this study oscillation probabilities are calculated in the 3+1 sterile neutrino model using a two-flavor approximation. The oscillation probabilities for beam ν_μ are

$$P(\nu_\mu \to \nu_\mu) = 1 - \sin^2 2\theta_{\mu\mu} \sin^2 \left(\frac{1.267 \Delta m^2 L}{E} \right) \quad (24)$$

$$P(\nu_\mu \to \nu_e) = \sin^2 2\theta_{\mu e} \sin^2 \left(\frac{1.267 \Delta m^2 L}{E} \right) \quad (25)$$

$$P(\nu_\mu \to \nu_s) = \left(\sin^2 2\theta_{\mu\mu} - \sin^2 2\theta_{\mu e} \right) \sin^2 \left(\frac{1.267 \Delta m^2 L}{E} \right) \quad (26)$$

with similar expressions for the oscillations of intrinsic beam ν_e. In order to treat the rapid-oscillation regime, the oscillation probability is averaged analytically over the true energy bin.

Systematic uncertainties are included to account for the expected uncertainties in the beam flux, neutrino interaction, and detector response models used in the simulation at the time of the analysis. The impact of systematic uncertainties is included by adding additional nuisance parameters into the fit. Each of these parameters can have arbitrary effects on the Monte Carlo prediction, and can affect the various samples and channels within each sample in different ways. These parameters are profiled over in the production of the result. The range of these parameters is controlled by the use of Gaussian penalty terms to reflect our prior knowledge of reasonable variations.

For each systematic parameter under consideration, the matrices $M_{ij}^{\alpha\beta}$ are evaluated for a range of values of the parameter, by default $\pm 1, 2, 3\sigma$. The predicted spectrum at any combination of systematic parameters can then be found by interpolation. Cubic interpolation is used, which guarantees continuous and twice-differentiable results, advantageous for gradient-based fitters such as MINUIT. The SBN analysis files treat systematic uncertainties with a "multiverse" approach. For each randomly thrown systematic universe the value taken by each systematic parameter, and the corresponding factor in the overall event weight are stored. This allows CAFAna to identify universes where a specific parameter takes desired values, and isolate the effect of that single parameter in order to fill the required matrices. CAFAna also has the capability to treat systematic uncertainties by directly adjusting the event record; for example, an energy scale uncertainy would change

the reconstructed energy. When these systematics are applied, all downstream calculations and selections will be based on the shifted value, so that the full effect on the analysis is included.

6.2.1. Assumptions and Details

The true baseline and true neutrino energy, taken from the Monte Carlo event record, is used to calculate the oscillation probability for the Monte Carlo prediction. [Include details of how we oscillate based on true interaction type here]

Systematic uncertainties: At least three types of uncertainty to describe (though some of this is done above): systematics with weights in the event record, systematics where we use PCA and take first x components, systematics where we adjust the event record (though none of these are included in the final analysis because we haven't cross-validated the detector systs yet. Show a plot of our detector systs in this section?

Joint fits - brief description here - again, not part of the results shown in this technote.

6.3. SBNFit

6.3.1. Introduction

In Progress The SBNfit framework is a spiritual successor to the covariance matrix-based fitting approach that has been followed in MiniBooNE, and was originally developed for an independent phenomenological study of SBN's ability to resolve 3+N oscillations and leptonic CP violation associated with a sterile neutrino sector [28]. It has since been generalized, extended and adopted by the MicroBooNE collaboration as its primary fitting tool, e.g. for its recent searches for an anomalous low-energy excess [29, 30, 31, 32, 33].

The SBNfit framework [**?**] offers the capability of performing fits to 3+N sterile neutrino oscillations with an arbitrary number of detectors (baselines) and final state selected samples (e.g. ν_e CC, ν_μ CC, or NC selections). This is possible through a simultaneous, side-by-side fit of multiple event spectra by way of a full covariance matrix that contains the full statistical and systematic uncertainties as well as systematic correlations among the different samples (and across different baselines).

The test statistic, as utilized by SBNfit for the sensitivity studies presented in this note, is a χ^2 calculated over the concatenated ν_e CC inclusive and/or ν_μ CC inclusive selected

spectra for each of the three detectors (SBND, MicroBooNE, and ICARUS), defined as

$$\chi^2(\Delta m^2_{i1}, U_{\alpha i}) = \sum_{k=1}^{M}\sum_{l=1}^{M}\left[D_k - P^{\rm osc}_k(\Delta m^2_{i1}, U_{\alpha i})\right] E^{-1}_{kl}\left[D_l - P^{\rm osc}_l(\Delta m^2_{i1}, U_{\alpha i})\right] \ , \qquad (27)$$

where D_k is the number of observed or hypothetical data events in the $k^{\rm th}$ bin of reconstructed neutrino energy; $P^{\rm osc}_k(\Delta m^2_{i1}, U_{\alpha i})$ is the number of signal and background events predicted to be observed in reconstructed neutrino energy bin k under an oscillation hypothesis described by the set of parameter values $(\Delta m^2_{i1}, U_{\alpha i})$; and E_{kl} is a full $M \times M$ covariance matrix containing the total systematic and statistical uncertainty squared, including systematic correlations between any two bins k and l, corresponding to $P^{\rm osc}_k(\Delta m^2_{i1}, U_{\alpha i})$. (Details of the covariance matrix construction are provided below). Alternate χ^2 statistics are possible; for example, the Combined Neyman-Pearson χ^2 (χ^2_{CNP}) definition of [34] can be used, which has been shown to yield less biased results specifically for a covariance matrix based approach, and has been used for that reason in [29, 30, 31, 32, 33]. This metric is defined as above, but with a modified covariance matrix

$$E^{CNP}_{kl} = E^{syst}_{kl} + \frac{3}{1/D_k + 2/P_k}\delta_{kl} \ , \qquad (28)$$

where the second term in the above equation replaces the statistical uncertainty in E_{kl} (nominally, $P^{\rm osc}_k\delta_{kl}$) with the CNP statistical uncertainty metric.

6.3.2. Construction of Predicted Oscillated Spectra

For assessing SBN's sensitivity to either $\nu_\mu \to \nu_e$ appearance or ν_e disappearance, we fit exclusively to the ν_e CC selected spectra at each detector. When assessing sensitivity to ν_μ disappearance, we fit exclusively to the ν_μ CC selected spectra at each detector. In principle, improved sensitivity could be obtained by fitting both ν_e CC and ν_μ CC spectra simultaneously, regardless of oscillation channel being probed, further utilizing correlations between the two samples to cancel systematic uncertainties.

In general, for any given 3+N model, both appearance and disappearance effects are expected to occur simultaneously. In the case of the ν_e disappearance search presented in this note, we consider only the disappearance of true ν_e (and $\bar{\nu}_e$) events in the selected ν_e CC spectra; disappearance of ν_μ background is assumed to be negligible, and ignored, as is $\nu_\mu \to \nu_e$ appearance. In that respect, the search is equivalent to a 3+1 search with $U_{\mu 4} = 0$. Similarly, we ignore ν_e background disappearance in the case of the ν_μ disappear-

ance search (equivalent to a 3+1 search with $U_{e4} = 0$). In the case of $\nu_\mu \to \nu_e$ search, we consider only $\nu_\mu \to \nu_e$ oscillations, and assume that disappearance of background ν_e and ν_μ events is negligible.This is illustrated in Fig. 6. We note that this approach is taken only for the purposes of allowing comparisons of sensitivity to that of other fitters; one of the advantages of SBNfit is the ability to perform these searches by fully accounting for all oscillation channels simultaneously (see, e.g. [28]).

When working with vacuum oscillation probabilities, or in the short-baseline approximation, where matter effects can safely be ignored, all neutrino appearance and disappearance oscillation probabilities for any arbitrary number of additional sterile neutrinos can be re-written in the following representative form:

$$P^{3+N}_{\nu_\alpha \to \nu_\beta}(E_\nu, L_{\rm osc}, \Delta m^2_{i1}, U_{\alpha i}) = \sum A(U_{\alpha i}) \sin^2\left(\frac{\Delta m^2_{i1} L_{\rm osc}}{4E_\nu}\right) + \sum B(U_{\alpha i}) \sin\left(\frac{\Delta m^2_{i1} L_{\rm osc}}{2E_\nu}\right), \tag{29}$$

i.e., as a sum of sin and $\sin^2$ frequencies, which are functions of energy and baseline, scaled by amplitudes (A, B) which are functions of the mixing elements of an expanded $(3 + N) \times (3 + N)$ mixing matrix. SBNfit takes advantage of this simplification to pre-calculate the individual sin and $\sin^2$ frequency spectra for any given mass-splittings ahead of a (Δm^2_{i1},$U_{\alpha i}$)-grid-based search; then, at during fitting, any complete oscillated spectra can be found by merely scaling the tabulated oscillation frequency spectra (frequency templates) by the appropriate amplitudes and adding them together. As the frequency templates are constructed directly from oscillating the MC prediction on an event-by-event basis, the true true energy and true baseline of each event is explicitly used to evaluate the oscillation probability, with no approximation or binning in true energy/baseline needed. Note that, even though one can always rewrite the oscillation probabilities in this form, even in the case of arbitrary matter potentials, for non-zero matter potentials the amplitudes become a function of Δm^2 and $L_{\rm osc}$, and thus this approach no longer offers a computational advantage. We also note that summing up the scaled, pre-calculated oscillation frequency spectra doesn't allow accurate estimation of the Monte Carlo intrinsic error, and results shown in this technote do not have Monte Carlo intrisinc error included.

6.3.3. Construction of Covariance Matrix

All bin-by-bin statistical and systematic uncertainties and bin-to-bin systematic uncertainty correlations are accounted for during the fit via the combined covariance matrix E_{ij}. At

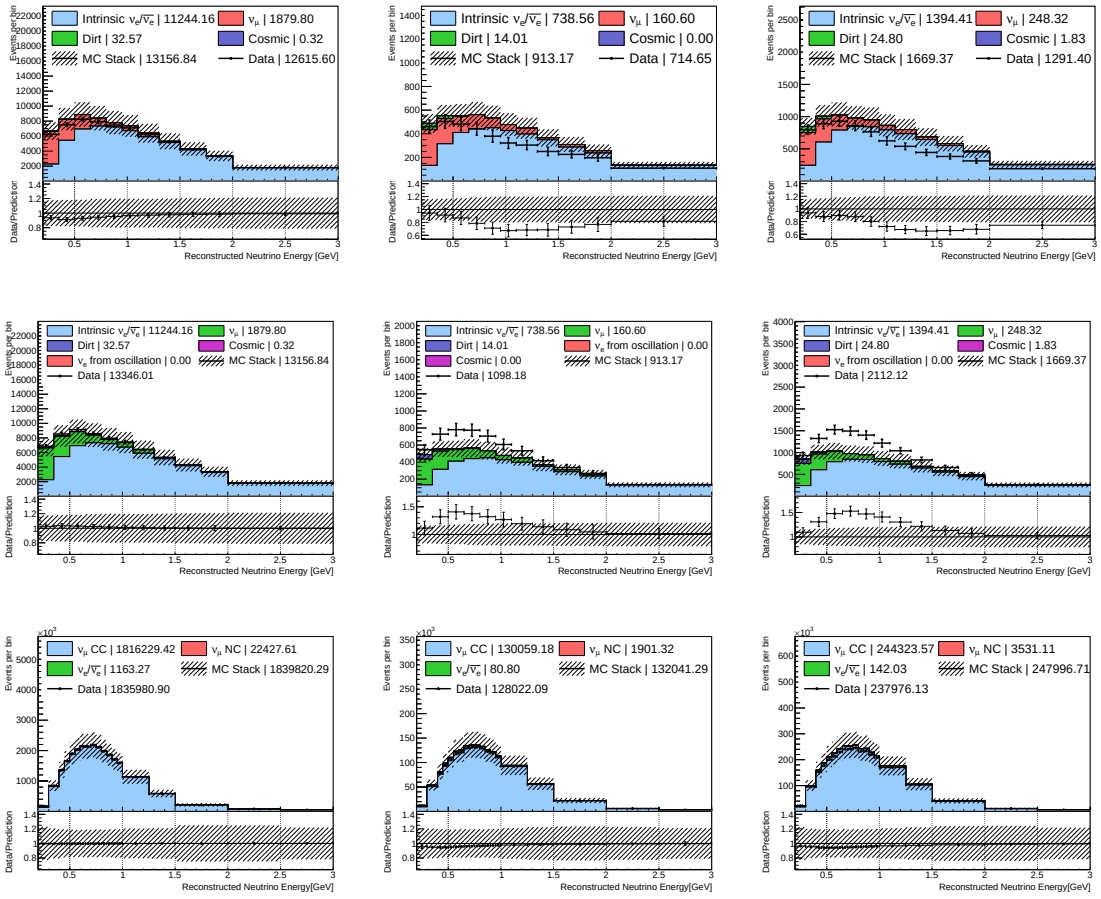

Figure 6: Top: Side-by-side ν_e CC selected spectra predicted at SBND, MicroBooNE, and ICARUS, illustrating the true $\nu_e(\bar{\nu}_e)$ and non-true-$\nu_e(\bar{\nu}_e)$ oscillation assumptions in the ν_e disappearance search at point $\Delta m^2 = 3$ eV^2, $U_{e4} = 0.4$. Middle: Side-by-side ν_e CC selected spectra predicted at SBND, MicroBooNE, and ICARUS, illustrating the signal and background true $\nu_e(\bar{\nu}_e)$ and non-true-$\nu_e(\bar{\nu}_e)$ oscillation assumptions in the $\nu_\mu \rightarrow \nu_e$ appearance search at point $\Delta m^2 = 1.32$ eV^2, $U_{e4} = 0.003$. Bottom: Side-by-side ν_μ CC selected spectra predicted at SBND, MicroBooNE, and ICARUS, illustrating the true $\nu_\mu(\bar{\nu}_\mu)$ and non-true-$\nu_\mu(\bar{\nu}_\mu)$ oscillation assumptions in the ν_μ disappearance search at point $\Delta m^2 = 1.32$ eV^2, $U_{\mu 4} = 0.07$. The histogram labeled as "Data" and drawn in data style is not real data, instead it's MC predictions at respective oscillation points.

the moment, no detector systematic is taken into account for sensitivity evaluation. Of the systematic uncertainties used, flux and interaction cross-section uncertainties are estimated via reweighting the Monte Carlo central value prediction (CV). The reweighting of the CV for flux and cross-section systematics is stored in the eventweight class. This eventweight class in SBNcode is defined as a `std::map<std::string,std::vector<float>>`, and SBNfit utilizes the same structure for maximum compatibility and convenience. The strings are a unique tag that defines the variation, e.g. GENIE CCQE MA, or a given Sandford-Wang flux variation, and the `vector<float>` is the series of N weights, were N is the number of universes that have been thrown for this variation. For each source of flux or cross-section variation (v), defined in this way, we can construct an independent covariance matrix E^v from looping over the total number of universes in this variation (N^v):

$$E^v_{i,j} = \frac{1}{N^v}\sum_{k=1}^{N^v}(P_i^{\mathrm{CV}} - P_i^k) * (P_j^{\mathrm{CV}} - P_j^k) \ , \tag{30}$$

where P_i^{CV} is central value prediction for bin i, and P_i^k is the prediction of k universe for bin i. The total flux and cross-section systematic covariance matrix is then the linear sum of all individual flux and cross-section covariance matrices:

$$E^{\mathrm{tot}}_{i,j} = \sum_{\mathrm{flux}} E^v_{i,j} + \sum_{\mathrm{interaction}} E^v_{i,j} \tag{31}$$

Note that the number of universes that each variation is associated with, N^v, do not have to be the same, and variations which are expected to yield more dominant systematic uncertainties generally make use of more universes (larger N) to ensure good coverage.

The total covariance matrix is computed by breaking down the selected spectra into each of its respective contributing signal or background category, and scaling corresponding uncertainties according to the size of that contributing subcomponent, after oscillations. For example, in the $\nu_\mu \to \nu_e$ appearance search, CC ν_e inclusive selected events have components coming from intrinsic ν_e backgrounds, mis-identified ν_μ backgrounds, and oscillated $\nu_\mu \to \nu_e$ events, each with different contributing systematic uncertainties. This breakdown requires input covariance matrices which are significantly larger than the final covariance matrix used in the fit (generally, for n subcategories, an $M \times M$ covariance matrix requires an $nM \times nM$ input covariance matrix). Having the full covariance matrix with each subcategory split out allows for correct treatment of uncertainties and correlations, since the relative contribution of different subcategories changes as a function of oscillation pa-

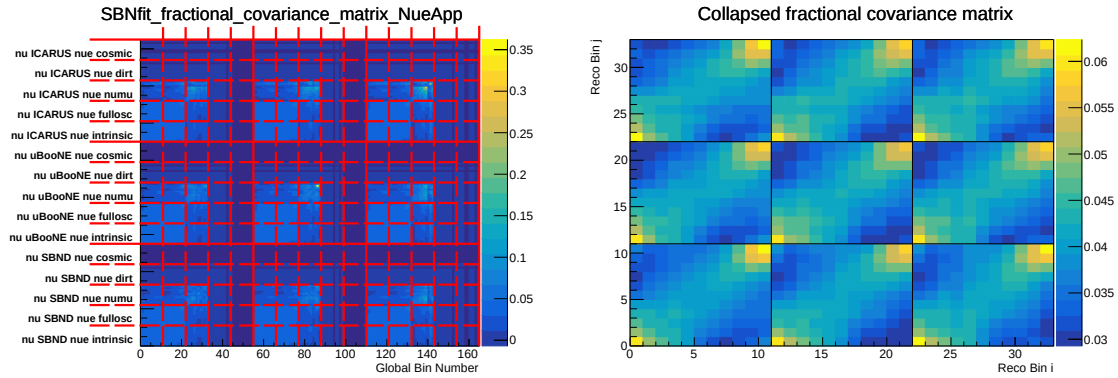

Figure 7: Collapse of ν_e CC inclusive selection covariance matrix in the case of $\nu_\mu \rightarrow \nu_e$ appearance search: (left) fractional covariance matrix, (right) collapsed fractional covariance matrix. Each detector's selection, corresponding to 165 bins, includes contributions from intrinsic ν_e backgrounds, mis-identified ν_μ backgrounds, mis-identified dirt and cosmic background, and oscillated $\nu_\mu \rightarrow \nu_e$ events (fullosc). After scaling each contribution according to the appropriate oscillation probability for any given grid point, the subcomponent blocks are added together to obtain the collapsed covariance matrix used in the fit.

rameters. To go from the broken down full covariance to the reduced one used in the fit, we collapse by superimposing each sub-component block together into a single block, as illustrated in Fig. 7.

6.3.4. Sensitivity Evaluation Assumptions with SBNfit

The SBNfit fitting framework uses pre-calculated oscillation spectra in the form of oscillation frequency histogram templates for any given Δm^2_{i1}. As such, it makes use of the true baseline and true energy information available in the Monte Carlo on an event-by-event basis. The baseline information is available via the SBNreco TTree's variable "truth.neutrino.baseline" and "truth.neutrino.energy". The "modern" MonteCarlo data sets properly simulate and account for the exact SBND location under the "truth.neutrino.baseline" variable.[3] There is also an additional event-by-event "reco.weight" applied per event, which is used to normalize event rates. The oscillation or survival probability evaluated for each event, according to its true baseline and true energy, is used to multiply each event's "reco.weight", thus accounting

[3]For the "proposal" datasets, however, an incorrect location for SBND was simulated, and although a 10 m correction shift in the SBND location was taken into account for the overall flux normalization within the SBNreco input files, the baseline was not changed in the truth.neutrino.baseline variable. To correct this, a manual 10 m shift was included when calculating the frequency templates for SBNfit. This is not an issue in the case of the "modern" samples, since those properly simulate the SBND location

for oscillation effects.

The systematic uncertainty included in the sensitivity evaluations are fourty-eight (48) independent sources of systematic uncertainties. Of these, thirteen (13) are flux uncertainties:

`expskin_FluxUnisim`, `horncurrent_FluxUnisim`, `kminus_PrimaryHadronNormalization`, `kplus_PrimaryHadronFeynmanScaling`, `kzero_PrimaryHadronSanfordWang`, `nucleoninexsec_FluxUnisim`, `nucleonqexsec_FluxUnisim`, `nucleontotxsec_FluxUnisim`, `piminus_PrimaryHadronSWCentralSplineVariation`, `pioninexsec_FluxUnisim`, `pionqexsec_FluxUnisim`, `piontotxsec_FluxUnisim`, `piplus_PrimaryHadronSWCentralSplineVariation`

Thirty-three (33) are cross-section uncertainties:

`DISAth`, `DISBth`, `DISCv1u`, `DISCv2u`, `IntraNukeNabs`, `IntraNukeNcex`, `IntraNukeNinel`, `IntraNukeNmfp`, `IntraNukeNpi`, `IntraNukePIabs`, `IntraNukePIcex`, `IntraNukePIinel`, `IntraNukePImfp`, `IntraNukePIpi`, `NC`, `NonResRvbarp1piAlt`, `NonResRvbarp1pi`, `NonResRvbarp2piAlt`, `NonResRvbarp2pi`, `NonResRvp1piAlt`, `NonResRvp1pi`, `NonResRvp2piAlt`, `NonResRvp2pi`, `ResDecayGamma`, `ccresAxial`, `ccresVector`, `cohMA`, `cohR0`, `ncelAxial`, `ncelEta`, `ncresAxial`, `ncresVector`, `qema`

The extra two (2) systematic uncertainties are an extra 100% normalisation uncertainty for MEC events and an extra 2% POT accounting uncertainty (fully correlated). Tables 11 and 12 shows the size of overall normalization uncertainty of each systematic variation on the ν_e and ν_μ central value predictions (no oscillation effects) respectively at each detector.

It is worth noting that in particular, `piplus_PrimaryHadronSWCentralSplineVariation`, is known to have a large effect in the low Δm^2 sensitivity region.

We note that for comparative purposes to the other fitting groups, the intrinsic statistical uncertainty of the generated MonteCarlo samples is being ignored currently. The effect of low MC statistics can be important for sparse regions of phase space and should be included for the final sensitivity calculations in the future.

6.3.5. Beyond Initial Sensitivity Evaluations

One of the key advantages of SBNfit is that it facilitates expansion of the fits to multiple selected samples that can be fit simultaneously, as well as simultaneous appearance and

disappearances searches. In doing so, even for the simplest, 3+1 oscillation scenario, and under the two-neutrino approximation, one must still scan over a 3-dimensional parameter space: Δm^2, U_{e4}, and $U_{\mu 4}$. In the case of simultaneous fits to NC event rates, one may further probe sensitivity to U_{s4} (or, equivalently, $U_{\tau 4}$, elevating the grid dimension from 3 to 4. This creates additional requirements for computational resources, especially for applying frequentist corrections to the fit—a procedure which can be rather computationally expensive even in a 2-dimensional grid search. To enable multi-dimensional Feldman-Cousins correlctions, SBNfit has been recently adapted [35], making use of vectorization through Eigen3 [36], to yield significant execution speed-up and allow for further parallelization for High-Performance Computing (HPC) sites. Through these improvements, a single-core speed-up of a factor of 350 compared to the original implementation was achieved, which can also leverage HPC parallelization.

6.4. VALOR

6.4.1. Introduction

VALOR[4] is a modern oscillation analysis framework, that was first established within the T2K experiment in 2010 and named after its initial participants (VALencia-Oxford-Rutherford), a name that was maintained although the group has since expanded substantially. Since 2010, the VALOR group performed around 20 iterations of T2K electron-(anti)neutrino appearance, muon-(anti)neutrino disappearance, and joint 3-flavour analyses and it contributed to nearly all published T2K oscillation results. 2019 saw the completion of a large-scale code refactoring, painstakingly carving a generic, CPU efficient and highly flexible oscillation analysis *framework*, the VALOR Software Development Kit (VALOR SDK), out of a leading 3-flavour oscillation analysis. The development of the VALOR SDK has streamlined use of VALOR in several experimental setups without the need to maintain multiple separate forks: Currently several oscillation analyses across several experiments are built as a thin layer of experiment-specific definitions and data inputs on top of that common VALOR SDK. A VALOR adaptation for the SBN, implementing at first the same analysis paradigm as the one used for the SBN proposal, was completed in 2019. The following subsections give a brief overview of VALOR SDK, and of the tools used to construct the SBN physics parameterization (as encapsulated in the fit likelihood), and to interpret the SBN data.

[4] https://valor.pp.rl.ac.uk

6.4.2. Construction of neutrino event rate predictions

The main inputs to the oscillation sensitivity calculation are the predicted (Monte Carlo) neutrino interaction event rates, which may be parametrised in many ways. For instance, the predictions can be defined for any combination of,

- Beam configurations, b
- Detectors, d
- Observed final state topologies, s,

in terms of the desired observable kinematic parameters in a reconstructed parameter bin, r. The Monte Carlo prediction will be constructed with both true and reconstructed quantities, as an $(N_R \times N_T)$ matrix, where N_R is the total number of reconstructed bins and N_T is the total number of true bins in the parameter space.

For instance, one may choose to construct the prediction in the SBND detector, using the FHC BNB configuration, for the CC 0π final state topology in terms of the reconstructed neutrino energy, E_r. These dependencies are summarised for the event rate predictions in Monte Carlo Templates (MCT's),

$$T = T_{b;d;s;m}(r, t), \tag{32}$$

an $(N_R \times N_T)$ matrix which maps between the event rate in true and reconstructed kinematic parameter space such that t is a bin in the true kinematic parameter space and m is the true interaction mode which took place in each event.

The definition of T can then be used to construct Monte Carlo predictions of the observable event rate, $n^{pred}_{b;d;s}(r; \vec{\theta}; \vec{f})$ for all of the pre-defined dependencies. The event rate prediction may also encapsulate physics effects (for instance the oscillation hypothesis) and/or systematic variations, through the incorporation of the relevant set of physics, $\vec{\theta}$ and systematic[5], $\vec{f}$ parameters,

[5]Systematic parameters are also referred to as nuisance parameters and these may be used interchangeably from hereon.

$$n^{pred}_{b;d;s}(r;\vec{\theta};\vec{f}) = \sum_m \sum_t P_{b;d;m}(t;\vec{\theta}) \cdot R_{b;d;s;m}(r,t;\vec{f}) \cdot T_{b;d;s;m}(r,t) \cdot N^{MC}, \quad (33)$$

where $P_{b;d;m}(t;\vec{\theta})$ parametrises the impact of a physics effect on the event rate for a given true kinematic bin and will be defined in section vi, $R_{b;d;s;m}(r,t;\vec{f})$ defines the response of the event rate to variations of each systematic parameter in true-reconstructed parameter space and will be defined for the SBN analysis in section vii. Finally, $N^{MC} = \mathrm{POT}^{data}_{b;d}/\mathrm{POT}^{MC}_{b;d}$ is the normalisation by which to scale the event rate, to account for the POT which was used to construct the sample of neutrino events with respect to the nominal POT in the analysis. The SBN-specific components of equation 33 followed by the fitting method they are applied to will be discussed in the following sections.

6.4.3. Statistical inference: Point and interval estimation

Oscillation fits are performed by comparing MC predictions with real or fake sets of data using the approach outlined in this section. First, for each of the predefined d, b, s in the reconstructed kinematic parameter space, the MC predictions, $n^{pred}_{b;d;s}(r;\vec{\theta};\vec{f})$, are constructed using equation 33 and the real or fake data, $n^{data}_{b;d;s}(r)$, is measured or defined. The binned-likelihood method is used for comparing between the two event rates through the minimisation of,

$$\chi^2 = -2\ln\mathscr{L}(\vec{\theta};\vec{f}) = -2\ln\mathscr{L}_0(\vec{\theta};\vec{f}) - 2\ln\mathscr{L}_{phys}(\vec{\theta};\vec{f}) - 2\ln\mathscr{L}_{syst}(\vec{f}), \quad (34)$$

where,

$$\chi^2_0 = -2\ln\mathscr{L}_0(\vec{\theta};\vec{f}) = 2\sum_{b,d,s,r}\Big(n^{data}_{b;d;s}(r)\cdot\ln\frac{n^{data}_{b;d;s}(r)}{n^{pred}_{b;d;s}(r;\vec{\theta};\vec{f})} + (n^{pred}_{b;d;s}(r;\vec{\theta};\vec{f}) - n^{data}_{b;d;s}(r))\Big), \quad (35)$$

is the contribution to the likelihood ratio from an experiment's own data. In addition, two penalty terms are added in Eq. 34. The term

$$\chi^2_{phys} = -2\ln\mathscr{L}_{phys}(\vec{f}), \quad (36)$$

is a penalty term based on prior constraints on new physics parameters. For example, this may be used to add optional constraints on oscillation parameters coming from previous experiments or global fits.

Since $\ln \mathscr{L}(\vec{\theta}; \vec{f})$ is a function of several (typically, of the order of 100-1000) new physics and systematic parameters, when calculating limits, typically for 1 or 2 interesting parameters, several parameters (called *nuisance* parameters in that context) will need to be eliminated. VALOR can eliminate nuisance parameters in one of two ways: profiling or marginalization.

TODO: add some details on marginalization

In the SBN analyses, the systematic parameters are eliminated by profiling in the fits, through the inclusion of a penalty term in the definition of χ^2 to account for prior constraints and correlations of systematic parameters. This penalty term takes the form,

$$\chi^2_{syst} = -2 \ln \mathscr{L}_{syst}(\vec{f}) = (\vec{f} - \vec{f}_0)^T \cdot \mathbf{V^{-1}} \cdot (\vec{f} - \vec{f}_0), \tag{37}$$

where $\vec{f}_0$ is the set of nominal systematic parameter values, $\vec{f}$ is the set of systematic parameter values currently set by the fit and $\mathbf{V}$ is a covariance matrix with the prior uncertainty assignments. This contribution is essentially a systematic penalty which is intended to penalise the fit increasingly with larger systematic pulls.

These uncertainty assignments, typically, are coming from theoretical considerations, external data (e.g. hadro-production measurements constraining the flux, external cross-section measurements), or other complementary data (e.g. cosmic ray, light source, or other calibration data) not explicitly included in the oscillation fit.

The advantage of the likelihood ratio method used in VALOR is that in the large-sample limit, when there are many events in every fitted bin, the quantity $-2 \ln \mathscr{L}(\vec{\theta}; \vec{f})$ has a χ^2 distribution and it can therefore be used as a goodness-of-fit test. The MIGRAD minimisation method is used to execute the fits, along with the HESSE (Hessian) error determination, and are both implemented inside MINUIT [37].

6.4.4. VALOR SBN sensitivity calculation specifics

i. Types and construction of SBN confidence regions.

The sensitivity of SBN to sterile neutrino oscillation parameters can be defined in two ways. The first is known as an 'exclusion' sensitivity, and corresponds to the region of parameter space in which the hypothesis of no oscillations (the 'null' hypothesis) can be excluded with a given confidence. The second is known as an 'allowed' sensitivity, and corresponds to the region of parameter space that is allowed with a given confidence from the analysis of samples with an injected oscillation signal.

Both methods utilise an 'Asimov' dataset, which serves as the representative sample in which all quantities are set to their nominal values [38]. When determining the exclusion sensitivity, the Asmiov dataset corresponds to the nominal MC sample with all systematics set to their prior values, and $\sin^2 2\theta_{\mu\mu}$ and Δm^2_{41} are set to 0 as per the null oscillation hypothesis. For the allowed region, the nominal sample is once again constructed, but this time the oscillation parameters are set to the values of the injected signal. The method for constructing both forms of the sensitivity is as follows,

- Separate the phase space into a 40x40-point grid, logarithmically-spaced. The choice to use 40 points in each dimension is driven only by the amount of processing required to perform the fits
- At each grid point in the parameter space, a fit is performed between the relevant Asimov dataset and the MC template constructed with the ν_μ disappearance parameters set to the value at the current grid point
- If a set of systematic parameters has been included in the fit, they are allowed to float between their $\pm 5\sigma$ limits whilst the profiling and minimisation procedures defined in section 6.4.3 are performed
- The value of χ^2 is extracted from every fit in the parameter space to form a 2D surface in a 3D volume, from which confidence regions can be extracted.

The constant-$\Delta\chi^2$ method is employed to construct the SBN sensitivity curves at the chosen confidence level, in which lines of constant-$\chi^2_{critical}$ are drawn in the 2D parameter space.

The regions of parameter space in which $\chi^2 > \chi^2_{critical}$ are those which are sensitive to discriminating a real physics (or null) result from a systematic discrepancy.

Values of $\chi^2_{critical}$ are defined separately for the exclusion and allowed sensitivity definitions. The χ^2 surface across the 2-dimensional exclusion parameter space is constructed by performing a raster scan at each Δm^2_{41} point to define a 1-dimensional limit, therefore 1 degree-of-freedom is used to define the value of $\chi^2_{critical}$ at each confidence level. The raster-scanning method is not employed in the construction of the allowed distributions, and instead 2-dimensional limits are determined, therefore 2 degrees-of-freedom are used in the definition of each $\chi^2_{critical}$ value. Table 13 lists the relevant values of $\chi^2_{critical}$ for a range of confidence levels.

ii. Initial parameter values and ranges allowed in fits.

When the (3+1) sterile neutrino oscillation hypothesis is implemented, the mixing parameters which are not held constant under the ν_μ disappearance hypothesis are allowed to float in the fits between their physical parameter limits, $0 < \sin^2 2\theta < 1$. Initially, they are set to the current global best-fit values shown in Table 14.

In all fits, the relevant set of systematic parameters are initially set to their nominal value, and are allowed to float between $-5\sigma_f < f < 5\sigma_f$, where σ_f is the prior uncertainty on the parameter f. The aforementioned penalty is applied as an incentive to minimise the magnitude of any single pull.

iii. Choice of true reaction modes in MC templates.

The reaction modes, m, in the oscillation analysis define the topology of the neutrino interaction within the nucleus, before any FSI take place. Contributions from each reaction mode to the event rate predictions directly depend on the model used as input to the physics simulation. The beam configuration, b, defines the primary neutrino content of the beam and is set to FHC in all SBN analyses, since the BNB currently only runs in neutrino mode.

The list of reaction modes used in the SBN oscillation analysis comes in two forms, fine and coarse. The fine list consists of all possible neutrino interaction modes, categorised by neutrino flavour and current, and is used in the construction of the systematic response

functions and MC templates. The coarse list is defined separately for every analysis based on specific features, such as energy and topology of the sample, to absorb the dominant signal interaction modes along with an informative set of background modes. The coarse list is more often used in the presentation of results, and ensures the maximum amount of information is demonstrated concisely. The fine list of reaction modes is given for each neutrino flavour in Table 15. The coarse list of reaction modes for the SBN ν_μ CC oscillation analysis is given in Table 16.

Note that intranuclear pion production reaction modes, such as resonant interactions and DIS, are combined to form the pion multiplicity modes. This is clearer for studies of final state pion multiplicities in neutrino interactions on heavy nuclei, in which hadron transport plays such a huge part.

iv. Choice of kinematic binning in MC templates.

The SBND neutrino energy distributions shown in Figure 8 are taken into consideration when defining the true and reconstructed binning schemes for the ν_μ disappearance oscillation analysis in SBN. The shape of the true and reconstructed energy distributions helps make a number of decisions. First, since the location of the neutrino energy peaks remains consistent between underlying models, the same binning scheme can be used in all iterations of the analysis. Second, the general location and widths of the distributions guides the specification of the variable bin widths across the true and reconstructed space. Although not shown in Figure 8, the peak locations and widths are also consistent between SBND, MicroBooNE and ICARUS. The same binning schemes are therefore used across all 3 detectors within the analysis and are defined in Table 17.

The ν_μ binning (edge-to-edge) has 19 reconstructed and 33 true bins which are arranged as per Table 17.

The ν_e binning (edge-to-edge) has 33 true bins which are the same as the ν_μ ones.

v. Variable SBN baseline parameterization.

In SBN sterile oscillation searches, the d component of equation 33 effectively defines the baseline input to the oscillation probability. Initially, the baselines used at each of the SBN detectors were defined as the single, average value at each location,

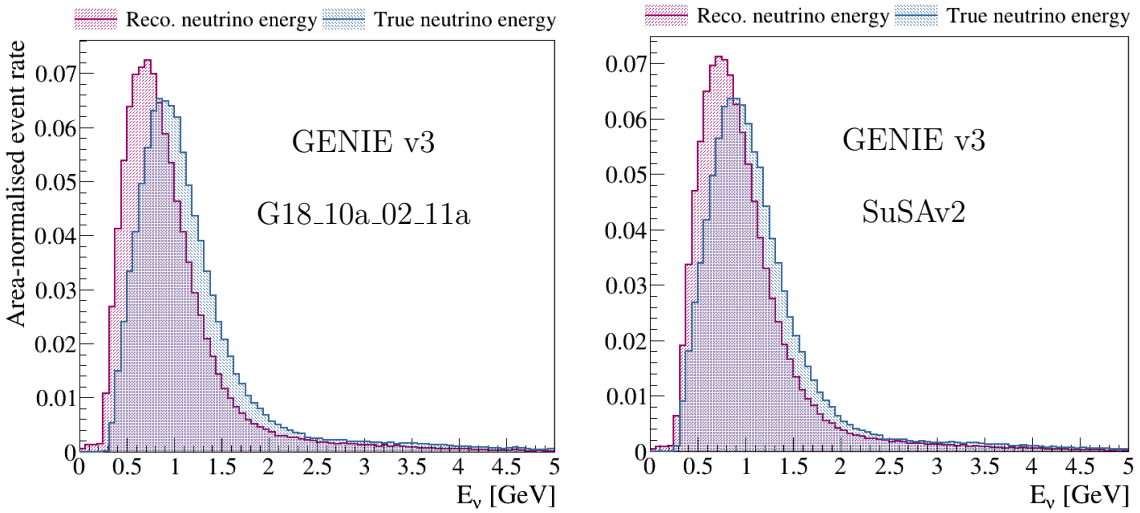

Figure 8: Shapes of the true and reconstructed neutrino energy distributions following the truth-level ν_μ CC Inclusive event selection in SBND. These energy distributions are considered when defining the ν_μ disappearance oscillation analysis true and reconstructed neutrino energy binning schemes. Two of the model configurations discussed are shown, G18_10a_02_11a and SuSAv2 from GENIE v3.

- SBND, 87.6m
- MicroBooNE, 446m
- ICARUS, 574m,

such that the probability was calculated once in each of the true energy bins defined in Table 17. The true shapes of the baseline distribution in each detector, from which the averages are calculated, are shown in Figure 9.

Looking instead at the energy dependence of the baseline in each detector raises a concern about the validity of using such a simple approximation. Figure 10 shows that in all three SBN detectors, the baselines distributions are not constant as a function of energy, which is a critical requirement for the approximation to hold.

Having determined that simply using the average value at each detector is not sufficient to describe the baseline, a simple validation procedure was defined. The SBND oscillation probability distribution was constructed as a function of true neutrino energy at a single point in the ν_μ disappearance parameter space, $\sin^2 2\theta_{\mu\mu} = 0.01$, $\Delta m^2_{41} = 50$ eV^2. The distribution was first constructed using the true value of L/E in every event, before being

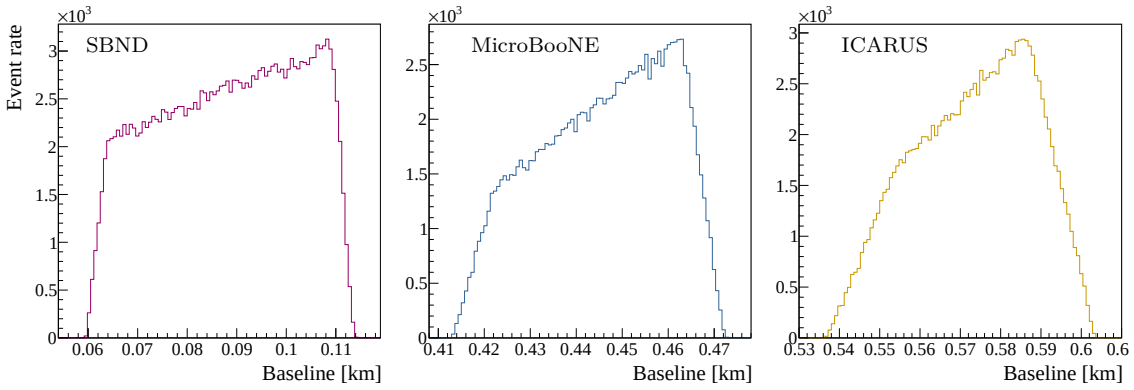

Figure 9: Baseline distributions at each of the SBN detectors

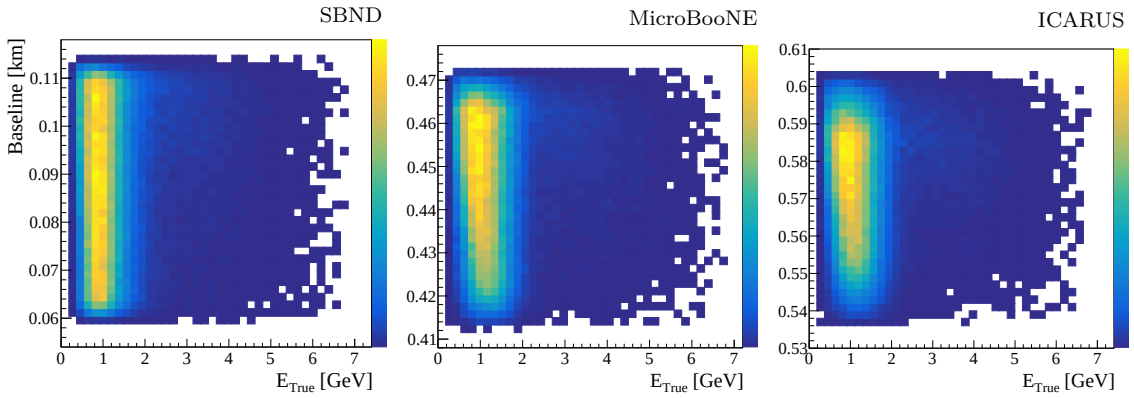

Figure 10: Energy vs baseline distributions in each of the SBN detectors.

compared against the calculation with L_{avg}/E. A number of iterative improvements to the baseline definition were implemented in attempts to improve the parametrisation without drastically increasing the computational expense, after each iteration the oscillation probability was calculated and compared against the previous methods and ultimately, truth.

The first iteration involved defining the baseline in splines at 4 points in energy space, in the hopes it would better-represent the true behaviour. This was quickly superseded by the construction of many such splines at many points in energy space. Each incrementally improved the agreement with truth, whilst increasing the computational cost. Ultimately, it was determined that using the true baseline in every event was the only sufficient option for performing physics studies at the precision required in SBN. The oscillation probabilities at the aforementioned point in ν_μ disappearance parameter space for each of the baseline

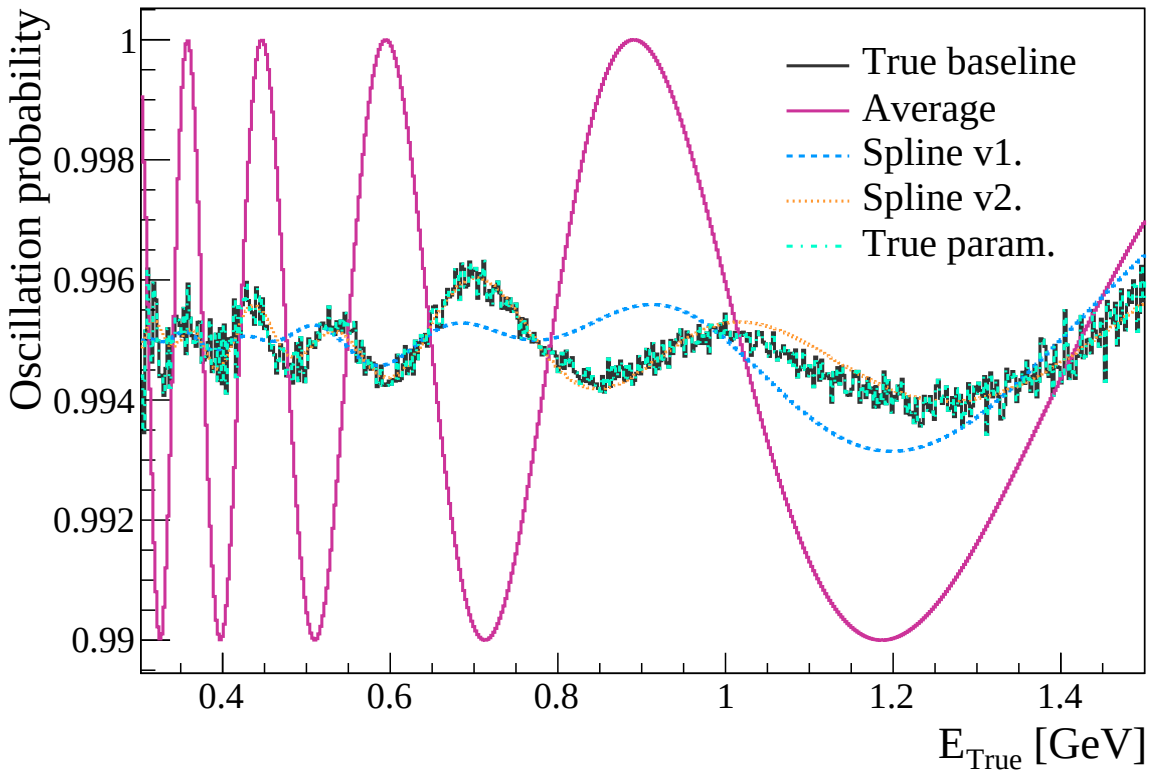

Figure 11: SBN ν_μ disappearance oscillation probability in the (3+1) sterile neutrino framework at $\sin^2 2\theta_{\mu\mu} = 0.01$ & $\Delta m^2_{41} = 50$ eV^2 for each of the methods of parametrising the baseline in SBND.

definition iterations are shown in Figure 11.

vi. Parameterization of oscillation effects.

This note will present analyses of the SBN sensitivity to the (3+1) sterile oscillation model through the observation of ν_μ disappearance and ν_e appearance in SBN. The physics hypotheses, $P_{b;d;m}(t;\vec{\theta})$, used in the construction of the MCT's for this analysis will be discussed here.

Given that existing results suggest $\Delta m^2_{41} \gg \Delta m^2_{sol,atm}$ in the (3+1) sterile neutrino hypothesis, the effective two-flavour oscillation probability can be employed. This probability is parametrised by Δm^2_{41} and $\sin^2 2\theta_{\mu\mu}$ for ν_μ disappearance searches, and by Δm^2_{41} and $\sin^2 2\theta_{\mu e}$ for ν_e appearance searches as per equations 24 and 25 respectively. SBN will be sensitive to the same region of parameter space previously explored by Mini-

BooNE, MINOS/MINOS+ and many other experiments, where $10^{-2} < \Delta m^2_{41}$ eV^2 and $10^{-3} < \sin^2 2\theta_{\mu\mu}$, $\sin^2 2\theta_{\mu e} < 1$. SBN will aim to push below the existing $\sin^2 2\theta_{\mu\mu}$ and $\sin^2 2\theta_{\mu e}$ limits.

Due to the short baseline of the SBN experiment, along with the validity of the approximation that $\Delta m^2_{41} \gg \Delta m^2_{sol,atm}$, $\Delta m^2_{sol} = \Delta m^2_{atm} = 0$, SBN is completely insensitive to active neutrino oscillations. The active neutrino oscillation hypothesis is therefore not applied alongside the sterile hypothesis in the SBN (3+1) sensitivity analyses and $\sin^2 2\theta_{\mu\mu}$, $\sin^2 2\theta_{\mu e}$ are the relevant mixing parameter in the two-flavour approximation for the disappearance and appearance measurements respectively.

vii. Parameterization of systematic effects.

The systematic inputs to the oscillation analysis together define $R_{b;d;s;m}(r,t;\vec{f})$ in equation 33. This section will define and validate how the flux, interaction and detector systematic parameter sets are parametrised in the oscillation analysis.

The flux and interaction systematic uncertainties are separated into two categories by construction. The first are known as 'unisims' in which the prior uncertainty on each parameter is either defined by,

(a) Determining the magnitude of a single, 1σ variation of the parameter

(b) By generating two samples with the parameter switched on in the first and off in the second, and setting the observed rate difference to be the 1σ variation

(c) By generating multiple samples with different underlying models of the parameter and assuming a Gaussian variation of the models, such that the standard deviation corresponds to a 1σ variation of the parameter.

Treating every parameter independently, the magnitude of the prior 1σ uncertainty can then be used as an input to a generation of many MC universes, to determine the effect of varying the parameter with respect to its prior uncertainty on the content and kinematics of neutrino interactions observed in the detector. All unisim parameters must consequently be entirely uncorrelated. The second category contains 'multisim' parameters, in which each

universe is constructed following the variation of multiple, correlated parameters within their prior 1σ uncertainties.

Every flux and interaction systematic parameter is represented in the analysis samples by a set of weights, with one weight taken from each of the aforementioned MC universes. In the case of unisim parameters, every weight corresponds to a single n σ variation of the parameter. Whereas for the multisim parameters, every weight corresponds to a unique throw of all correlated parameters used in the construction of the multisim universes.

In order to proceed with the analysis, the weights must be converted into a format which can be processed by the fitter. In the case of unisim parameters, a set of 1D responses[6] are constructed at each point in the 2D true and reconstructed neutrino energy parameter space (E_{True}, E_{Reco}) for every neutrino interaction mode listed in section 6.4.4. The knots, $\mathscr{R}_{m;t,r}(k)$, of the spline are defined as follows,

$$\mathscr{R}_{m;t,r}(k) = \frac{N^{v}_{m;t,r}(k)}{N^{n}_{m;t,r}},\ k \in \{0, \pm 0.5, \pm 1, \pm 1.5, \pm 2, \pm 2.5, \pm 3\}, \tag{38}$$

for reaction mode, m, in the (E_{True}, E_{Reco}) bins, t, r. Each of the 13 knots in the response function are defined as the ratio of the $k\sigma$-varied event rate, $N^{v}_{m;t,r}(k)$, to the nominal event rate, $N^{n}_{m;t,r}$ in the corresponding mode and bin.

In the case of the multisim parameters it is not trivial to construct response functions to represent them. This is due to the fact that $n > 1$ correlated parameters are used to construct each event weight such that a single knot does not represent a single variation, and it is not possible to efficiently process high-dimensionality ($\mathcal{O}(10)$) splines. Instead, a covariance matrix is constructed in E_{True} parameter space to define how the multisim systematic variations behave as a function of energy.

The covariance matrix, $\mathbf{C_{ij}}$, is constructed by computing the event rates in each of the U universes and finding,

$$\mathbf{C_{ij}} = \frac{1}{U}\sum_{u=1}^{U}(N^{u}_{i} - N^{cv}_{i})(N^{u}_{j} - N^{cv}_{j}), \tag{39}$$

[6]Systematic parameter response functions are also known as 'splines'. The two will be referred to interchangeably throughout the setup and discussion of the analysis.

where $N^{u}_{i,j}$ is the event rate in universe u in bin i or j and $N^{cv}_{i,j}$ is the central value, or nominal, event rate in bin i or j.

Frequently throughout the introduction to the analysis procedure as well as within the analysis itself, the neutrino event rate spectra will be shown as a function of the reconstructed neutrino energy with a representative $\pm 1\sigma$ error envelope. These envelopes are produced by constructing 1000 toy MC samples with the specified set of systematic parameters randomised and taking the $\pm 1\sigma$ spread of the 1000 toys with all correlations considered.

Systematic Variation	Uncertainty Size on ν_e selection (%)		
	SBND	MicroBooNE	ICARUS
expskin_FluxUnisim	1.38	1.75	1.55
horncurrent_FluxUnisim	0.350	0.376	0.394
kminus_PrimaryHadronNormalization	0.0757	0.0650	0.0361
kplus_PrimaryHadronFeynmanScaling	2.12	2.08	2.23
kzero_PrimaryHadronSanfordWang	2.55	2.43	2.45
nucleoninexsec_FluxUnisim	0.922	0.884	0.910
nucleonqexsec_FluxUnisim	2.75	2.69	2.71
nucleontotxsec_FluxUnisim	0.770	0.758	0.801
piminus_PrimaryHadronSWCentralSplineVariation	0.0284	0.0592	0.0734
pioninexsec_FluxUnisim	0.498	0.516	0.486
pionqexsec_FluxUnisim	0.297	0.310	0.279
piontotxsec_FluxUnisim	0.448	0.488	0.465
piplus_PrimaryHadronSWCentralSplineVariation	2.63	2.52	2.35
DISAth	0.0113	0.0112	0.00964
DISBth	0.0165	0.0165	0.0145
DISCv1u	0.0109	0.0105	0.00895
DISCv2u	0.0109	0.0105	0.00902
IntraNukeNabs	6.38	6.24	6.27
IntraNukeNcex	0.967	0.822	0.758
IntraNukeNinel	7.08	6.87	6.85
IntraNukeNmfp	2.79	2.77	2.78
IntraNukeNpi	0.390	0.404	0.416
IntraNukePIabs	3.78	3.93	4.01
IntraNukePIcex	0.188	0.643	0.617
IntraNukePIinel	3.48	3.27	3.35
IntraNukePImfp	0.991	1.07	1.01
IntraNukePIpi	0.501	0.478	0.473
NC	0.983	1.09	0.797
NonResRvbarp1piAlt	0	0	0
NonResRvbarp1pi	0	0	0
NonResRvbarp2piAlt	0	0	0
NonResRvbarp2pi	0	0	0
NonResRvp1piAlt	0	0	0
NonResRvp1pi	0	0	0
NonResRvp2piAlt	0	0	0
NonResRvp2pi	0	0	0
ResDecayGamma	0.116	0.113	0.108
ccresAxial	5.57	5.89	5.94
ccresVector	4.52	4.82	4.82
cohMA	0.00437	0	0
cohR0	0.00437	0	0
ncelAxial	0.0152	0.0224	0.0197
ncelEta	0.000693	0.000723	0.000507
ncresAxial	1.47	1.70	1.48
ncresVector	0.594	0.699	0.613
qema	1.47	1.38	1.42
MEC normalization	11.0	10.3	10.6
POT	2.00	2	2.00

Table 11: The size of overall normalization uncertainty of systematic variations in the ν_e CC central value prediction.

Systematic Variation	Uncertainty Size on ν_μ selection (%)		
	SBND	MicroBooNE	ICARUS
expskin_FluxUnisim	3.31	4.41	4.33
horncurrent_FluxUnisim	0.540	0.653	0.642
kminus_PrimaryHadronNormalization	0.0115	0.00460	0.0100
kplus_PrimaryHadronFeynmanScaling	0.394	0.330	0.340
kzero_PrimaryHadronSanfordWang	0.0229	0.0247	0.0224
nucleoninexsec_FluxUnisim	0.895	0.854	0.857
nucleonqexsec_FluxUnisim	2.64	2.59	2.59
nucleontotxsec_FluxUnisim	0.812	0.774	0.776
piminus_PrimaryHadronSWCentralSplineVariation	0.120	0.145	0.136
pioninexsec_FluxUnisim	1.23	1.30	1.29
pionqexsec_FluxUnisim	0.827	0.856	0.855
piontotxsec_FluxUnisim	0.857	0.949	0.944
piplus_PrimaryHadronSWCentralSplineVariation	4.22	4.43	4.43
DISAth	0.0279	0.0213	0.0233
DISBth	0.0444	0.0341	0.0369
DISCv1u	0.0246	0.0196	0.0213
DISCv2u	0.0242	0.0194	0.0210
IntraNukeNabs	6.57	6.61	6.59
IntraNukeNcex	0.608	0.504	0.668
IntraNukeNinel	6.96	6.95	7.03
IntraNukeNmfp	2.79	2.86	2.85
IntraNukeNpi	0.290	0.307	0.319
IntraNukePIabs	3.53	3.89	3.88
IntraNukePIcex	0.889	1.00	1.06
IntraNukePIinel	2.44	2.68	2.61
IntraNukePImfp	0.803	0.886	0.884
IntraNukePIpi	0.233	0.258	0.247
NC	0.00404	0.00420	0.00393
NonResRvbarp1piAlt	0.0842	0.110	0.114
NonResRvbarp1pi	1.15	1.25	1.28
NonResRvbarp2piAlt	0.0372	0.0412	0.0456
NonResRvbarp2pi	0.672	0.760	0.746
NonResRvp1piAlt	0.00656	0.00639	0.00570
NonResRvp1pi	0.0442	0.0459	0.0372
NonResRvp2piAlt	0.0412	0.0573	0.0528
NonResRvp2pi	0.400	0.467	0.458
ResDecayGamma	0.00298	0.00127	0.00219
ccresAxial	5.09	5.56	5.53
ccresVector	4.05	4.46	4.44
cohMA	0	0	0
cohR0	0	0	0
ncelAxial	0.00617	0.00640	0.00676
ncelEta	6.48e-05	0.000235	0.000164
ncresAxial	0.220	0.252	0.250
ncresVector	0.102	0.121	0.122
qema	1.71	1.60	1.61
MEC normalization	12.1	12.2	12.2
POT	2	2	2

Table 12: The size of overall normalization uncertainty of systematic variations in the ν_μ CC central value prediction.

Contour type	Confidence Level			
	68%	90%	3σ	5σ
Exclusion limits	0.23	1.64	7.74	23.66
Allowed regions	2.30	4.61	11.83	28.74

Table 13: Values of $\chi^2_{critical}$ at various confidence levels defined in the construction of exclusion limit and allowed region sensitivity contours.

Parameter	Global Best Fit
$\lvert U_{e4}\rvert$	0.116
$\lvert U_{\mu 4}\rvert$	0.135
$\sin^2 2\theta_{\mu\mu}$	0.0716
$\sin^2 2\theta_{\mu e}$	0.000981
$\sin^2 2\theta_{ee}$	0.0531
Δm^2_{41}	1.32

Table 14: Global best fit sterile neutrino oscillation parameters [3]

ν_μ, $\bar{\nu}_\mu$	ν_e, $\bar{\nu}_e$
CC QE	CC QE
NC Elastic	NC Elastic
CC, NC 2p2h	CC, NC 2p2h
CC, NC $1\pi^\pm$	CC, NC $1\pi^\pm$
CC, NC $1\pi^0$	CC, NC $1\pi^0$
CC, NC $2\pi^\pm$	CC, NC $2\pi^\pm$
CC, NC $2\pi^0$	CC, NC $2\pi^0$
CC, NC $\pi^\pm\pi^0$	CC, NC $\pi^\pm\pi^0$
CC, NC Coh	CC, NC Coh
CC, NC Elastic Scattering	CC+NC Elastic Scattering
NC 1γ	NC 1γ
CC, NC Other	CC, NC Other
Cosmic & Dirt	

Table 15: The extensive list of reaction modes used in the construction of MC templates and systematic response functions in the SBN analysis procedure. These modes correspond to the primary topology of the neutrino interaction, before any FSI take place. Note that many such modes will have negligible contributions from events in the SBN ν_μ CC disappearance analysis, but are still included for validation and completeness purposes. The cosmic and dirt modes represent external backgrounds though are not yet generated as part of the sample.

Reaction modes
Signal
ν_μ CC QE
ν_μ CC 2p2h
ν_μ CC 1π
ν_μ CC 2π
ν_μ CC ¿2π
Background
$\bar{\nu}_\mu$ CC
ν_e & $\bar{\nu}_e$ CC
NC 0π
NC Other
Cosmic
Dirt

Table 16: The signal and background reaction modes used in the SBN ν_μ CC disappearance analysis. Note, the external background contributions, *Cosmic* and *Dirt*, are not yet generated as part of the ν_μ CC sample.

E_{Reco}				E_{True}	
ν_e		ν_μ		ν_μ & ν_e	
Range [GeV]	Width [GeV]	Range [GeV]	Width [GeV]	Range [GeV]	Width [GeV]
0.2-1.1	0.15	0.0-0.2	0.2	0.0-0.3	0.3
1.1-1.5	0.2	0.2-0.4	0.1	0.3-0.6	0.1
1.5-2.0	0.25	0.4-1.0	0.05	0.6-1.2	0.05
2.0-3.0	1.0	1.0-1.5	0.25	1.2-1.5	0.3
-	-	1.5-3.0	0.5	1.5-3.0	0.5
-	-	3.0-10.0	7.0	3.0-5.0	2.0
-	-	-	-	5.0-10.0	5.0

Table 17: The true and reconstructed binning scheme used in the construction of MC templates in the SBN ν_μ disappearance analysis. Different binning schemes are used in reconstructed and true space as they are each defined according to the shape and rate of the uniformly-binned reconstructed and true neutrino energy distributions, shown in Figure 8.

7. Systematic Validation

7.1. CAFAna

7.2. SBNFit

7.3. VALOR

a. Flux systematics

The unisim flux systematic parameters are those associated with hadronic (p, n & $\pi^{\pm}$) interaction cross-sections in the Beryllium target and Aluminium horn, along with optical, beam-focusing parameters. The multisim parameters comprise the differential cross-section associated with the production of π^{+}, π^{-}, K^{+}, K^{-} & K^{0}, in inelastic proton-Beryllium interactions. The subsequent decay of each of these hadrons are the primary neutrino production mechanisms which were discussed in section i.

The left-hand plot in Figure 12 demonstrates the 1σ uncertainty envelopes introduced by the flux unisim parameter set with respect to the ν_{μ} CC Inclusive sample of events in SBND. The systematic variations are applied in two ways: first, with the uncertainties taken directly from the universe input files and second, with the uncertainties calculated from the systematic parameter response functions.

The right-hand plot in Figure 12 serves as a validation of the systematic parametrisation. The validation involves a double ratio, which is constructed by first taking the ratio of the event rate from the 1σ variation of all flux parameters to the nominal event rate, and then calculating a second ratio, between the spline-based parametrisation and the variations taken from the input universes. A flat line at 1 would indicate perfect agreement between the input variations and the spline-based variations. Although this is not quite the case, the discrepancies are well below 1% across the entire energy range.

In summary, the response functions defined to represent the flux unisim parameters in all SBN oscillation analyses serve as an excellent approximation of the input systematic variations. These studies have been repeated for all input samples, s, and detectors, d, and

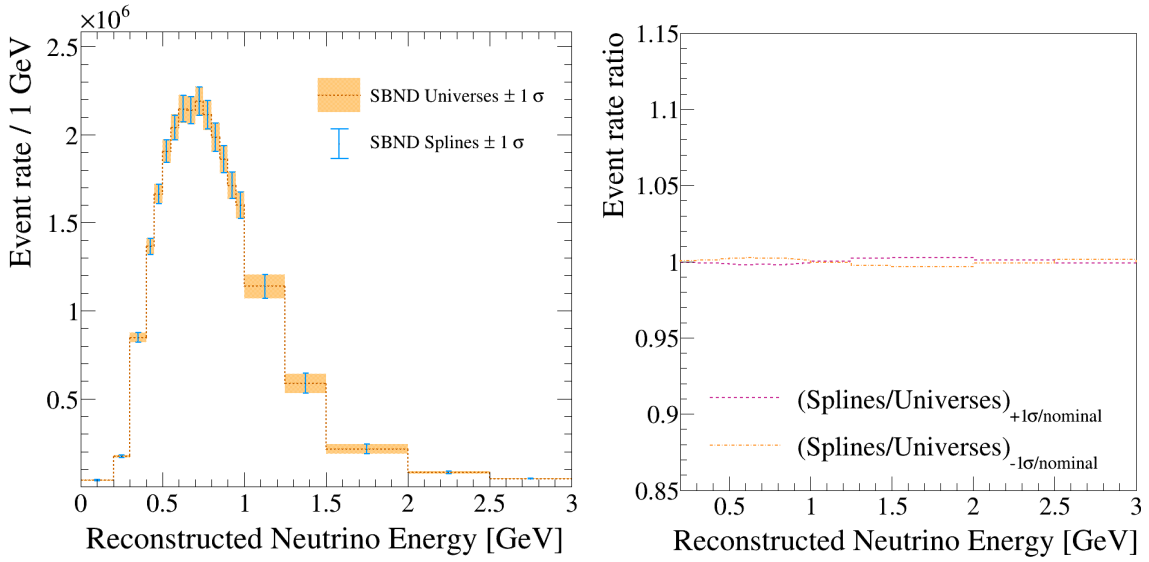

Figure 12: On the left is the SBND ν_μ CC Inclusive event rate plotted with the 1σ SBN uncorrelated flux parameter uncertainty envelope constructed in two ways. The blue band takes the 1σ variation directly from the input universes, and the orange band constructs the 1σ variation from the response functions. On the right is a more quantitative assessment of this comparison, the $\pm1\sigma$/nominal event rate in each energy bin is calculated in the universe and spline-based uncertainty definitions which is in turn taken as a ratio, pink line.

a comparable level of agreement is observed in all cases. Each of the flux spline parameters are applied to all reaction modes.

The multisim flux parameters are defined in a covariance matrix parametrised in E_{True} bins as per equation 39. The covariance matrix elements are also separated into neutrino flavour with an appropriate binning defined based on their relative rates. These bin edges are given in Table 18 and closely follow the E_{True} scheme laid out in Table 17 for muon neutrinos. Figure 13 shows the true and covariance-defined 1σ variation envelopes as well as the double ratio which more-quantitatively assesses the performance. The covariance matrix approach is naturally less precise than the response function approach, however the disagreement still does not exceed 1%.

b. Interaction systematics

ν_μ		$\bar{\nu}_\mu$	ν_e	$\bar{\nu}_e$
Range [GeV]	Width [GeV]	Bin edges [GeV]		
0.3-0.6	0.1	0.0	0.0	0.0
0.6-1.2	0.05	0.7	0.5	2.5
1.2-1.5	0.3	1.0	0.7	10.0
1.5-3.0	0.5	1.5	0.8	-
3.0-10.0	7.0	2.5	1.5	-
	-	10.0	2.5	-
	-	-	10.0	-

Table 18: The binning defintions in each neutrino flavour which are used in the construction of the flux multisim covariance matrix.

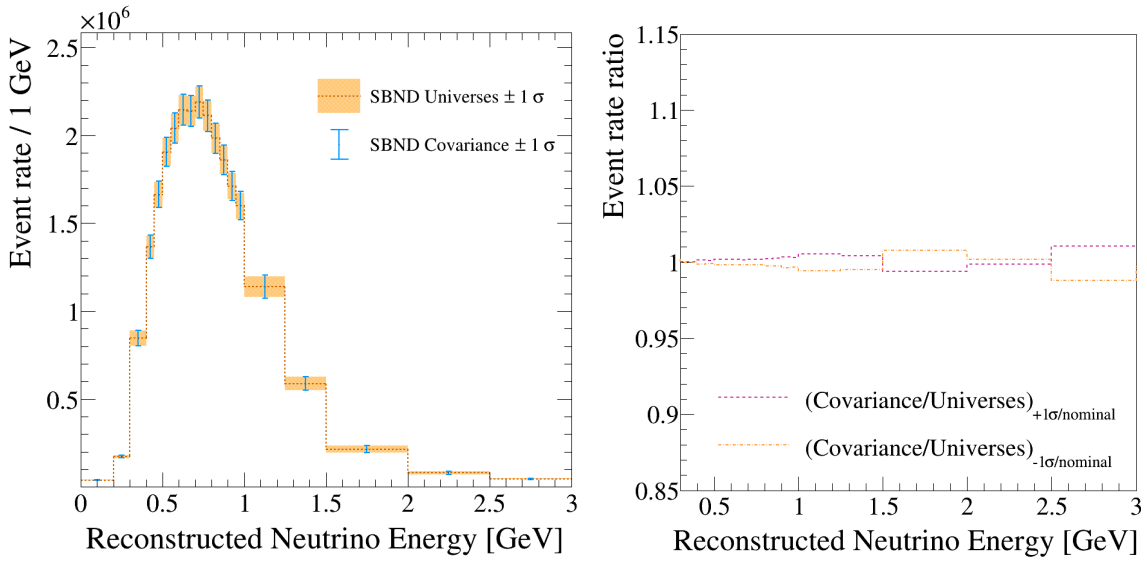

Figure 13: On the left is the SBND ν_μ CC Inclusive event rate plotted with the 1σ SBN correlated flux parameter uncertainty envelope constructed in two ways. The blue band takes the 1σ variation directly from the input universes, and the orange band constructs the 1σ variation from the covariance matrix. On the right is a more quantitative assessment of this comparison, the $\pm1\sigma$/nominal event rate in each energy bin is calculated in the universe and covariance-based uncertainty definitions which is in turn taken as a ratio, pink line.

The two interaction parameter sets are validated using the same procedure as that of the flux, the results of which are given for the proposal parameter set in Figure 14 and the modern parameter set in Figure 15. Although there are 20 and 22 proposal and modern parameters respectively, compared with the 8 from the flux, the agreement between the input and parametrised SBN proposal-era systematic uncertainties is extremely precise.

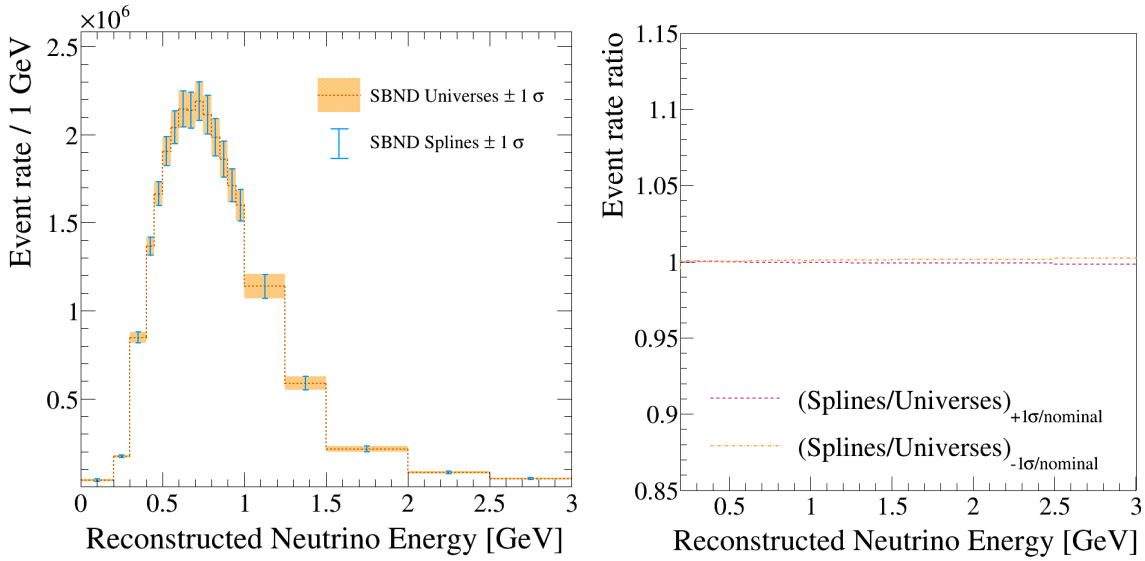

Figure 14: On the left is the SBND ν_μ CC Inclusive event rate plotted with the 1σ SBN proposal-era interaction systematic uncertainty envelope constructed in two ways. The blue band takes the 1σ variation directly from the input universes, and the orange band constructs the 1σ variation from the response functions. On the right is a more quantitative assessment of this comparison, the $\pm1\sigma$/nominal event rate in each energy bin is calculated in the universe and spline-based uncertainty definitions which is in turn taken as a ratio, pink line.

The modern-era systematic agreement between the universe input and parametrised approach is a little less precise. This is predominantly due to the parameters in the set which only impact reaction modes that occur relatively infrequently in the SBN analysis, such that the rate of events used to construct the splines is low. That being said, only 2 reconstructed neutrino energy bins have a magnitude of the disagreement exceeding 1% of the event rate in that bin. Finally, a full list of the interaction modes which are affected by each of the proposal and modern interaction parameters is given in Table 19 and 20 respectively.

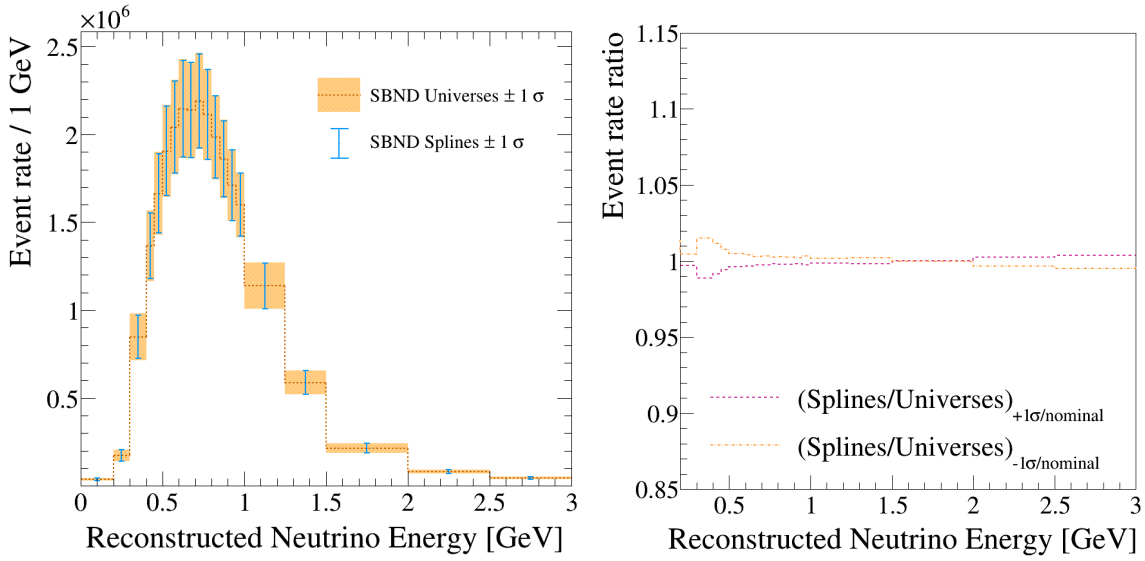

Figure 15: On the left is the SBND ν_μ CC Inclusive event rate plotted with the 1σ modern-era interaction systematic uncertainty envelope constructed in two ways. The blue band takes the 1σ variation directly from the input universes, and the orange band constructs the 1σ variation from the response functions. On the right is a more quantitative assessment of this comparison, the $\pm 1\sigma$/nominal event rate in each energy bin is calculated in the universe and spline-based uncertainty definitions which is in turn taken as a ratio, pink line.

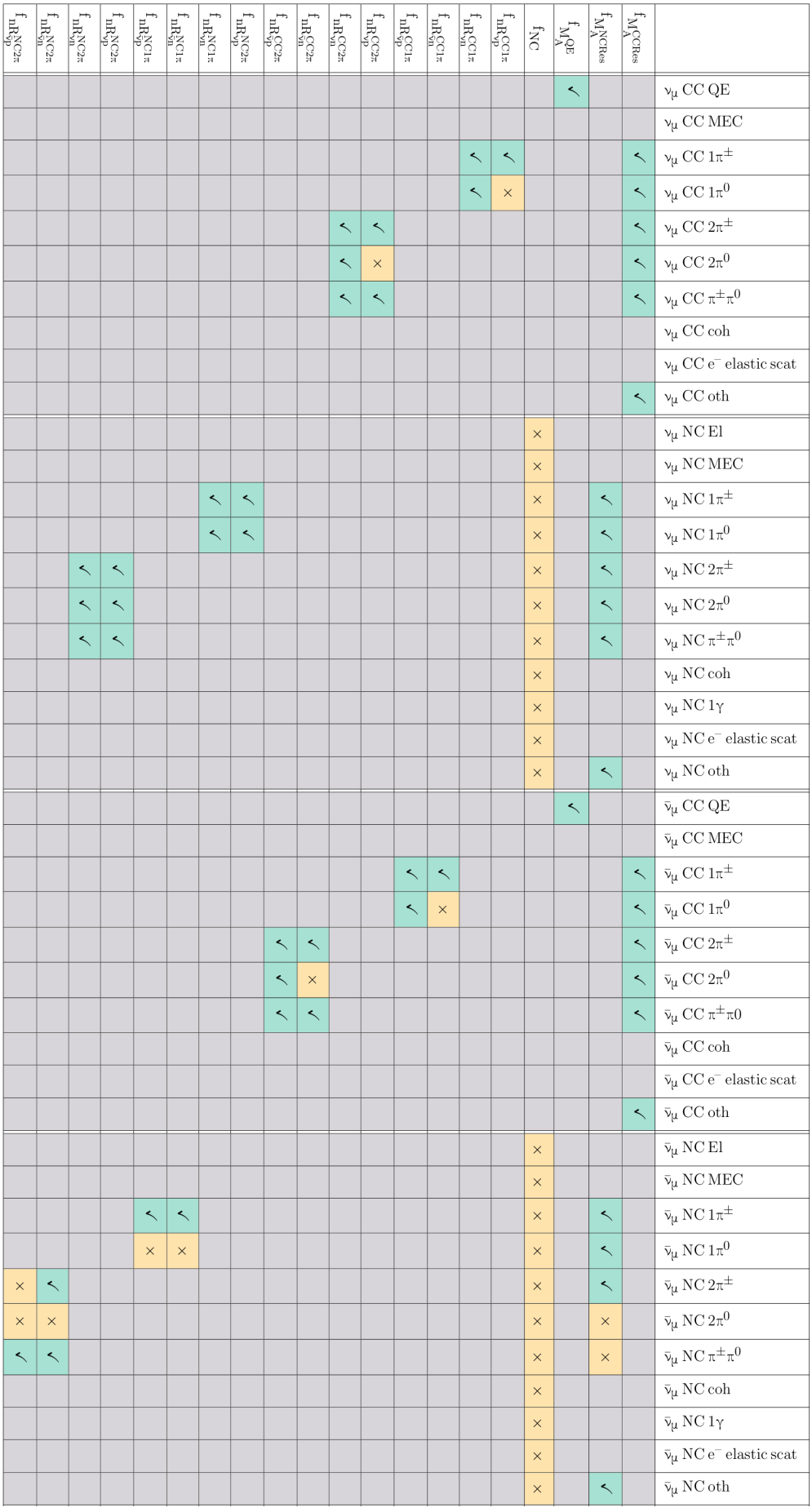

Table 19: A list of interaction modes impacted by the proposal interaction spline parameters. A green tick indicates that the mode should have been affected, and was. An orange cross indicates that the mode could have been affected, but there were too few events in the relevant mode and binning scheme to pass the spline-construction threshold.

f_{2p2h}	$f_{\eta^0}^{NCEl}$	$f_{M_A^{NCEl}}$	$f_{R_0^{COH}}$	$f_{M_A^{COH}}$	$f_{M_V^{NCRes}}$	$f_{M_V^{CCRes}}$	$f_{\Delta\to N\gamma}$	$f_{R_\pi^\pi}$	f_{λ_π}	$f_{R_\pi^{Inel}}$	$f_{R_\pi^{CEx}}$	$f_{R_\pi^{Abs}}$	$f_{R_N^\pi}$	f_{λ_N}	$f_{R_N^{Inel}}$	$f_{R_N^{CEx}}$	$f_{R_N^{Abs}}$	$f_{C_{V2u}}$	$f_{C_{V1u}}$	$f_{B_{HT}}$	$f_{A_{HT}}$	
													✓	✓	✓	✓	✓					ν_μ CC QE
✓													✓	✓	✓	✓	✓					ν_μ CC MEC
						✓	✓	✓	✓	✓	✓	✓	✓	✓	✓	✓	✓	✓	✓	✓	✓	ν_μ CC $1\pi^\pm$
						✓	✓	✓	✓	✓	✓	✓	✓	✓	✓	✓	✓	✓	✓	✓	✓	ν_μ CC $1\pi^0$
						✓	✓	✓	✓	✓	✓	✓	✓	✓	✓	✓	✓	✓	✓	✓	✓	ν_μ CC $2\pi^\pm$
						✓	✓	✓	✓	✓	✓	✓	✓	✓	✓	✓	✓	✓	✓	✓	✓	ν_μ CC $2\pi^0$
						✓	✓	✓	✓	✓	✓	✓	✓	✓	✓	✓	✓	✓	✓	✓	✓	ν_μ CC $\pi^\pm\pi^0$
			×	×																		ν_μ CC coh
																						ν_μ CC e^- elastic scat
						✓	✓	✓	✓	✓	✓	✓	✓	✓	✓	✓	✓	✓	✓	✓	✓	ν_μ CC oth
	✓	✓											×	✓	×	×	×					ν_μ NC El
✓													×	×	×	×	×					ν_μ NC MEC
					✓		✓	✓	✓	✓	✓	✓	✓	✓	✓	✓	✓	✓	✓	✓	✓	ν_μ NC $1\pi^\pm$
					✓		✓	✓	✓	✓	✓	✓	✓	✓	✓	✓	✓	✓	✓	✓	✓	ν_μ NC $1\pi^0$
					✓		✓	✓	✓	✓	✓	✓	✓	✓	✓	✓	✓	✓	✓	✓	✓	ν_μ NC $2\pi^\pm$
					✓		✓	✓	✓	✓	✓	✓	✓	✓	✓	✓	✓	✓	✓	✓	✓	ν_μ NC $2\pi^0$
					✓		✓	✓	✓	✓	✓	✓	✓	✓	✓	✓	✓	✓	✓	✓	✓	ν_μ NC $\pi^\pm\pi^0$
			×	×																		ν_μ NC coh
																						ν_μ NC 1γ
																						ν_μ NC e^- elastic scat
					✓		✓	✓	✓	✓	✓	✓	✓	✓	✓	✓	✓	✓	✓	✓	✓	ν_μ NC oth
													✓	✓	✓	✓	✓					$\bar{\nu}_\mu$ CC QE
✓													✓	✓	✓	✓	✓					$\bar{\nu}_\mu$ CC MEC
						✓	✓	✓	✓	✓	✓	✓	✓	✓	✓	✓	✓	×	×	×	×	$\bar{\nu}_\mu$ CC $1\pi^\pm$
						✓	✓	✓	✓	✓	✓	✓	✓	✓	✓	✓	✓	✓	✓	✓	✓	$\bar{\nu}_\mu$ CC $1\pi^0$
						✓	✓	✓	✓	✓	✓	✓	✓	✓	✓	✓	✓	×	×	×	×	$\bar{\nu}_\mu$ CC $2\pi^\pm$
						✓	✓	✓	✓	✓	✓	✓	✓	✓	✓	✓	✓	×	×	×	×	$\bar{\nu}_\mu$ CC $2\pi^0$
						✓	✓	✓	✓	✓	✓	✓	✓	✓	✓	✓	✓	✓	✓	✓	✓	$\bar{\nu}_\mu$ CC $\pi^\pm\pi0$
			×	×																		$\bar{\nu}_\mu$ CC coh
																						$\bar{\nu}_\mu$ CC e^- elastic scat
						✓	×	✓	✓	✓	✓	✓	✓	✓	✓	✓	✓	×	×	×	×	$\bar{\nu}_\mu$ CC oth
	×	×											×	×	×	×	×					$\bar{\nu}_\mu$ NC El
✓													×	×	×	×	×					$\bar{\nu}_\mu$ NC MEC
					✓		✓	×	✓	✓	✓	✓	×	✓	✓	✓	✓	×	×	×	×	$\bar{\nu}_\mu$ NC $1\pi^\pm$
					✓		✓	✓	✓	✓	✓	✓	✓	✓	✓	✓	✓	×	×	×	×	$\bar{\nu}_\mu$ NC $1\pi^0$
					✓		✓	×	✓	×	×	×	✓	✓	✓	✓	✓	×	×	×	×	$\bar{\nu}_\mu$ NC $2\pi^\pm$
					×		×	×	×	×	×	×	×	×	×	×	×	×	×	×	×	$\bar{\nu}_\mu$ NC $2\pi^0$
					×		×	×	✓	✓	✓	✓	×	×	×	×	×	×	×	✓	✓	$\bar{\nu}_\mu$ NC $\pi^\pm\pi^0$
			×	×																		$\bar{\nu}_\mu$ NC coh
																						$\bar{\nu}_\mu$ NC 1γ
																						$\bar{\nu}_\mu$ NC e^- elastic scat
					✓		×	×	×	×	×	×	×	×	×	×	×	×	×	×	×	$\bar{\nu}_\mu$ NC oth

Table 20: A list of interaction modes impacted by the modern interaction spline parameters. A green tick indicates that the mode should have been affected, and was. An orange cross indicates that the mode could have been affected, but there were too few events in the relevant mode and binning scheme to pass the spline-construction threshold.

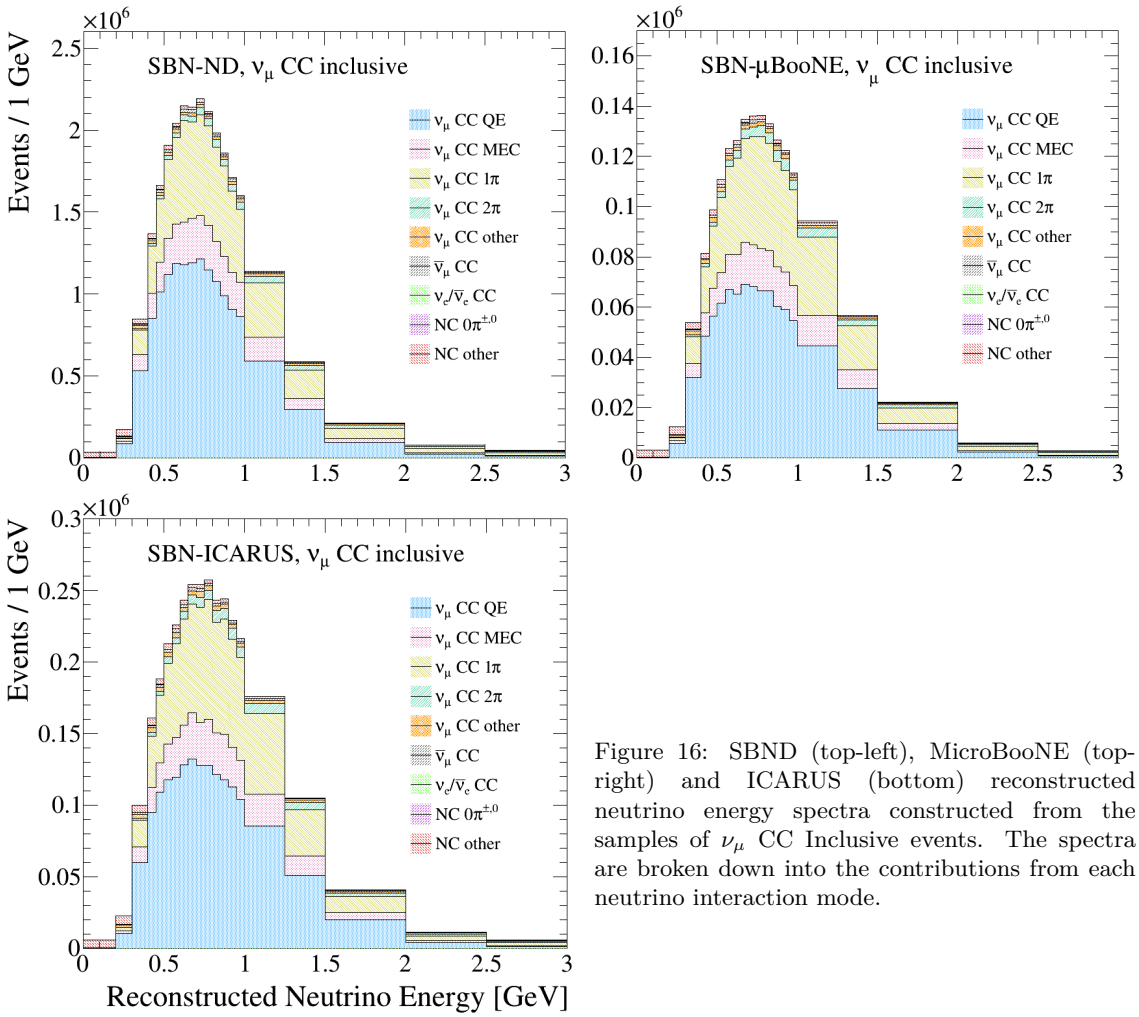

Figure 16: SBND (top-left), MicroBooNE (top-right) and ICARUS (bottom) reconstructed neutrino energy spectra constructed from the samples of ν_μ CC Inclusive events. The spectra are broken down into the contributions from each neutrino interaction mode.

8. Oscillation Sensitivity Calculations and Discussion

8.1. Muon-neutrino disappearance

8.1.1. Event rates in the SBN program

The reconstructed neutrino energy spectra which are the inputs to the oscillation sensitivity fits are presented for each of the three SBN detectors in the ν_μ CC Inclusive samples in Figure 16. The spectra are broken down into the pre-FSI neutrino interaction modes, in order to demonstrate the signal and background contributions to the samples.

The top left plot of Figure 17 shows the ν_μ disappearance statistical-only exclusion contour

and allowed region. The injected point $\Delta m^2_{41} = 1.32$ eV^2, $sin^2 2\theta_{\mu\mu} = 0.007$, used when producing the global best fit allowed region is shown along with two further points on the exclusion contour at $\Delta m^2_{41} = 1$ eV^2, $sin^2 2\theta_{\mu\mu} = 0.0185$ and $\Delta m^2_{41} = 100$ eV^2, $sin^2 2\theta_{\mu\mu} = 0.0065$. ν_μ appearance spectra are produced using oscillation parameters corresponding to each of these three points for each of the three SBN detectors. The ratio of each of these oscillated spectra to the nominal for each detector are shown in the the remaining plots in Figure 17 and highlight the expected oscillation signal.

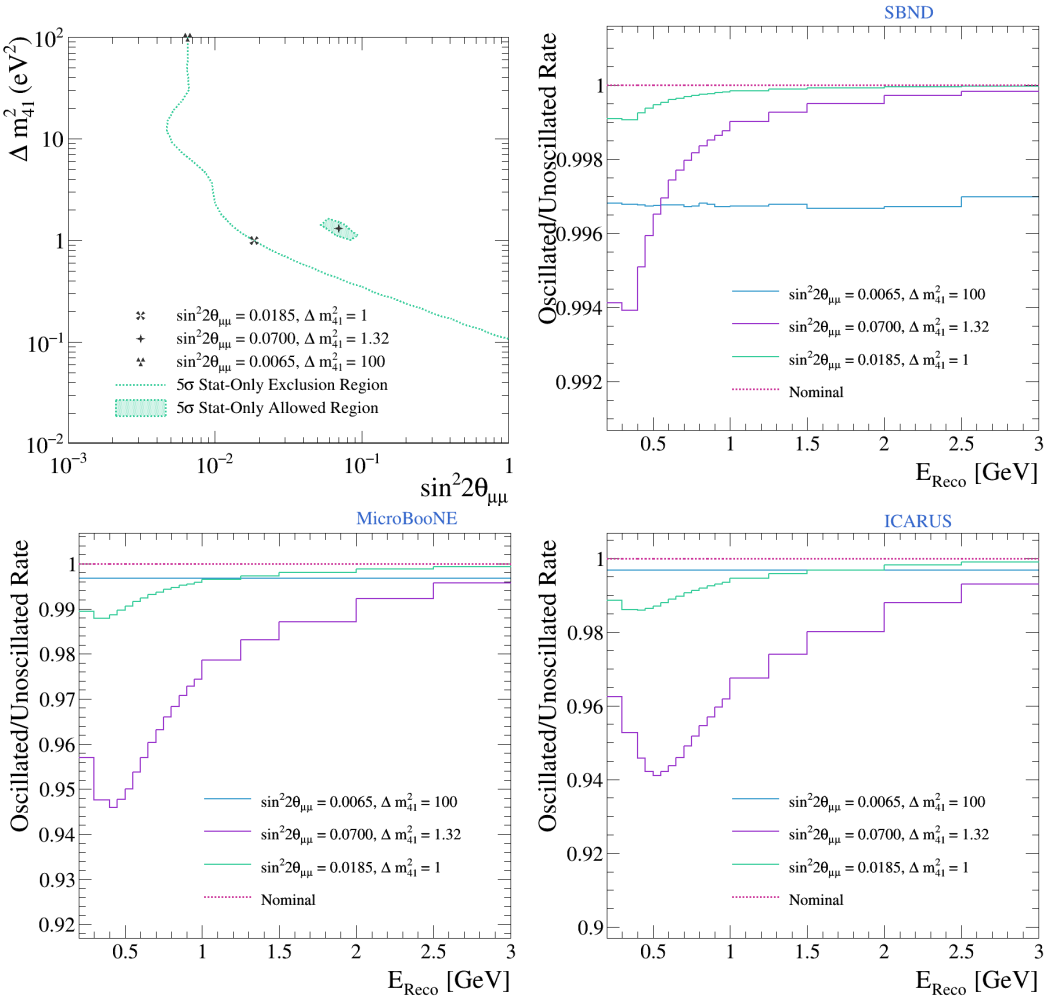

Figure 17: ν_μ disappearance stat-only exclusion contour and allowed region. The global best fit injected point at $sin^2 2\theta_{\mu\mu} = 0.007$, $\Delta m^2_{41} = 1.32$ eV^2 used for the allowed region is shown along with two further points at $sin^2 2\theta_{\mu\mu} = 0.0185$, $\Delta m^2_{41} = 1$ eV^2 and $sin^2 2\theta_{\mu\mu} = 0.00165$, $\Delta m^2_{41} = 100$ eV^2 (top left). The ratio of spectra with oscillation parameters corresponding to the three points mentioned versus nominal are shown for sbnd (top right), MicroBooNE (bottom left) and ICARUS (bottom right).

8.1.2. Cross-fitter event rate and oscillation sensitivity validation, no systematic variations, ν_μ disappearance

This section will outline comparisons performed between the three fitters to ensure the independent oscillation implementation methods yield comparable event rate spectra when produced using the same sample as input. The first iteration of this cross-fitter validation is performed with no systematic parameter variations, consequently the event rates observed by each fitter should be identical to one another.

Event rates are calculated by each fitter at three physical points in the oscillation parameter space. One hypothesis assumes no oscillations, the other two are chosen to represent slow and fast oscillations, based on regions of interest for the SBN sensitivity.

1. No oscillations occur: $\sin^2 2\theta_{\mu\mu} = 0, \Delta m^2_{41} = 0$
2. Low mass splitting: $\sin^2 2\theta_{\mu\mu} = 3 \times 10^{-3}, \Delta m^2_{41} = 2$
3. High mass splitting: $\sin^2 2\theta_{\mu\mu} = 2 \times 10^{-3}, \Delta m^2_{41} = 100$

8.1.3. Characteristics of the systematic uncertainties in VALOR

Figure 18 shows the integrated event rate spectra in each of the three detectors and two sample topologies with 1σ error envelopes corresponding from the uncertainty contributions from the full set of interaction, flux and pseudo-detector systematic parameters. The integrated event rates in each detector are given in Table 21 alongside the 1σ statistical and systematic uncertainties. All events are contained within the fiducial of each detector.

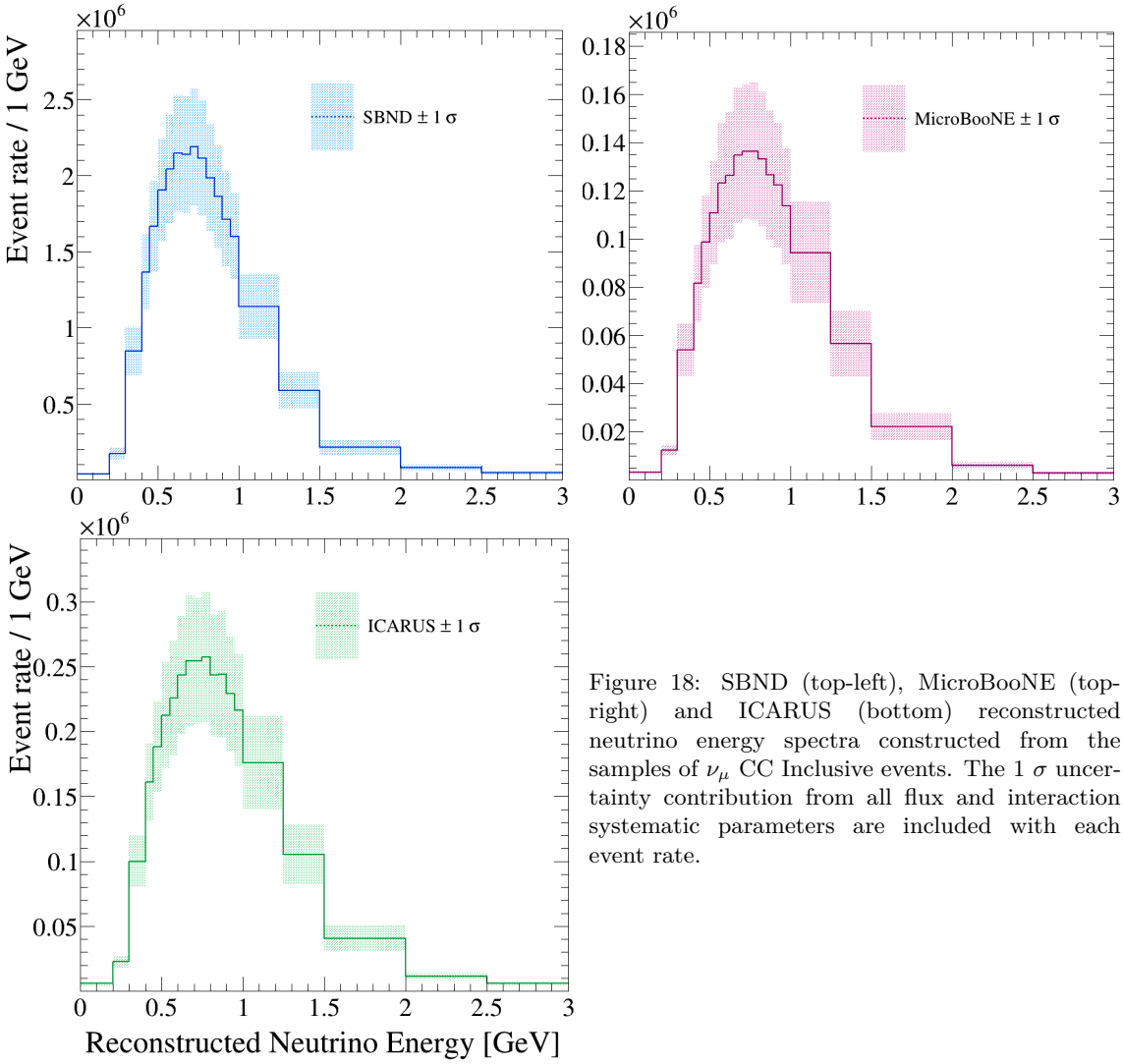

Figure 18: SBND (top-left), MicroBooNE (top-right) and ICARUS (bottom) reconstructed neutrino energy spectra constructed from the samples of ν_μ CC Inclusive events. The 1 σ uncertainty contribution from all flux and interaction systematic parameters are included with each event rate.

Detector	ν_μ CC Inclusive		
	Rate	Stat. %	Syst. %
SBND	1,885,340	0.07	18.85
MicroBooNE	135,400	0.27	21.70
ICARUS	254,200	0.20	20.40

Table 21: SBN event rates as inputs to the sensitivity study following the pseudo-selection of ν_μ CC Inclusive events scaled to the full 6.6×10^{20} POT in SBND and ICARUS and 13.2×10^{20} POT in MicroBooNE. Statistical and systematic uncertainties are quoted separately as a percentage of the full event rate. All events are contained within the fiducial volume.

8.1.4. Cross-fitter systematic validation

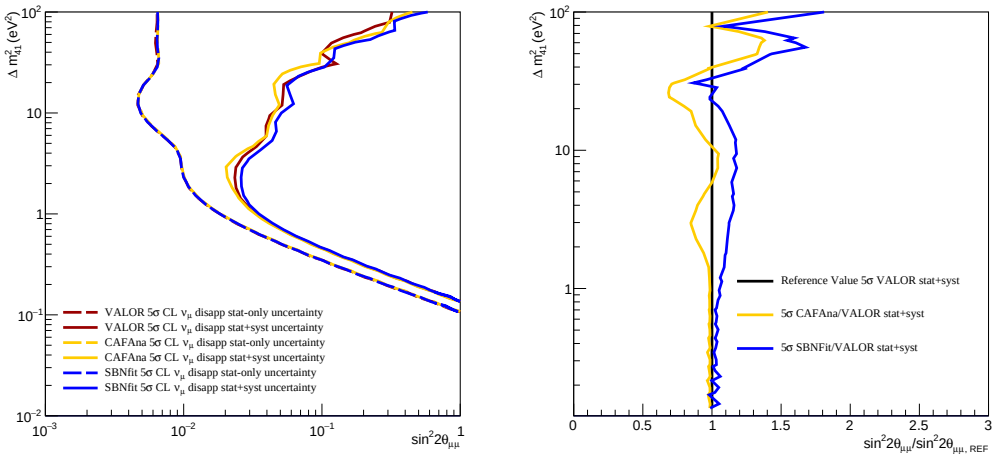

Figure 19: Comparison of the SBN ν_μ disappearance exclusion sensitivities from the VALOR, SBNFit and CAFAna fitting groups for statistical-only and statistical plus flux and interaction systematics (left). Ratio of the contours including systematics from the different fitters (right).

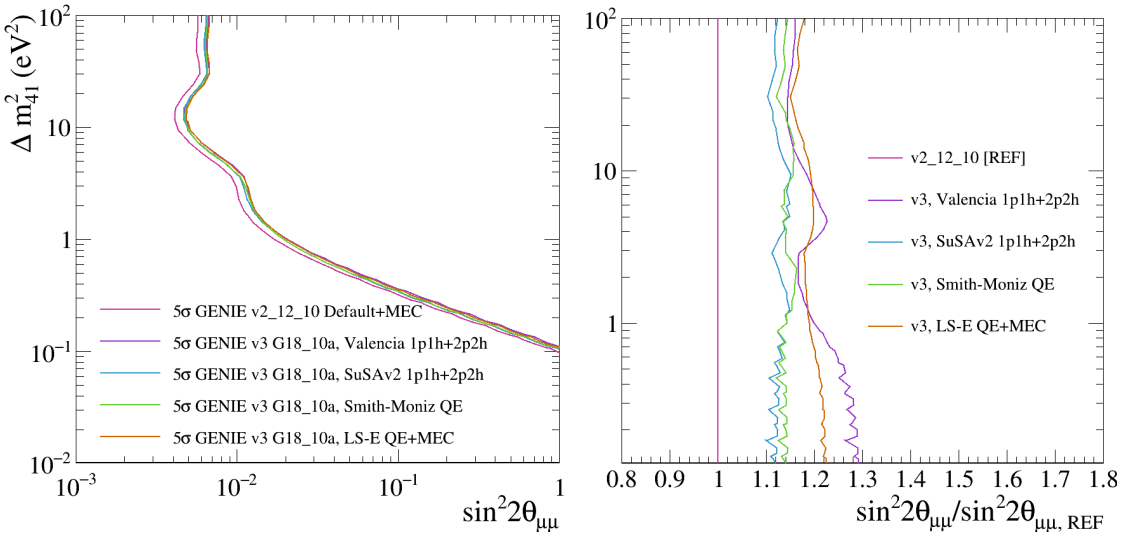

Figure 20: Variations to the SBND+ICARUS statistics-only sensitivity when changing the theoretical model used in the construction of the sample. The left plot shows the region of oscillation parameter space each model is sensitive to. The right plot shows the relative location of the 5σ contour in $\sin^2 2\theta_{\mu\mu}$ space for each model, with respect to the GENIE v2_12_10 Default+MEC model. The fractional contours are shown across the active Δm^2_{41} phase space.

8.1.5. Oscillation sensitivities

Impact of multiple theoretical models

The SBN sterile oscillation sensitivity in this study was calculated following joint SBND and ICARUS fits using each of the model configurations defined in section 3.3. Since the systematic parameters were defined and validated in section 6.4.1 for a single model configuration, only statistical exclusion contours were constructed in this comparison.

The plots in Figure 20 therefore demonstrate the impact of the shape and rate variations between the energy distributions of the samples on the oscillation sensitivity. The left-hand plot shows that the most substantial variation is between GENIE v2 and all model configurations from GENIE v3, due to the almost 25% reduction in the event rates in each case. The similarities between the GENIE v3 configurations arise because the only the QE+2p2h models are altered.

The right-hand plot in Figure 20 provides slightly more information about the relative sensitivities. Across the Δm^2_{41} parameter space, the ratio of $\sin^2 2\theta_{\mu\mu}$ between each model configuration and GENIE v2_12_10 Default+MEC model is shown. A higher fraction corre-

sponds to a larger value of $\sin^2 2\theta_{\mu\mu}$ at the point where the contour is drawn, and therefore to a reduction in the sensitivity.

Although there are statistical fluctuations in the region of the contour in which ICARUS is most-sensitive, it is clear that the largest model variations occur in this low-Δm^2_{41} range. In addition, when considering the region above $\Delta m^2_{41} > 8$ eV^2, the GENIE v3 LS-E QE+MEC model appears to have the least sensitivity to the sterile oscillations, however when $\Delta m^2_{41} < 1$ eV^2, it is the Valencia 1p1h+2p2h model which is the least sensitive. This demonstrates the model-dependence of the L/E distribution.

Impact of systematic groups

Having assessed the sensitivity of SBN to observing sterile neutrino oscillations through various statistical-only fits, studies of how this sensitivity changes with the inclusion of systematics were then performed. The systematic parameter sets defined and quantified in section 5 were added to the fits individually. The left plot in Figure 21 shows the exclusion contours for each of the flux, proposal interaction, modern interaction and proposal+modern interaction systematics with respect to the statistical-only sensitivity. The impact in the region where $\Delta m^2_{41} > 1$ eV^2 is immediately apparent, and is exacerbated in the right-hand ratio plot.

The flux systematics conduce the largest reduction in sensitivity in this region, however these parameters have been thoroughly validated by both the MiniBooNE and MicroBooNE experiments, and are unlikely to be constrained much further. The proposal interaction systematic parameters contribute the smallest reduction to the sensitivity whilst the full interaction parameter set has a comparable effect to the detector systematics. Some of these parameters are still being constrained and therefore may have their impact reduced. Ultimately, the overall interaction systematic contribution is model-dependent, the impact of which cannot be tested here.

Impact of the three SBN detectors

The statistical contributions to the sterile oscillation sensitivity from each SBN detector is shown in the left-hand plot of Figure 22. Combining the near and far detectors in the fits shows a substantial improvement to the sensitivity compared to their individual contributions. Adding in the MicroBooNE detector improves the sensitivity further still, across most of the parameter space.

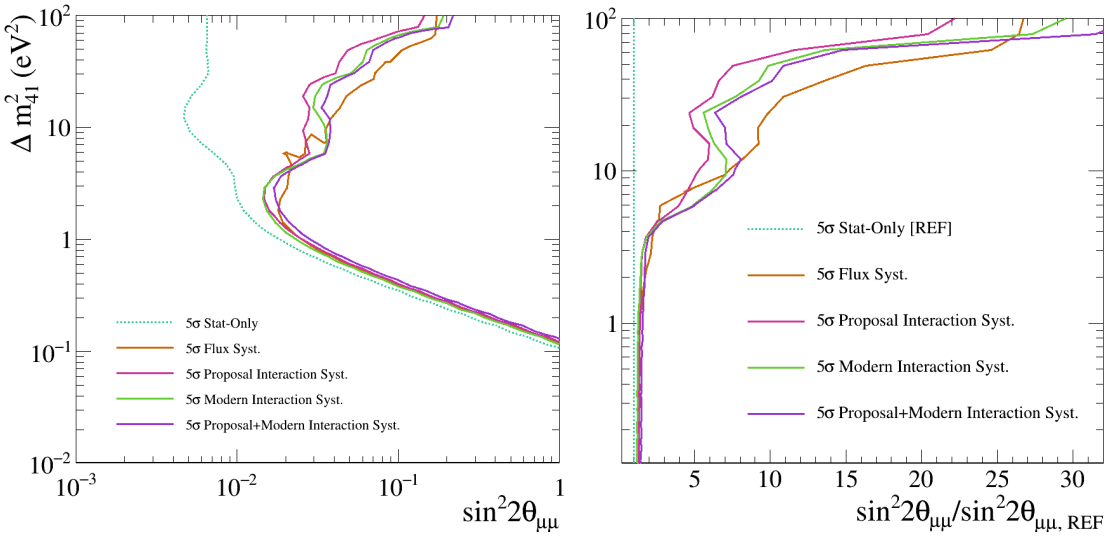

Figure 21: The left plot shows the reduction in sensitivity from the stat-only contour when including each set of systematic parameters in the fits. The right plot shows the relative location of each systematic contour in $\sin^2 2\theta_{\mu\mu}$ space, with respect to the statistical-only case, for the active region of Δm^2_{41} phase space.

The left-hand plot in Figure 22 also highlights the locations in which each detector is most sensitive. The short baseline of SBND lends itself to the region in which $\Delta m^2_{41} > 4$ eV^2, MicroBooNE improves the sensitivity between $1 < \Delta m^2_{41} < 4$ eV^2 and ICARUS, the far detector, is most sensitive below $\Delta m^2_{41} < 1$ eV^2.

The ν_μ CC Inclusive fits used to create the contours in the right-hand plot in Figure 22 include the flux, interaction and pseudo-detector systematic parameters. This quantifies the substantial reduction in sensitivity when adding systematics to the individual detector analyses, whilst also highlighting the level of improvement in the sensitivity which is possible when combining multiple detectors in the joint analysis. The improvement comes primarily from combining the near and far detector in the fits, with a slight increase in sensitivity in some regions of the parameter space (where $\Delta m^2_{41} > 1$ eV^2) from the inclusion of MicroBooNE.

8.1.6. SBN allowed-region sensitivity studies

This section will present allowed-region (3+1) sterile neutrino oscillation sensitivities following joint inclusive three-detector SBN fits with all flux and interaction systematic parameters. Each contour will depict the region of $\sin^2 2\theta_{\mu\mu}$, Δm^2_{41} parameter space in which the SBN experiment is sensitive to an injected hypothesis at the 5σ confidence level. The injec-

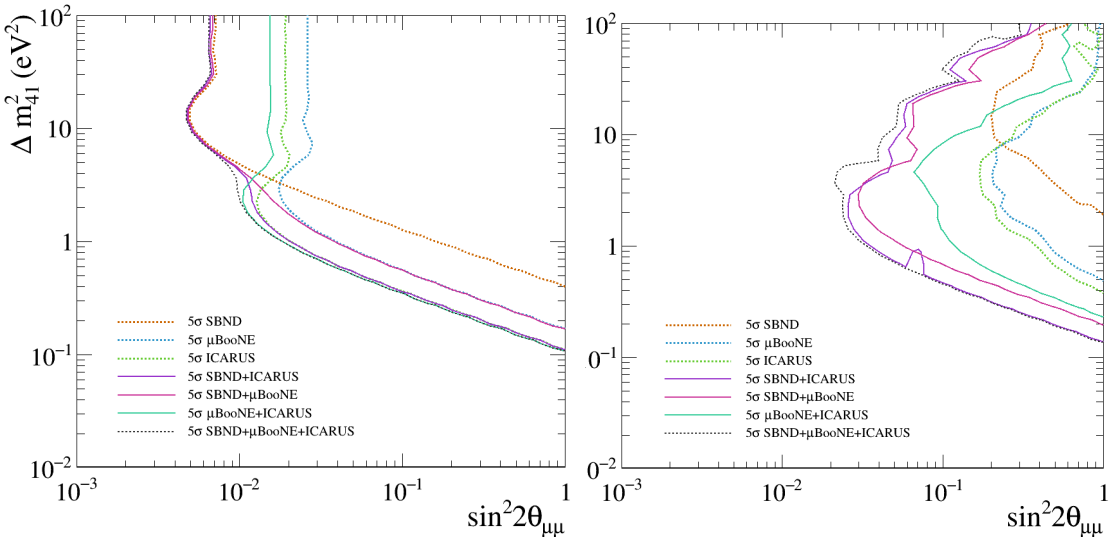

Figure 22: Contributions to the SBN sterile oscillation sensitivity from each detector and combinations of detectors in the SBN program. The statistical-only plots in the left-hand figure show that SBND is most sensitive to the region $\Delta m^2_{41} > 4$ eV^2, MicroBooNE is sensitive between $1 < \Delta m^2_{41} < 4$ eV^2 and ICARUS is most sensitive below $\Delta m^2_{41} < 1$ eV^2. The right-hand figure includes flux and interaction systematic parameters and highlights the considerable improvement in the oscillation sensitivity when including multiple detectors in the fits.

tion point corresponds to the global best fit values, $\sin^2 2\theta_{\mu\mu} = 0.07$ and $\Delta m^2_{41} = 1.32$ [3]. All fits are performed with the ν_μ CC Inclusive sample of pseudo-reconstructed events, generated using the GENIE v3 G18_10a Valencia 1p1h+2p2h model.

Figure 23 shows the statistical-only allowed region along with the impact of adding the flux and interaction systematic parameters, which results in a decrease in sensitivity from the statistical-only case in all directions. Two fitting frameworks were used in the construction of these sensitivities, SBNFit and VALOR.

8.1.7. Global sensitivity studies

Finally, the SBN sensitivity to ν_μ disappearance under the (3+1) sterile neutrino hypothesis is compared to the existing global data. The SBN contours involved in this comparison were constructed with the three-detector inclusive joints fits, and include all systematic parameters. Figure 24 demonstrates how the 5σ SBN exclusion confidence limits compare with MiniBooNE and MINOS/MINOS+ data at the 90% confidence level [39] [40] as well as eight years of IceCube data at the 90 and 99% confidence levels [41]. In IceCube, $\theta_{\mu\mu}$ depends on both θ_{24} and θ_{34}, however in this particular dataset the assumption $\theta_{34} = 0$

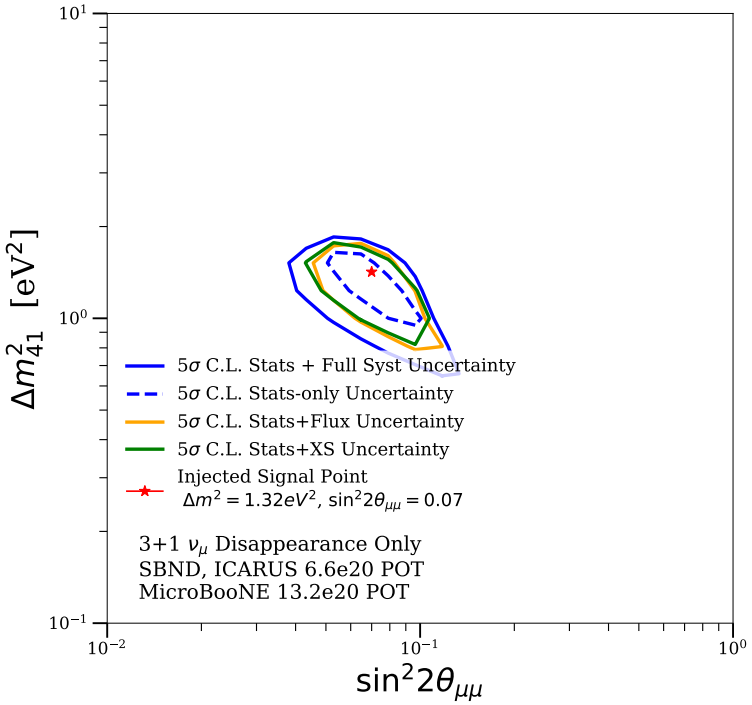

Figure 23: SBN allowed region contours following the three-detector inclusive joint fits of ν_μ CC Inclusive sample with the global best fit injected point $\Delta m^2_{41} = 1.32$, $\sin^2 2\theta_{\mu\mu} = 0.07$. The allowed regions are generated by SBNfit, where the green, orange and blue solid contours are 5σ confidence level contours when considering statistical + cross section, statistical + flux, and statistical + flux + cross section systematic uncertainties respectively.

from [41] allows for the approximation $\theta_{24} = \theta_{\mu\mu}$.

The SBN sensitivity is comparable to that of MINOS/MINOS+ in the region $\Delta m^2_{41} > 1\text{eV}^2$, and supersedes the MiniBooNE sensitivity across the entire parameter space. The IceCube 99% exclusion limit is strong for $\Delta m^2_{41} < 1$ eV^2 and reduces as the mass splitting increases, in the opposite way to the SBN sensitivity. The IceCube 90% closed contour does not quite overlap with the global best-fit point in the 5σ SBN allowed region.

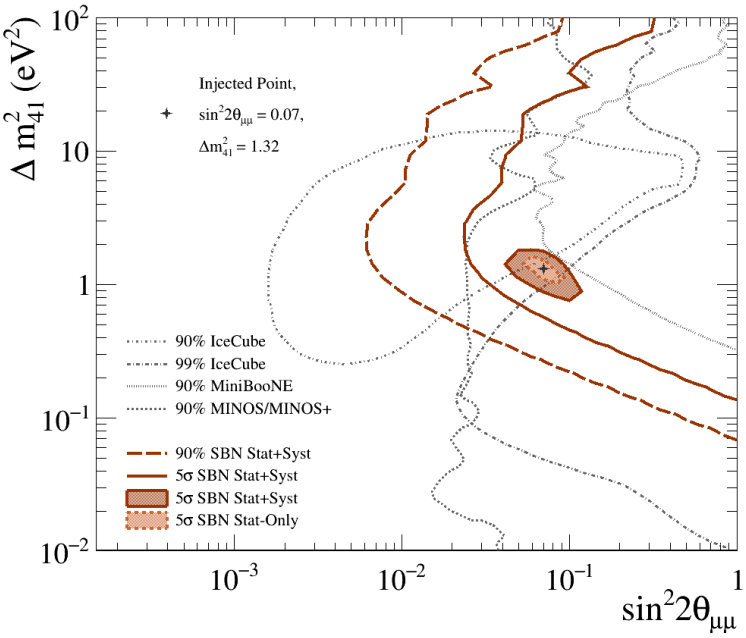

Figure 24:
This plot includes two confidence intervals (90% and 5σ) of the SBN exclusion-region sensitivities to ν_μ disappearance under the (3+1) sterile neutrino hypothesis along with the 5σ statistics-only and statistics+systematics allowed-region sensitivities. All interaction and flux systematic parameters are included in the three-detector inclusive joint fits. Also added to the plot are the contours produced with MiniBooNE data [39], MINOS/MINOS+ data [40] and two confidence intervals from eight years of IceCube data [41]. The confidence levels are specified for each contour in the legend.

8.2. Electron-neutrino appearance

8.2.1. Event rates in the SBN program

The reconstructed neutrino energy spectra which are the inputs to the oscillation sensitivity fits are presented for each of the three SBN detectors in the ν_e CC Inclusive samples in Figure 25. The spectra are broken down into the pre-FSI neutrino interaction modes, in order to demonstrate the signal and background contributions to the samples.

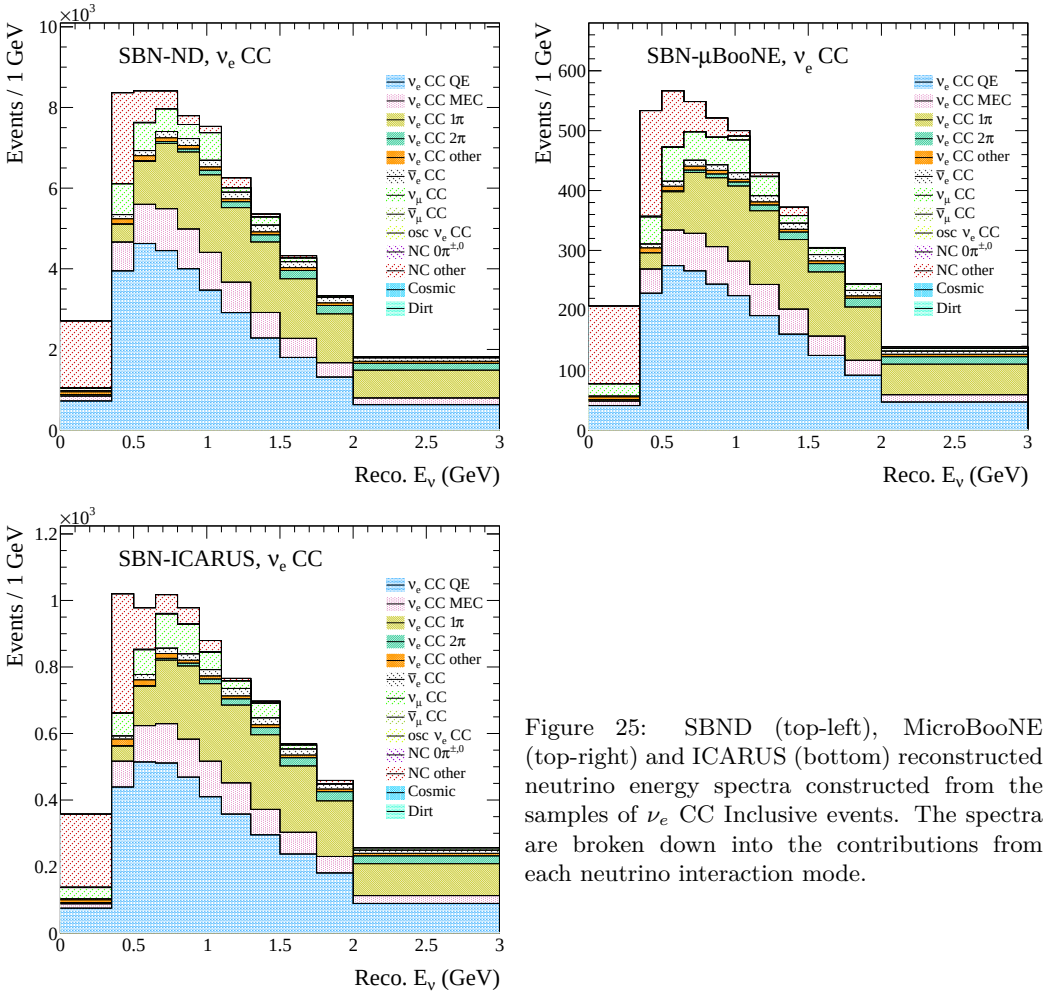

Figure 25: SBND (top-left), MicroBooNE (top-right) and ICARUS (bottom) reconstructed neutrino energy spectra constructed from the samples of ν_e CC Inclusive events. The spectra are broken down into the contributions from each neutrino interaction mode.

The top left plot of Figure 26 shows the ν_e appearance stat only exclusion contour and allowed region. The injected point $\Delta m^2_{41} = 1.32$ eV^2, $sin^2 2\theta_{\mu e} = 0.003$, used when producing the allowed region is shown along with two further points on the exclusion contour at

$\Delta m^2_{41} = 1$ eV^2, $sin^2 2\theta_{\mu e} = 0.0014$ and $\Delta m^2_{41} = 100$ eV^2, $sin^2 2\theta_{\mu e} = 0.0005$. ν_e appearance spectra are produced using oscillation parameters corresponding to each of these three points for each of the three SBN detectors. The ratio of each of these oscillated spectra to the nominal for each detector are shown in the the remaining plots in Figure 26 and highlight the expected oscillation signal.

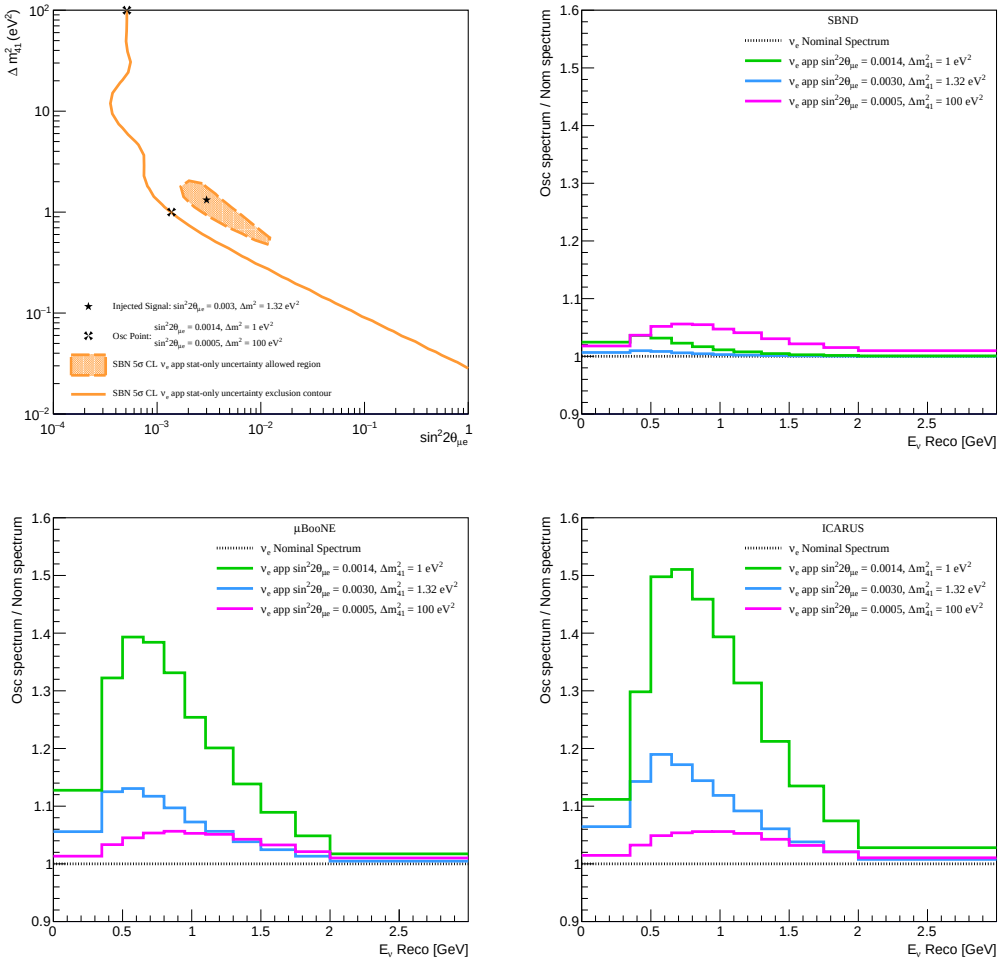

Figure 26: ν_e appearance stat-only exclusion contour and allowed region. The injected point at $sin^2 2\theta_{\mu e} = 0.003$, $\Delta m^2_{41} = 1.32$ eV^2 used for the allowed region is shown along with two further points at $sin^2 2\theta_{\mu e} = 0.0014$, $\Delta m^2_{41} = 1$ eV^2 and $sin^2 2\theta_{\mu e} = 0.0005$, $\Delta m^2_{41} = 100$ eV^2 (top left). The ratio of spectra with oscillation parameters corresponding to the three points mentioned versus nominal are shown for sbnd (top right), MicroBooNE (bottom left) and ICARUS (bottom right).

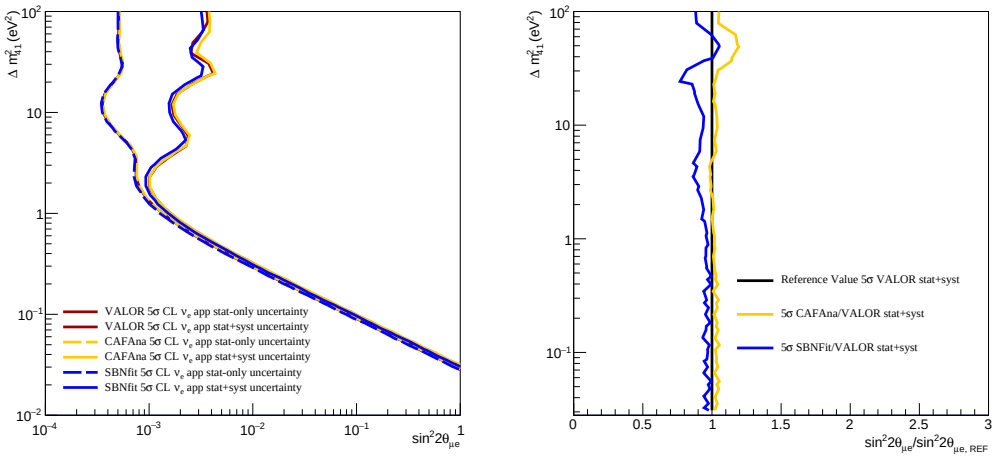

Figure 27: Comparison of the SBN ν_e appearance exclusion sensitivities from the VALOR, SBNFit and CAFAna fitting groups for statistical-only and statistical plus flux and interaction systematics (left). Ratio of the contours including systematics from the different fitters (right).

8.2.3. Oscillation sensitivities

Impact of systematic groups

Similarly to the ν_μ case, Figure 28 shows the impact of flux, proposal interaction, modern interaction and proposal+modern interaction systematics on the ν_e appearance sensitivity compared to the stat-only case. As is the case for ν_μ disappearance, the impact of the systematics is very apparent at $\Delta m^2_{41} > 1$ eV^2, however it should be noted that the relative size of the impact from each systemtic group is quite different. In this case, the modern interaction systematics dominate, whilst the proposal interaction systematics have the smallest impact.

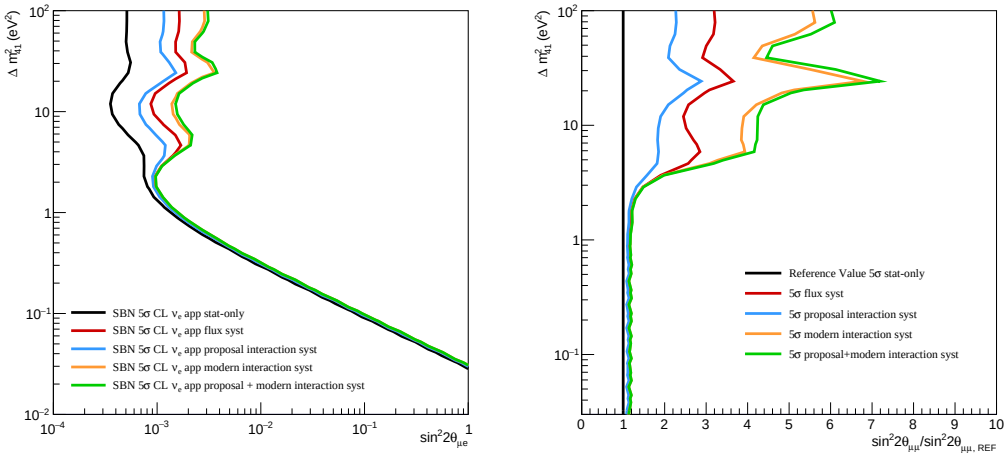

Figure 28: The left plot shows the reduction in sensitivity from the stat-only contour when including each set of systematic parameters in the fits and was produced by the VALOR fitting framework. The right plot shows the relative location of each systematic contour in $\sin^2 2\theta_{\mu e}$ space, with respect to the statistical-only case for the active region of Δm^2_{41} phase space.

Impact of the three SBN detectors

The contribution of each detector and combination of detectors to the overall SBN ν_e appearance sensitivity are shown in Figure 29 for the stat-only case and for fits including flux and interaction systematics. For $\Delta m^2_{41} > \sim 3$ eV^2, the sensitivity is dominated by the SBND detector and for $\Delta m^2_{41} < \sim 3$ eV^2 the sensitivity is dominated by ICARUS. Combining fits from both SBND and ICARUS gives the most dramatic improvement to the sensitivity and with the inclusion of the MicroBooNE detector the sensitivity improves a little further.

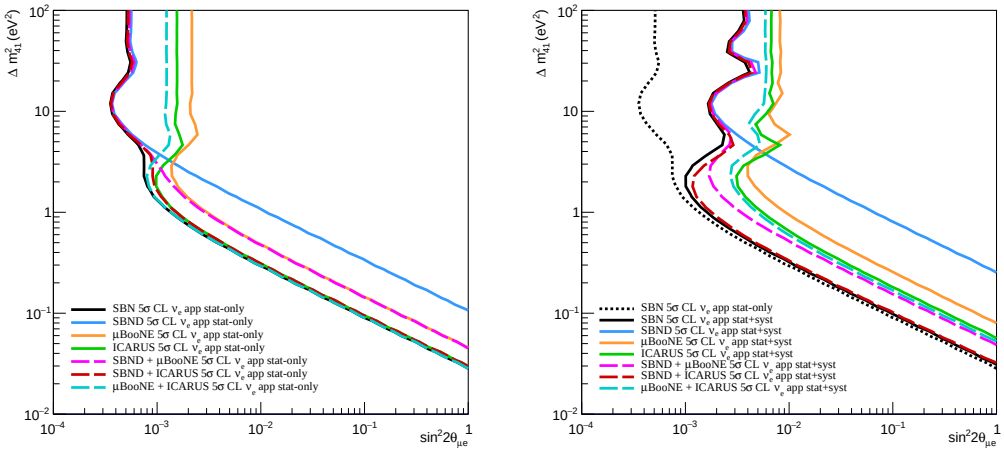

Figure 29: Contributions to the SBN ν_e appearance sterile oscillation sensitivity from each detector and combinations of detectors in the SBN programme produced by the VALOR fitting framework. The statistical-only plots in the left-hand figure show that SBND is most sensitive to the region $\Delta m^2_{41} > \sim 3$ eV^{2}and ICARUS is most sensitive to $\Delta m^2_{41} < \sim 3$ eV^2. The right-hand figure includes flux and interaction systematic parameters and highlights the considerable improvement in the oscillation sensitivity when including multiple detectors in the fits.

8.2.4. SBN allowed-region sensitivity studies

The statistical only allowed region and the allowed region produced when including the flux and interaction systematic sets resulting from an injected point of $\Delta m^2_{41} = 1.32$ eV^2, $\sin^2 2\theta_{\mu e} = 0.003$ are shown in Figure 30 and 31.

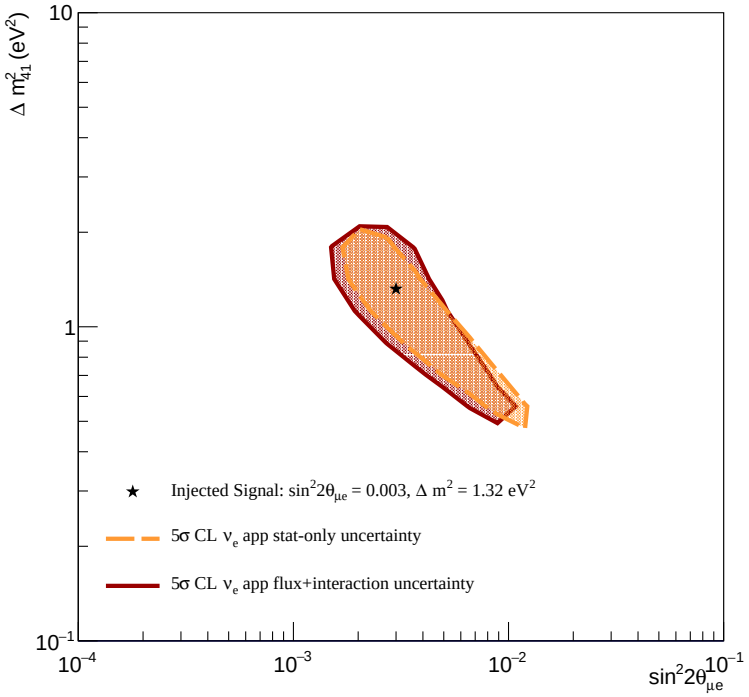

Figure 30: SBN ν_e appearance allowed region contours produced by the VALOR fitting framework. The injected point $\Delta m^2_{41} = 1.32$ eV^2, $\sin^2 2\theta_{\mu e} = 0.003$, is surrounded by the statistical-only contour in orange and the flux and interaction systematic parameters are added to the fits in red.

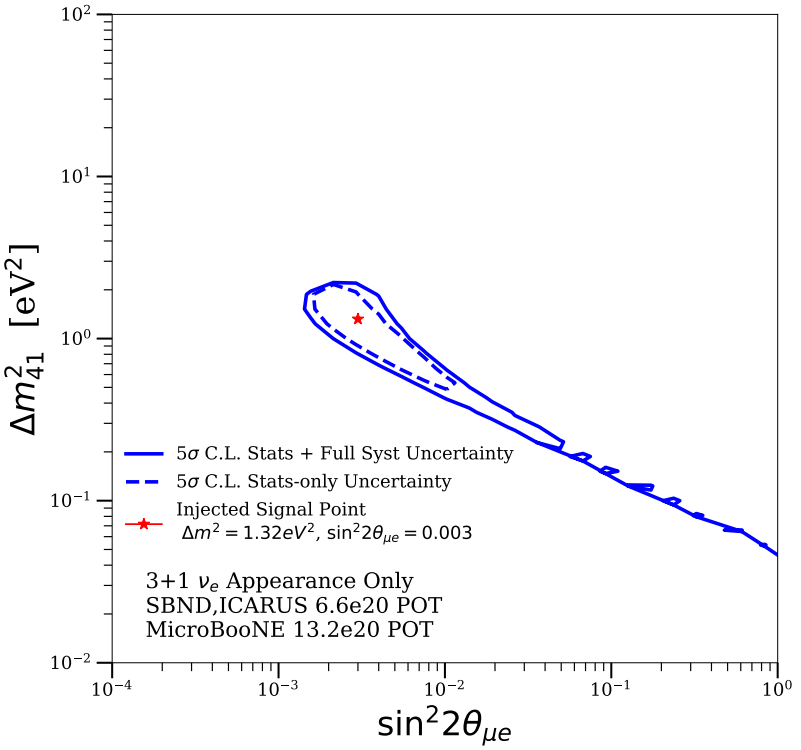

Figure 31: SBN ν_e appearance allowed region contours produced by the SBNfit fitting framework. The injected point $\Delta m^2_{41} = 1.32$ eV^2, $\sin^2 2\theta_{\mu e} = 0.003$, is surrounded by the 5σ confidence level allowed region contours, with statistical-only contour in dashed line and statistical and flux, cross section systematic contour in solid line.

8.2.5. Global sensitivity studies

The SBN ν_e appearance statistical only and statistical + flux and interaction systematic contours at the 5σ confidence level are overlayed with global data. Figure 32 shows the comparison of the expected SBN results with the 99% confidence level allowed region from LSND and the 99% confidence exclusion contour from KARMEN [42][43].

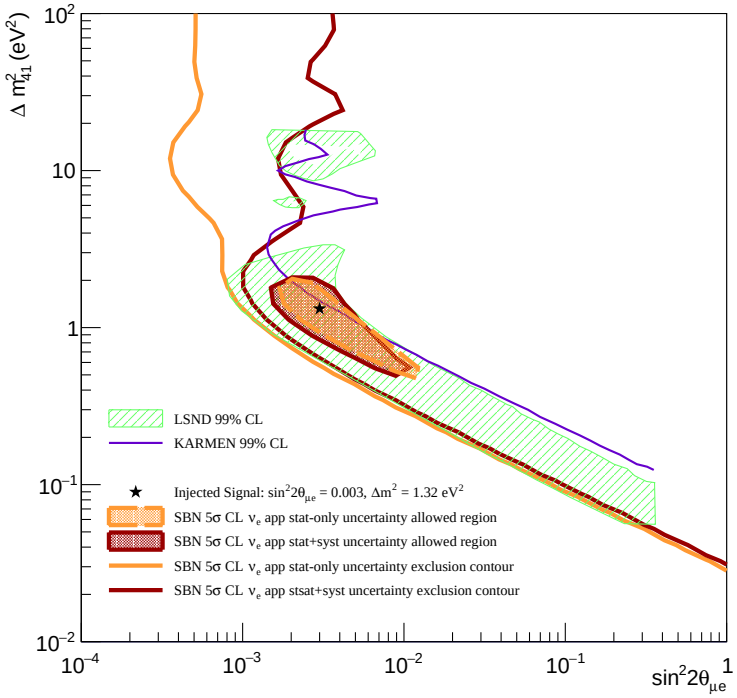

Figure 32: The SBN exclusion and allowed-region sensitivities to ν_e appearance under the (3+1) sterile neutrino hypothesis produced by the VALOR fitting framework. All interaction and flux systematic parameters are included in the fits. Also added to the plot are the allowed region produced with LSND data (green) [42] and the contour from KARMEN data (purple) [43]. The confidence levels are specified for each contour in the legend.

8.3. Electron-neutrino disappearance

8.3.1. Event rates in the SBN program

The top left plot of Figure 33 shows the ν_e disappearance stat only exclusion contour and allowed region. The injected point, $\Delta m^2_{41} = 3$ eV^2 , $sin^2 2\theta_{ee} = 0.4$, used when producing the allowed region is shown along with two further points on the exclusion contour at $\Delta m^2_{41} = 1$ eV^2 and $\Delta m^2_{41} = 100$ eV^2. ν_e disappearance spectra are produced using oscillation parameters corresponding to each of these three points for each of the three SBN detectors. The ratio of each of these oscillated spectra to the nominal for each detector are shown in the the remaining plots in Figure 33 and highlight the expected oscillation signal.

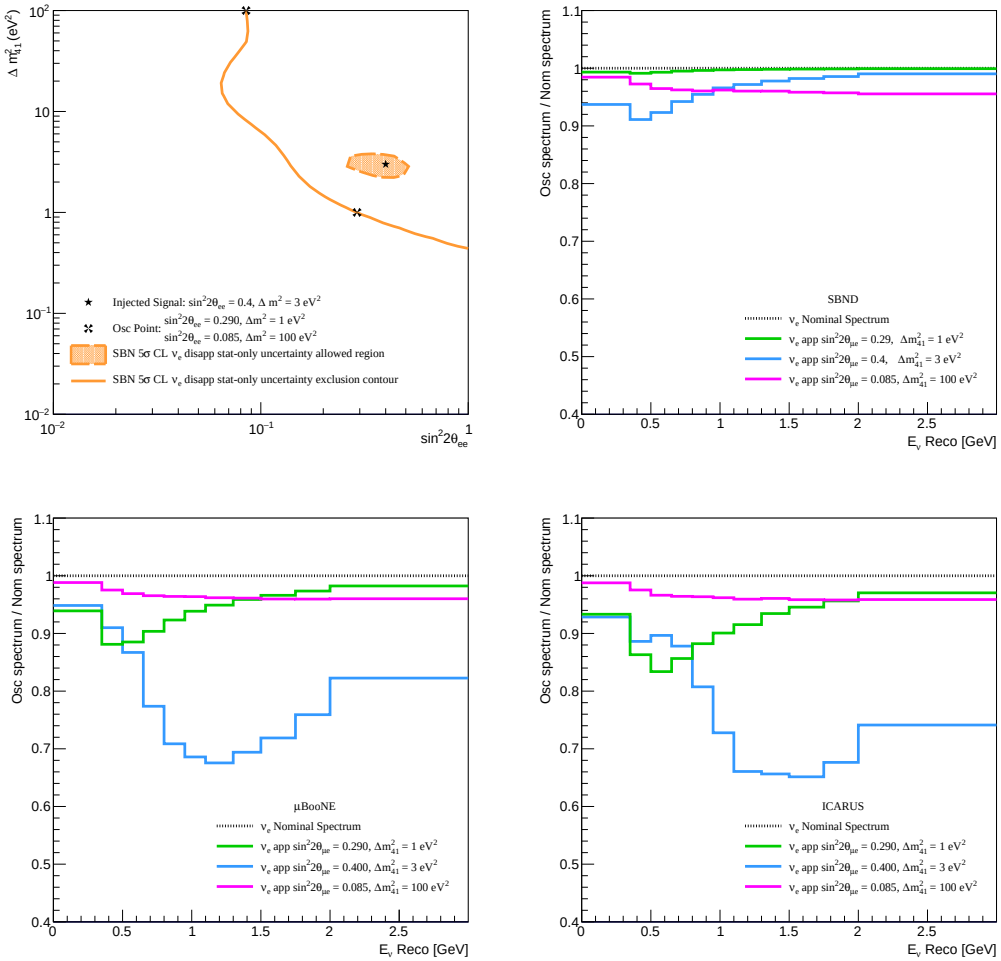

Figure 33: ν_e disappearance stat-only exclusion contour and allowed region. The injected point at $sin^2 2\theta_{ee} = 0.4$, $\Delta m^2_{41} = 3$ eV^2 used for the allowed region is shown along with two further points at $sin^2 2\theta_{ee} = 0.29$, $\Delta m^2_{41} = 1$ eV^2 and $sin^2 2\theta_{ee} = 0.085$, $\Delta m^2_{41} = 100$ eV^2 (top left). The ratio of spectra with oscillation parameters corresponding to the three points mentioned versus nominal are shown for sbnd (top right), MicroBooNE (bottom left) and ICARUS (bottom right).

8.3.2. Oscillation sensitivities

Impact of systematic groups

Figure 34 shows the impact of flux, proposal interaction, modern interaction and proposal+modern interaction systematics on the ν_e disappearance sensitivity compared to the stat-only case. As is the case for both ν_μ disappearance and ν_e appearance, the impact of the systematics becomes much more noticeable for $\Delta m^2_{41} > 1$ eV^2. Emulating what was seen in the ν_e appearance case, the modern interaction systematics again have the largest impact, whilst the proposal interaction systematics have the smallest impact.

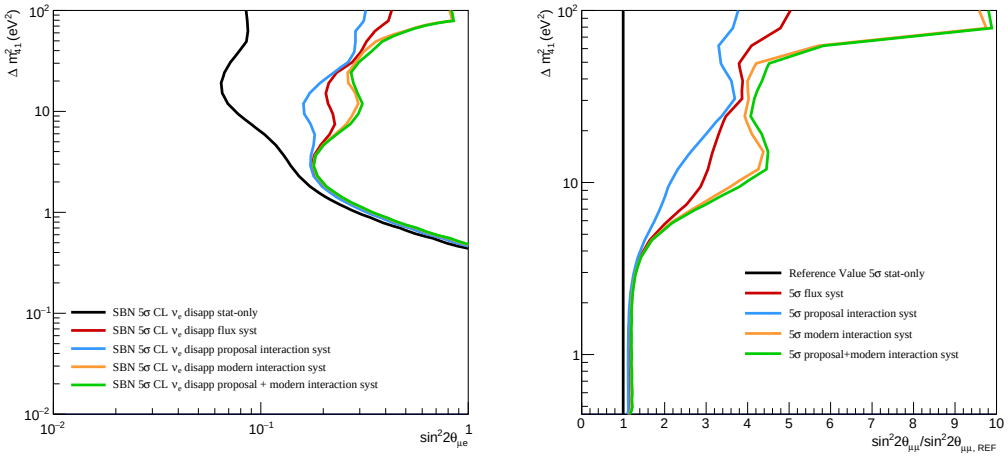

Figure 34: The left plot shows the reduction in sensitivity from the stat-only contour when including each set of systematic parameters in the fits and was produced by the VALOR fitting framework. The right plot shows the relative location of each systematic contour in $\sin^2 2\theta_{ee}$ space, with respect to the statistical-only case for the active region of Δm^2_{41} phase space.

Impact of the three SBN detectors

The contribution of each detector and combination of detectors to the overall SBN ν_e disappearance sensitivity are shown in Figure 35 for the stat-only case and for fits including flux and interaction systematics. For $\Delta m^2_{41} > \sim 3$ eV^2, the sensitivity is dominated by the SBND detector and for $\Delta m^2_{41} < \sim 3$ eV^2 the sensitivity is dominated by ICARUS. Combining fits from both SBND and ICARUS gives the most dramatic improvement to the sensitivity and with the inclusion of the MicroBooNE detector the sensitivity improves a little further.

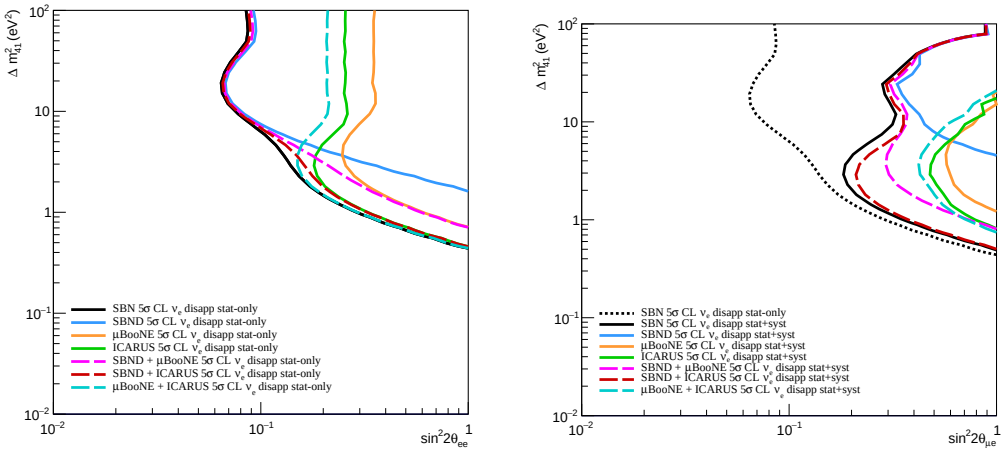

Figure 35: Contributions to the SBN ν_e disappearance sterile oscillation sensitivity from each detector and combinations of detectors in the SBN programme produced by the VALOR fitting framework. The statistical-only plots in the left-hand figure show that SBND is most sensitive to the region $\Delta m^2_{41} > 3$ eV^2 and ICARUS is most sensitive below $\Delta m^2_{41} < 3$ eV^2. The right-hand figure includes flux and interaction systematic parameters and highlights the considerable improvement in the oscillation sensitivity when including multiple detectors in the fits.

Full systematic sensitivity studies

8.3.3. SBN allowed-region sensitivity studies

The statistical only allowed region and the allowed region produced when including the flux and interaction systematic sets resulting from an injected point of $\Delta m^2_{41} = 3$ eV^2, $\sin^2 2\theta_{ee} = 0.4$ are shown in Figure 36.

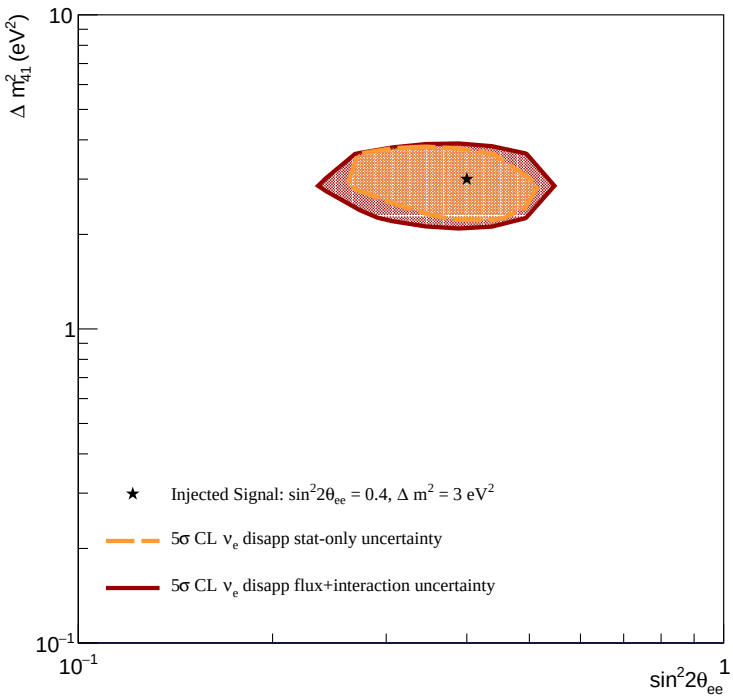

Figure 36: SBN ν_e disappearance allowed region contours produced by the VALOR fitting framework. The injected point $\Delta m^2_{41} = 3$ eV^2, $\sin^2 2\theta_{ee} = 0.4$, is surrounded by the statistical-only contour in orange and the flux and interaction systematic parameters are added to the fits in red.

8.3.4. Global sensitivity studies

The SBN ν_e disappearance statistical only and statistical + flux and interaction systematic contours at the 5σ confidence level are overlayed with global data. Figure 37 shows the comparison of the expected SBN results with the 90% and 68% confidence level allowed region and the 95% confidence level exclusion contour from T2K [44].

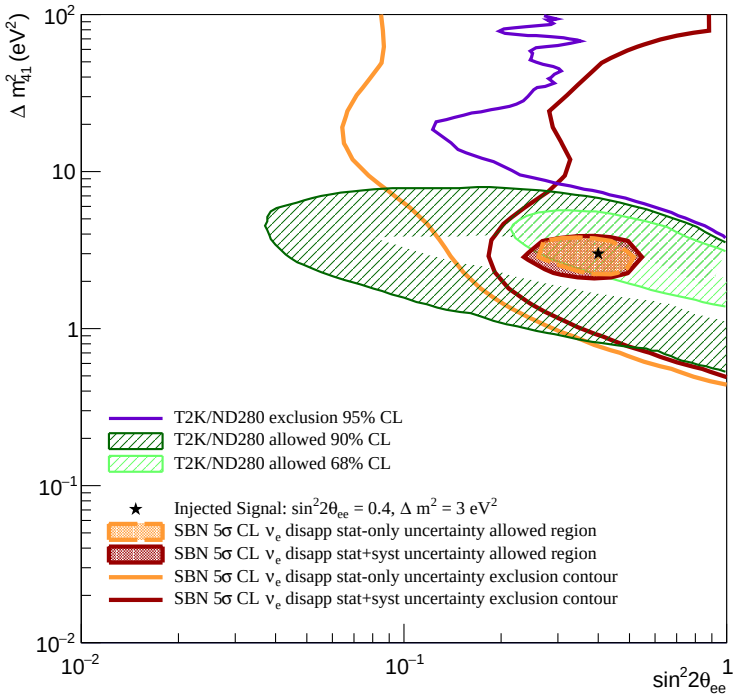

Figure 37: The SBN exclusion and allowed-region sensitivities to ν_e disappearance under the (3+1) sterile neutrino hypothesis produced by the VALOR fitting framework. All interaction and flux systematic parameters are included in the fits. Also added to the plot are the exclusion contour (purple) and two allowed regions (green) produced with T2K data [44]. The confidence levels are specified for each contour in the legend.

9. Summary

References

[1] D. Decamp, et al. (ALEPH), Determination of the Number of Light Neutrino Species, Phys. Lett. B 231 (1989) 519–529. doi:10.1016/0370-2693(89)90704-1.

[2] O. Adriani, et al. (L3), Determination of the number of light neutrino species, Phys. Lett. B 292 (1992) 463–471. doi:10.1016/0370-2693(92)91204-M.

[3] A. Diaz, C. Argüelles, G. Collin, J. Conrad, M. Shaevitz, Where Are We With Light Sterile Neutrinos? (2019). arXiv:1906.00045.

[4] P. Abratenko, et al. (MicroBooNE), First Measurement of Inclusive Muon Neutrino Charged Current Differential Cross Sections on Argon at E_ν ~0.8 GeV with the MicroBooNE Detector, Phys. Rev. Lett 123 (2019) 131801. doi:10.1103/PhysRevLett.123.131801. arXiv:1905.09694.

[5] C. Andreopoulos, et al., The GENIE Neutrino Monte Carlo Generator, Nucl. Instrum. Meth. A 614 (2010) 87–104. doi:10.1016/j.nima.2009.12.009. arXiv:0905.2517.

[6] C. Llewellyn Smith, Neutrino reactions at accelerator energies, Physics Reports 3 (1972) 261 – 379. URL: http://www.sciencedirect.com/science/article/pii/0370157372900105. doi:https://doi.org/10.1016/0370-1573(72)90010-5.

[7] J. Nieves, I. R. Simo, M. J. V. Vacas, Inclusive charged-current neutrino-nucleus reactions, Phys. Rev. C 83 (2011) 045501. URL: https://link.aps.org/doi/10.1103/PhysRevC.83.045501. doi:10.1103/PhysRevC.83.045501.

[8] G. Megias, et al., Meson-exchange currents and quasielastic predictions for charged-current neutrino-^{12}C scattering in the superscaling approach, Phys. Rev. D 91 (2015) 073004. doi:10.1103/PhysRevD.91.073004. arXiv:1412.1822.

[9] R. Smith, E. Moniz, NEUTRINO REACTIONS ON NUCLEAR TARGETS, Nucl. Phys. B 43 (1972) 605. doi:10.1016/0550-3213(75)90612-4, [Erratum: Nucl.Phys.B 101, 547 (1975)].

[10] H. Hassanabadi, A. Armat, L. Naderi, Relativistic Fermi-Gas Model for Nucleus, Found. Phys 44 (2014) 1188–1194. doi:10.1007/s10701-014-9836-7.

[11] L. Alvarez-Ruso, Neutrino interactions: Challenges in the current theoretical picture, Nuclear Physics B - Proceedings Supplements 229-232 (2012) 167 – 173. URL: http://www.sciencedirect.com/science/article/pii/S0920563212002447. doi:https://doi.org/10.1016/j.nuclphysbps.2012.09.027, neutrino 2010.

[12] L. Ahrens, et al., Measurement of Neutrino - Proton and anti-neutrino - Proton Elastic Scattering, Phys. Rev. D 35 (1987) 785. doi:10.1103/PhysRevD.35.785.

[13] T. Katori, Meson exchange current (mec) models in neutrino interaction generators (2013). arXiv:1304.6014.

[14] D. Rein, L. M. Sehgal, Neutrino-excitation of baryon resonances and single pion production, Annals of Physics 133 (1981) 79 – 153. URL: http://www.

sciencedirect.com/science/article/pii/0003491681902426. doi:https://doi.org/10.1016/0003-4916(81)90242-6.

[15] C. Berger, L. M. Sehgal, Lepton mass effects in single pion production by neutrinos, Phys. Rev. D 76 (2007) 113004. URL: https://link.aps.org/doi/10.1103/PhysRevD.76.113004. doi:10.1103/PhysRevD.76.113004.

[16] D. Rein, L. M. Sehgal, Coherent π^0 production in neutrino reactions, Nuclear Physics B 223 (1983) 29 – 44. URL: http://www.sciencedirect.com/science/article/pii/0550321383900901. doi:https://doi.org/10.1016/0550-3213(83)90090-1.

[17] C. Berger, L. Sehgal, PCAC and coherent pion production by low energy neutrinos, Phys. Rev. D 79 (2009) 053003. doi:10.1103/PhysRevD.79.053003. arXiv:0812.2653.

[18] A. Bodek, U. Yang, Higher twist, xi(omega) scaling, and effective LO PDFs for lepton scattering in the few GeV region, J. Phys. G 29 (2003) 1899–1906. doi:10.1088/0954-3899/29/8/369. arXiv:hep-ex/0210024.

[19] C. Andreopoulos, et al., Genie event generator, naming conventions, 2022. URL: https://hep.ph.liv.ac.uk/~costasa/genie/naming_conventions.html.

[20] S. A. et. al, Geant4—a simulation toolkit, Nuclear Instruments and Methods in Physics Research Section A: Accelerators, Spectrometers, Detectors and Associated Equipment 506 (2003) 250 – 303. URL: http://www.sciencedirect.com/science/article/pii/S0168900203013688. doi:https://doi.org/10.1016/S0168-9002(03)01368-8.

[21] E. Snider, G. Petrillo, LArSoft: toolkit for simulation, reconstruction and analysis of liquid argon TPC neutrino detectors, Journal of Physics: Conference Series 898 (2017) 042057. URL: https://doi.org/10.1088%2F1742-6596%2F898%2F4%2F042057. doi:10.1088/1742-6596/898/4/042057.

[22] M. Antonello, et al. (MicroBooNE, LAr1-ND, ICARUS-WA104), A Proposal for a Three Detector Short-Baseline Neutrino Oscillation Program in the Fermilab Booster Neutrino Beam (2015). arXiv:1503.01520.

[23] e. a. Ankowski, Measurement of through-going particle momentum by means of multiple scattering with the icarus t600 tpc, The European Physical Journal C 48 (2006) 667–676. URL: http://dx.doi.org/10.1140/epjc/s10052-006-0051-3. doi:10.1140/epjc/s10052-006-0051-3.

[24] A. A. Aguilar-Arevalo, et al. (MiniBooNE), The Neutrino Flux prediction at MiniBooNE, Phys. Rev D79 (2009) 072002. doi:10.1103/PhysRevD.79.072002. arXiv:0806.1449.

[25] R. e. a. Acciarri ((MicroBooNE Collaboration)), Booster neutrino flux predicion at microboone (2018). URL: https://microboone.fnal.gov/wp-content/uploads/MICROBOONE-NOTE-1031-PUB.pdf.

[26] C. Andreopoulos, C. Barry, S. Dytman, H. Gallagher, T. Golan, R. Hatcher, G. Perdue, J. Yarba, The GENIE Neutrino Monte Carlo Generator: Physics and User Manual (2015). arXiv:1510.05494.

[27] M. Tanabashi, et al. (Particle Data Group), Review of Particle Physics, Phys. Rev. D98 (2018) 030001. doi:10.1103/PhysRevD.98.030001.

[28] D. Cianci, A. Furmanski, G. Karagiorgi, M. Ross-Lonergan, Prospects of Light Sterile Neutrino Oscillation and CP Violation Searches at the Fermilab Short Baseline Neutrino Facility, Phys. Rev. D 96 (2017) 055001. doi:10.1103/PhysRevD.96.055001. arXiv:1702.01758.

[29] P. Abratenko, et al. (MicroBooNE), Search for Neutrino-Induced Neutral Current Δ Radiative Decay in MicroBooNE and a First Test of the MiniBooNE Low Energy Excess Under a Single-Photon Hypothesis (2021). arXiv:2110.00409.

[30] P. Abratenko, et al. (MicroBooNE), Search for an Excess of Electron Neutrino Interactions in MicroBooNE Using Multiple Final State Topologies (2021). arXiv:2110.14054.

[31] P. Abratenko, et al. (MicroBooNE), Search for an anomalous excess of charged-current quasi-elastic ν_e interactions with the MicroBooNE experiment using Deep-Learning-based reconstruction (2021). arXiv:2110.14080.

[32] P. Abratenko, et al. (MicroBooNE), Search for an anomalous excess of inclusive charged-current ν_e interactions in the MicroBooNE experiment using Wire-Cell reconstruction (2021). arXiv:2110.13978.

[33] P. Abratenko, et al. (MicroBooNE), Search for an anomalous excess of charged-current ν_e interactions without pions in the final state with the MicroBooNE experiment (2021). arXiv:2110.14065.

[34] X. Ji, W. Gu, X. Qian, H. Wei, C. Zhang, Combined neymanâpearson chi-square: An improved approximation to the poisson-likelihood chi-square, Nuclear Instruments and Methods in Physics Research Section A: Accelerators, Spectrometers, Detectors and Associated Equipment 961 (2020) 163677. URL: https://www.sciencedirect.com/science/article/pii/S0168900220302436. doi:https://doi.org/10.1016/j.nima.2020.163677.

[35] M. Wospakrik, H. Schulz, J. Kowalkowski, M. Paterno, S. Sehrish, W. Ketchum, G. Ge, G. Karagiorgi, M. Ross-Lonergan, Grid-based minimization at scale: Feldman-Cousins corrections for light sterile neutrino search, EPJ Web Conf. 251 (2021) 02065. doi:10.1051/epjconf/202125102065.

[36] G. Guennebaud, B. Jacob, Eigen v3 (2010). URL: http://eigen.tuxfamily.org.

[37] F. a. James, MINUIT: Function Minimization and Error Analysis Reference Manual (1998). URL: https://cds.cern.ch/record/2296388, cERN Program Library Long Writeups.

[38] G. Cowan, K. Cranmer, E. Gross, O. Vitells, Asymptotic formulae for likelihood-based tests of new physics, The European Physical Journal C 71 (2011). URL: http://dx.doi.org/10.1140/epjc/s10052-011-1554-0. doi:10.1140/epjc/s10052-011-1554-0.

[39] K. Mahn, et al. (SciBooNE, MiniBooNE), Dual baseline search for muon neutrino disappearance at $0.5eV^2 < \Delta m^2 < 40eV^2$, Phys. Rev. D 85 (2012) 032007. doi:10.1103/PhysRevD.85.032007. arXiv:1106.5685.

[40] P. e. a. Adamson (MINOS+ Collaboration), Search for sterile neutrinos in minos and minos+ using a two-detector fit, Phys. Rev. Lett 122 (2019) 091803. URL: https://link.aps.org/doi/10.1103/PhysRevLett.122.091803. doi:10.1103/PhysRevLett.122.091803.

[41] M. Aartsen, R. Abbasi, M. Ackermann, J. Adams, J. Aguilar, M. Ahlers, M. Ahrens, C. Alispach, N. min, K. Andeen, et al, ev-scale sterile neutrino search using eight years of atmospheric muon neutrino data from the icecube neutrino observatory, Physical Review Letters 125 (2020). URL: http://dx.doi.org/10.1103/PhysRevLett.125.141801. doi:10.1103/physrevlett.125.141801.

[42] A. Aguilar, L. B. Auerbach, R. L. Burman, D. O. Caldwell, E. D. Church, A. K. Cochran, J. B. Donahue, A. Fazely, G. T. Garvey, R. M. Gunasingha, et al., Evidence for neutrino oscillations from the observation of $\bar{\nu}_e$ appearance in a $\bar{\nu}_\mu$ beam, Physical Review D 64 (2001). URL: http://dx.doi.org/10.1103/PhysRevD.64.112007. doi:10.1103/physrevd.64.112007.

[43] M. Dentler, A. Hernandez-Cabezudo, J. Kopp, P. Machado, M. Maltoni, I. Martinez-Soler, T. Schwetz, Updated global analysis of neutrino oscillations in the presence of ev-scale sterile neutrinos, Journal of High Energy Physics 2018 (2018). URL: http://dx.doi.org/10.1007/JHEP08(2018)010. doi:10.1007/jhep08(2018)010.

[44] K. Abe, J. Adam, H. Aihara, T. Akiri, C. Andreopoulos, S. Aoki, A. Ariga, S. Assylbekov, D. Autiero, M. Barbi, et al., Search for short baseline ν_e disappearance with the t2k near detector, Physical Review D 91 (2015). URL: http://dx.doi.org/10.1103/PhysRevD.91.051102. doi:10.1103/physrevd.91.051102.